Aristotle University
of Thessaloniki
School of Geology

National Technical
University of Athens
**School of Mining &
Metallurgical
Engineering**

National and
Kapodistrian
University of Athens
**Department of
Geology and
Geoenvironment**

Democritus
University of Thrace
**School of
Economics**

Master Degree:

«**Hydrocarbon Exploration and Exploitation**»

KONSTANTINOS Ch. CHAVANIDIS

Geologist

GEOPHYSICAL INVESTIGATIONS IN THE THERMAIKOS BASIN

MASTER THESIS

Thessaloniki

2020

KONSTANTINOS Ch. CHAVANIDIS

Geologist

GEOPHYSICAL INVESTIGATIONS IN THE THERMAIKOS BASIN

Submitted to the School of Geology of the Aristotle University of Thessaloniki in the framework of the Master's Degree 'Hydrocarbon Exploration and Exploitation'

Date of Oral Examination: March, 4, 2020

Advisory Committee

Professor Grigorios Tsokas, Supervisor

Professor Antonios Vafidis, Member

Dr. Alexandros Stampolidis, Member

Geophysical Investigations in the Thermaikos Basin

dedicated to my parents, for their continuous support and tolerance

Table of Contents

FOREWORD

The purpose of the present Master Thesis is to describe the processing and interpretation of the main geophysical methods used (Seismic Reflection and Potential Field methods, i.e. magnetic and gravimetric) in the area of onshore Thermaikos basin, in northern Greece, aiming to detect closed subsurface geological structures which can act as hydrocarbon traps.

In the first chapter, the geology and tectonics of the onshore Thermaikos basin is analyzed, in addition with information regarding the wider Axios basin and its geotectonic zones. Also, a synopsis of the main geophysical and geological exploration surveys that have been conducted is presented.

In the second chapter, a description of the geophysical (gravity, magnetic, seismic) and borehole data which were used for this Thesis is made, as well as a brief mention on formation density logging basics.

The third and fourth chapters contain the theory about potential field and seismic processing methods, correspondingly, along with images of the methods' application to Thermaikos basin data. At the end of chapter 4, the above data are used, in addition with the available borehole logs, for the construction of 2-D depth models of the subsurface of onshore Thermaikos basin.

Finally, in the fifth chapter natural gas storage in Thermaikos basin is discussed, while the sixth chapter includes the conclusions of the Master Thesis.

Konstantinos Chavanidis

Thessaloniki, 2020

CHAPTER 1

GEOLOGY OF THERMAIKOS BASIN

1.1 Geology, Tectonics and brief Geotectonic Evolution of Thermaikos Basin

The onshore Thermaikos basin (or Thessaloniki – Katerini basin) is located in Northern Greece, lies in an area of about 4000 km^2 and is the northwestern extension of the offshore Thermaikos basin (Figure 1.1.1). The basin is located west of Thessaloniki and is enclosed by Yannitsa, Pella and Koufalia from North, Agios Athanasios, Anatoliko and Nea Malgara from East, Aliakmon river from South and Krya Vrysi and Galatades from West. The deepest part of the basin, where the sediments have their greatest thickness, is located at Chalastra (Pirgos) area, along Axios river. The basin's creation began above the metamorphic formations of Axios zone during Eocene.
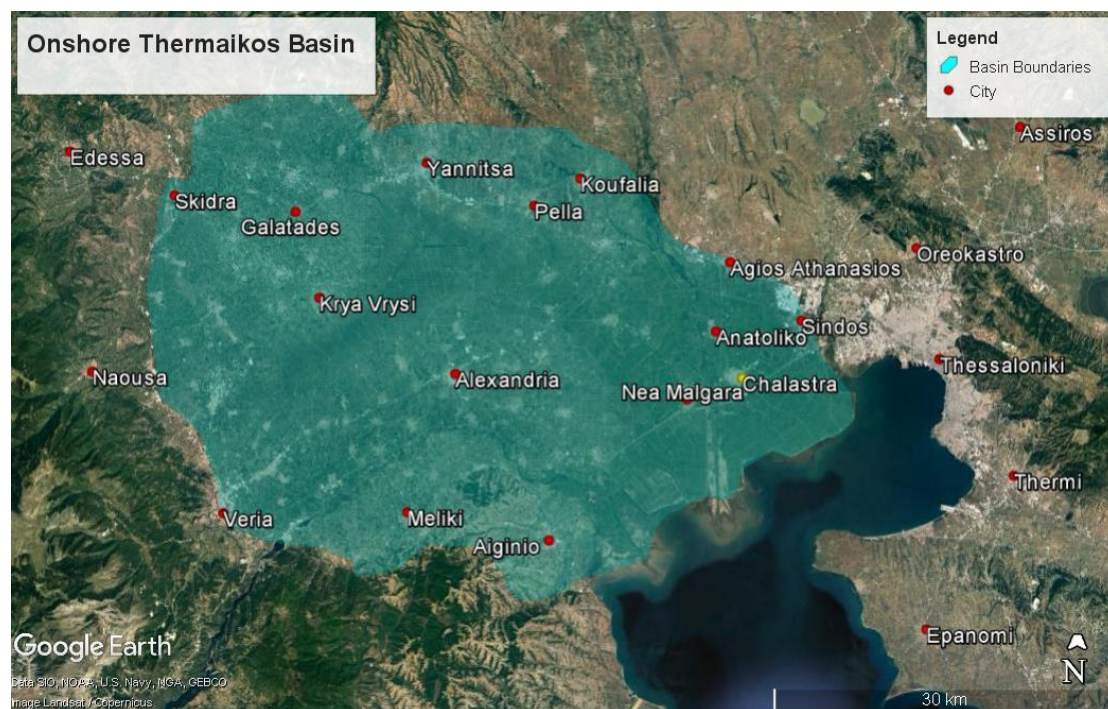
Figure 1.1.1: Map of the onshore Thermaikos basin. The yellow dot indicates the location of the deepest point of the basin, in Chalastra area (map created with Google Earth Pro).

1

The wider basin is known as Axios (or Vardar) basin and lies from the country of North Macedonia (approximately 70 km NW of the city of Thessaloniki), it continues inside Thermaikos gulf and reaches until Sporades Islands in Aegean Sea (Figure 1.1.2). Axios (or Vardar) river stems from the Sharr Mountains in Albania – Kosovo borders and runs the entire basin. The direction of Axios basin is NNW-SSE, its shape is oblong, and is developed over the Alpine Axios zone and the Tertiary "Molassic Axios Trench" (Mountrakis 2010) with unconformity.
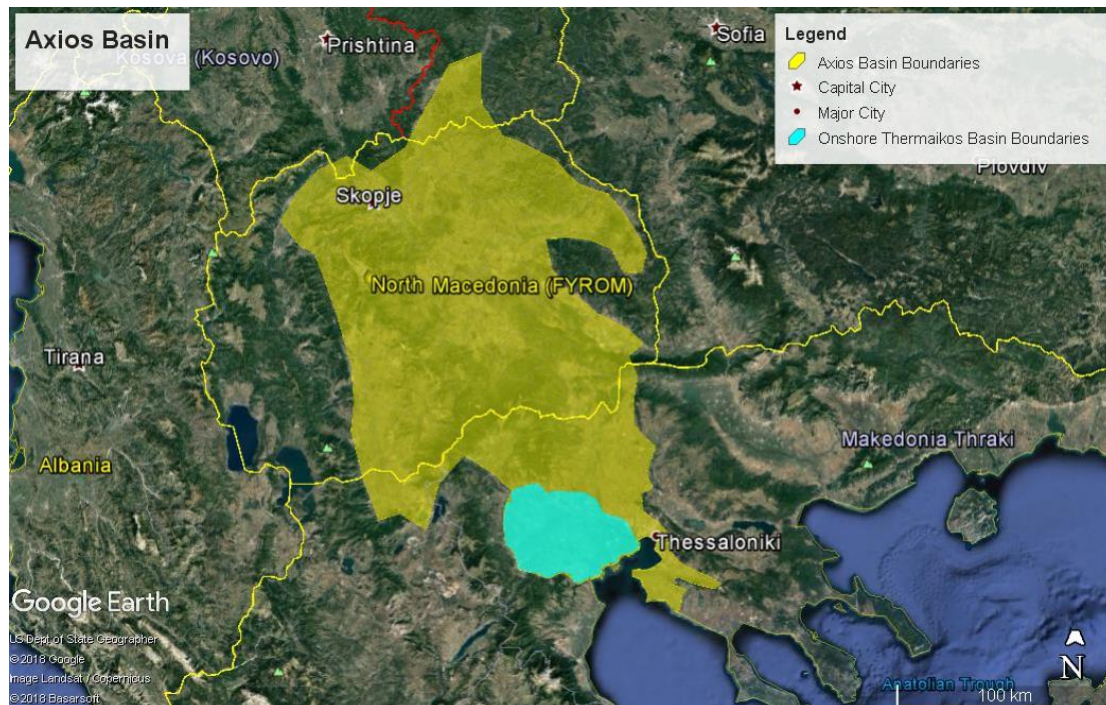
Figure 1.1.2: Onshore Axios basin boundaries and the location of the onshore Thermaikos basin in it (map created with Google Earth Pro).

"Axios Trench" was created and acted during Tertiary (Eocene – Oligocene) over the geologic formations of Peonias subzone. Today, it is covered by the sediments of Axios basin and eastern Thermaikos basin. The sediments which consist «Axios Trench» are of molassic type and of multiple depositional environments, i.e. marine, lacustrine and continental. They are sandstones, marls, conglomerates, breccias and limestones of Upper Eocene – Oligocene – Upper Miocene age. There is a remarkable presence of important fossils (e.g. *Ouranopithecus macedoniensis*, *Hipparion dietrichi*, *Choerolophodon pentelici*) in the continental sediments of Upper Miocene, as they were found in areas like Vathylakkos, Dytiko, Nea Mesimvria etc.

2

According to stratigraphic studies and deep boreholes that have been conducted in the area, the sediments of Axios basin can be divided into three groups:

- The Plio-Pleistocene deposits, which are mainly sandstones and marls with intercalations of clays and conglomerates at the upper part.
- The Miocene deposits, which consist of sandstones, marls and clays of continental and lacustrine origin.
- The sediments of "Molassic Axios Trench", as described in the previous paragraph.

The basement of Axios (and consequently Thermaikos) basin consists of strongly metamorphic rocks of Axios geotectonic zone and comes to the surface at the basin's circumference. These rocks are of pre-Paleogene age, mostly ophiolites (serpentinites, igneous rocks of basic composition etc.) and deep-sea sediments, that underwent metamorphism of greenschist phase (low pressure and temperature conditions). The basement is uplifted in the western basin boundary, between Katerini and Kariotissa region and in the eastern boundary, among the areas of Koufalia, Agios Athanasios and Thessaloniki. The boundaries of this ophiolite suture, though, are clearly discernible, both onshore and offshore (in Thermaikos Gulf).

According to Loukoyannakis et al. (1990), the average depth of the onshore Thermaikos basin in its SW area reaches 3000 meters. Strong folding of the Alpine basement has taken place there, with simultaneous presence of large anticline structures, reverse ruptures and small normal faults.

The Paleogene formations of Thermaikos basin are deposited with unconformity above the basement during Eocene Epoch. These formations come to the surface at the areas of Vasilitsa and Kastro in the northern part of the basin, with the form of fossiliferous conglomerates, sandstones, marls and coral limestones. They can be divided in two formations: the oldest dates at Lower Eocene, mostly lies at the NW part of the basin and is referred as Yannitsa Formation, and the newest dates at Upper Eocene – Oligocene, is composed of turbidites, lies at the central and eastern parts of the basin and covers with unconformity or pseudo-conformity the Yannitsa Formation. Turbidites are made of a sequence between clays and pelites with thin intercalations of fine-grained calcareous sandstones. Paleogene deposits become thinner at the eastern and western basin boundaries.

There are multiple references concerning Yannitsa Formation. Kellogg (1988) states that Yannitsa Formation is a representative Lower Eocene formation of the NW part of Thermaikos basin, found in Yannitsa 1 well. Lalechos (1983) described it as red argillaceous limestone of lacustrine phase dating on Pliocene, found on surface at Yannitsa area. Kolovos (1990), as mentioned on Sivenas et al. (1997), supports that the age of Yannitsa Formation, which is found on top of the amphibolitic basement in Litovoi 1 well, dates on Miocene. It is described by the same researcher as conglomerates with intercalations of clays, covered with red conglomerates, sands, gravels and clays, while on the upper part conglomerates with clay and pelite intercalations complete the sequence, indicating a continental to brackish water depositional environment, with local phases of sea influx. The boreholes drilled at onshore Thermaikos basin will be discussed in detail on Chapter 2.

Miocene deposits lay with unconformity (in an eroded surface) above the Paleogene formations. They appear at surface in the northern area of Katerini. Miocene stratigraphy generally consists of conglomerates with pelite and marl intercalations, that are followed by a series of clays, sands and sandstones with thin lignite layers. In the upper part, there are sandstones, sands and marls. These sediments indicate a lacustrine and a continental depositional environment. Miocene sediments become thinner at the eastern part of the basin, while at the south-western flank of the basin Miocene formations are wider, covering the eroded Eocene deposits.

Plio-Pleistocene sediments lay with pseudo-conformity above the Upper Eocene and with conformity above the Miocene deposits. Surficial, they can be observed at the basin's circumference, at the areas of Katerini, west of Agriosykia, Yannitsa, Litovoi, Agios Athanasios, at Kilkis area and up to the North and West of Thessaloniki. An augmentation in the sediments' thickness from the central to the western and, mainly, eastern part of the basin can be observed, which possibly indicates the direction of the basin filling during Upper Miocene – Lower Pliocene. At the western part of the basin, there are tuff intercalations in the upper sediments due to intense volcanic activity during Late Tertiary (Upper Pliocene) – Early Quaternary (Lower Pleistocene). These volcanic deposits appear to the surface in the areas western of the basin, between Veria and Naousa and they extent until Edessa and Aridaia regions. Only few quantities of these volcanic materials reached Thermaikos basin, as the greater expanse lies in the area of Mt. Voras, at the northern part of Almopias subzone.

4

The oldest geotectonic activity that was recorded in Axios zone basement has taken place during Upper Jurassic – Lower Cretaceous, with pre-Hercynian obductions in the metamorphic Jurassic formations. In the following Epochs, multiple Alpine obductions have, also, taken place on Axios and on Rhodope and Serbo-Macedonian zones, at Upper Cretaceous – Lower Eocene, Upper Eocene and Upper Oligocene. At Lower Eocene, Thermaikos basin was created. Tertiary sedimentation in Axios and Thermaikos basins began with Yannitsa Formation in the NW part (in a shallow water environment) and Kassandra Formation in the East and SE, which covered the basement with unconformity. The Paleogene sediments of Thermaikos basin were induced by the Alpine tectonic activity. Eocene deposits of Aiginio region in the South of the basin are more affected by tectonism. In the northern part, a similar situation is possible but cannot by proved due to lack of seismic data.

In Upper Eocene, compressional tectonism followed, with large-scale ophiolite obductions in Olympus-Ossa region and obductions of smaller scale, in addition to normal faulting, in Thermaikos basin. Until Lower Oligocene, turbidites were deposited in the deep-sea environment that was created due to rapid subduction conditions. In Upper Oligocene, SW ophiolite and deep-sea sediment obduction in Olympus-Ossa region and Pelagonian zone has taken place, which caused folding and normal faulting in Thermaikos basin's sediments, in add to locally extended compressional faults of NW-SE direction (similar to the main obduction) and intense erosion in the western basin boundary. Due to this ophiolite movement, a large active thrust fault of NW-SE direction was created, while smaller strike-slip faults perpendicular to the above direction are, also, present. The Tertiary sediments of Thermaikos basin followed the westward obduction movement and they have greater thickness in the central part of the basin (in Loudias area).

During Neogene, the intensity of tectonic activity decreased. Until today, tectonism is characterized mainly by normal faulting. From Miocene to Lower Pliocene, where the last subduction period took place, sediments of important thickness, rich in sand, were deposited above the eroded Eocene layers with angular unconformity and with pseudo-conformity above the Oligocene formations. In the eastern part of Thermaikos basin, there is a gravity fault system due to the sediment resettlement in the basin's slopes, which mainly affect the Miocene – Pliocene deposits.

5

The general basin's characteristic is a depositional environment of unvaried sedimentation, with decreasing porosity with depth, due to the sediments' compaction. The Upper Pleistocene sands show large porosity values, porosity decreases in Pliocene and Miocene sands and sandstones, while the Paleogene sandstones, which have generally clay cement, are of very low porosity.

1.2 The Formation of a Sedimentary Basin and an Anticline Trap

In a period of hundreds of millions of years, the combined action of eroded material deposition and precipitation of chemical and organic debris within water environment results in sedimentary basin creation.

Elevated land areas undergo erosion from water and wind action, forming areas of low-lying land. Water fills these areas, creating a water environment, where sedimentation takes place. Over years, continuing continental sedimentation and the additional sediments' weight cause subsidence. Organic matter and chemical components are deposited together with the eroded rock material, producing layering of strata (an individual layer of sediment that is defined by its lithology or physical breaks in sedimentation) in the basin and unconformities, if deposition is interrupted in the geological record. Tectonic activity that is, simultaneously, present due to the movement of earth's crust or possible volcanic action, causes faulting to appear in sediments. Folding and distortion is created due to land mass movement. Finally, the thick, complex structures that are formed result in the formation of sedimentary basin. Figure 1.2.1 represents schematically the formation of a sedimentary basin.

Initial basin formation

Faulting in the basin

Erosion surface

Unconformity creation

Sedimentary basin formation
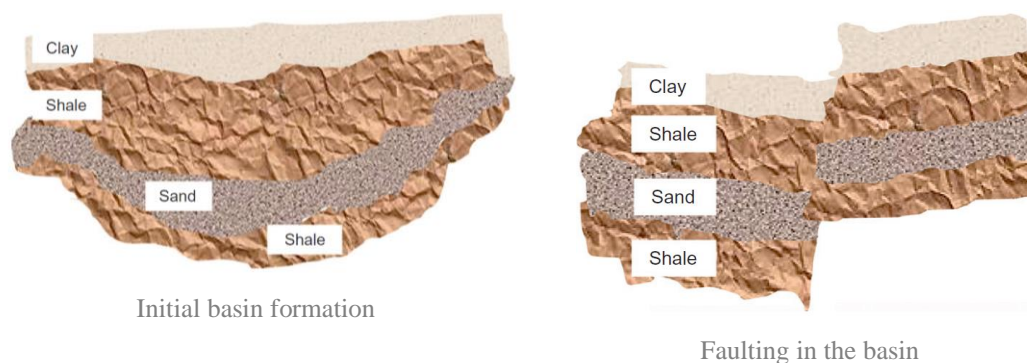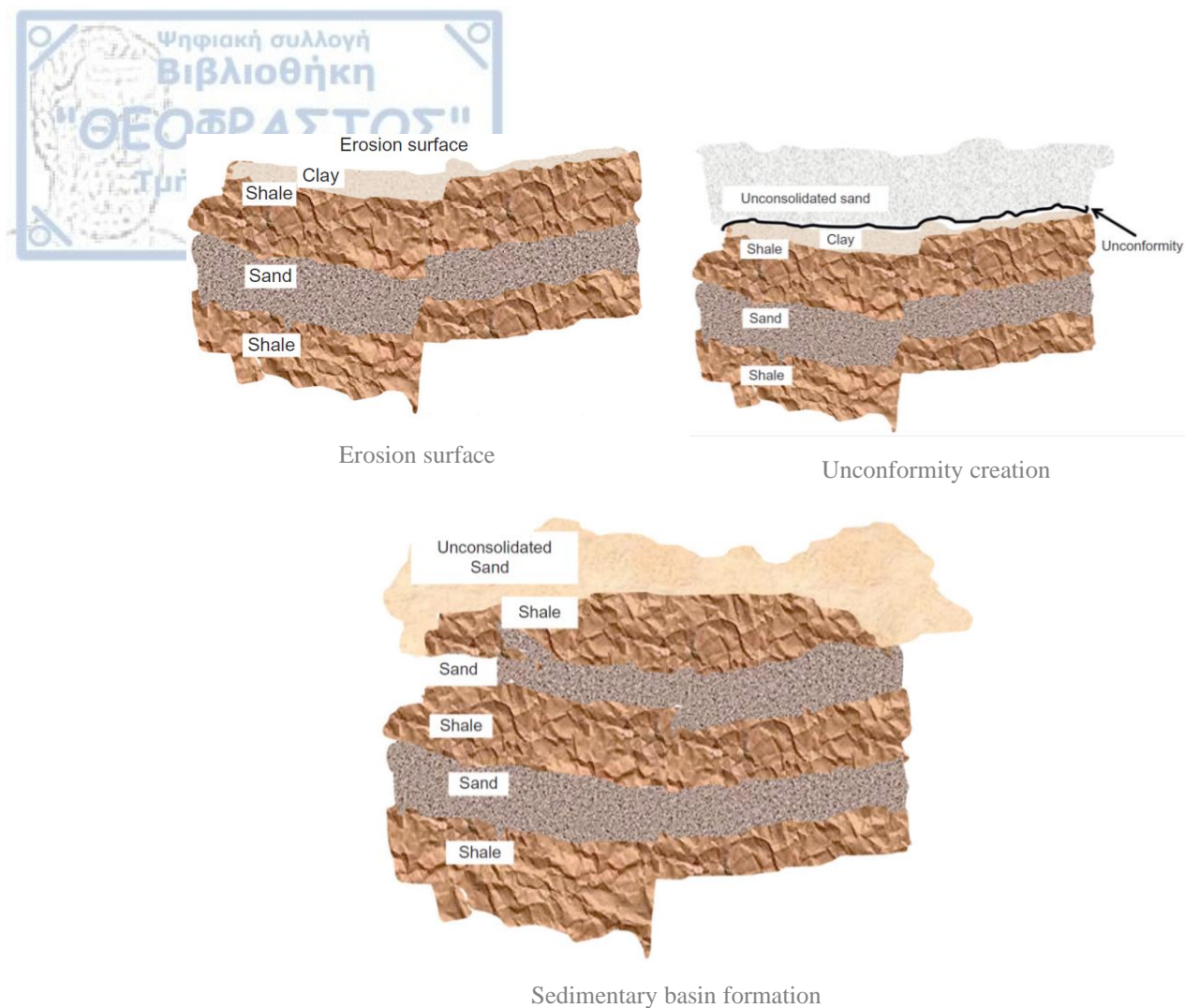
Figure 1.2.1: Sedimentary basin formation (after Onajide 2014).

Folding of rock strata due to earth movement into an arch-like shape creates an anticline. Anticlines, together with faults and salt diapirs, are characterized as structural traps. They can be identified at seismic sections by the closed loops that the structural contours create.

In order for the anticline to trap hydrocarbons (or water), the reservoir rock must be overlain by fine-grained rock at its top and sides, that acts as the seal or cap rock. The amount of hydrocarbon that an anticline can hold depends on the closure, i.e. the height of the closed crest above the lowest structural contour. If an anticline structure is filled with oil and there is more than enough gas to saturate it, the excess of gas will gather on top of the oil, giving the classic gas-oil-water system found in most hydrocarbon traps (Figure 1.2.2).

7
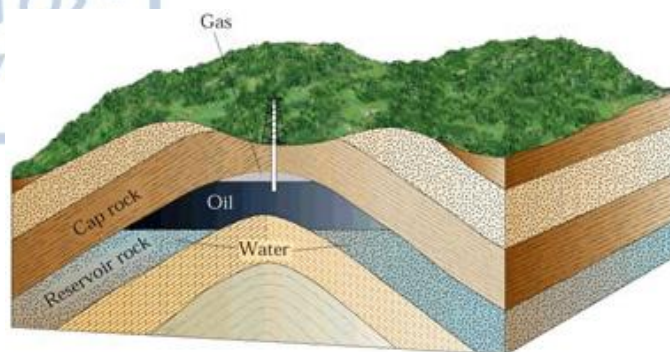
Figure 1.2.2: An anticline trap with a typical petroleum system (taken from: http://www.ingenieriadepetroleo.com/petroleum-traps).

1.3   General information on the lithology of Axios zone

The geotectonic zone of Axios is located between the Circum Rhodope (or Serbo-Macedonian according to some researchers) and the Pelagonian zones. It is divided into three subzones: Peonias to the East, Paikon in the middle and Almopias to the West.

The geological formations of Axios zone are encountered with the form of tectonic scales, creating obductions and thrusts of small scale but, also, of huge extent (of kilometers) with the main direction being that from East to West.

In the following paragraphs, a short description of the geologic formations of the three subzones is presented, as given by Mountrakis (2010).

The lithostratigraphy of **Almopias** subzone, from the oldest to the most recent formation, is (Figure 1.3.1):

- Rocks of strong metamorphism (augen gneisses, amphibolites, quartzites, schists). Paleozoic age.
- Alternations among schists, phyllites, marbles and cipollines. Triassic – Jurassic age.
- Carbonate rocks (marbles, crystalline limestones and dolomites) with insertions of schists. Triassic – Jurassic age (continuation of the previous formation).
- Ophiolitic mélanges. Formation which is placed tectonically above the previous, during the ophiolites' obduction in Upper Jurassic. They can be

8

observed as mega-breccia with parts of marbles and other metamorphic rocks into a mix of strong cleavage.

- Ophiolites (serpentinites, dolerites, lavas of basic composition). Upper Jurassic age. They constitute the most important formation of the subzone.

- Sedimentary (deep-sea sediments, radiolaritic cherts, clays, shales, pelagic limestones, calc-schists), volcanic-sedimentary (tuffs, pillow lavas, dolerites) and clastic (sandstones, volcanic conglomerates and breccias) series that overlay or are folded with the ophiolites. Upper Jurassic age.

- (Base) conglomerate. Lower Cretaceous age.

- Sediments of transgression (clastic sediments, such as sandstones, conglomerates and breccias, of important thickness in alternations with limestones). Middle – Upper Cretaceous age.

- Limestone horizon. Upper Cretaceous age.

- Flysch (sandstones, psammitic limestones, calc-schists, conglomerates). Upper Maastrichtian (Upper Cretaceous) – Lower Paleocene age.
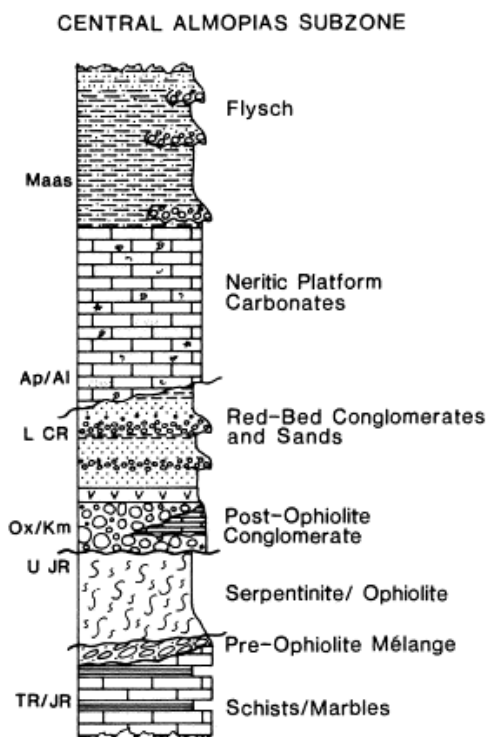
Figure 1.3.1: Lithostratigraphy of the central Almopias subzone (after Brown & Robertson 2004).

Peonias subzone is divided in seven units (Gevgeli, Oreokastro, Vafeiochori, Artzan, Aspri Vrysi, Metallikon, Leventochori), the lithostratigraphy of whom, from the oldest to the most recent formation, is:

- **Gevgeli unit** (Figure 1.3.2):
    - Gola Tsouka formation: recrystallized limestones and marbles. Triassic age.
    - Kastaneri formation: volcanic-sedimentary series (sericitic porphyroid rhyolites, tuffites, pyroclastic sandstones, lences and intercalations of squamous limestones, clastic sediments), quartz schists in the upper part and a body of granite metamorphosed into gneiss. Triassic – Jurassic age.
    - Grivas formation: limestones, sericitic and calc schists. Jurassic age.
    - Ophiolites (gabbro, dolerites, pillow lavas, microlithic basic volcanic rocks) and radiolaritic-chert sediments. Jurassic age.
    - A large granitic body intrudes inside the ophiolites after their placement. It is known as the Fanos/Axioupoli granite and dates at 150 Ma (Upper Jurassic).
    - Limestones, sandstones and micro-conglomerates. Upper Jurassic – Lower Cretaceous age.

- **Oreokastro unit** (the rocks of this unit appear inverted):
    - Gneisses and amphibolites of Serbo-Macedonian zone.
    - Black lyddites (cherts) with diabases. Carboniferous – Permian age.
    - Volcanic-sedimentary series made of red clastic sediments (conglomerates and sandstones) and volcanic rhyolitic rocks. Permian – Lower Triassic age.
    - Squamous limestones with foraminifera (*Meadrospira dinarica*) fossils of Middle Triassic age, that evolve to massive limestones of Anisian age.
    - Pelagic limestones. Ladinian (Upper Triassic) age.
    - Calc-clastic rocks. Late Triassic – Lower Jurassic age.
    - Ophiolites (gabbro mostly). Jurassic age.

- o Calcareous conglomerates with limestone and marl layers. Late Jurassic age.

- **Vafeiochori and Artzan units** (the formations of these units are similar) (Figure 1.3.2):
    - o Metamorphic rocks of greenschist phase (mica schists, quartzites, marbles, cipollines). Triassic – Jurassic age.
    - o Ophiolites (gabbro, dolerites etc.). Jurassic age.
    - o Transgressive series of important thickness (conglomerates with ophiolitic parts, sandstones, psammitic limestones and pelites), that contains Portlandian (Late Jurassic) limestones in the upper parts and displays a flysch structure in Cretaceous. Upper Jurassic – Lower Cretaceous age.

- **Metallikon, Leventochori and Aspri Vrysi units** (these units are considered part of Circum Rhodope zone by some researchers). They consist of two rock formations:
    - o The lower formations, made of recrystallized limestones dating at Triassic – Lower Jurassic age.
    - o The upper formations with ophiolites, made of deep-sea sediments (cherts, green schists, sandstones) folded with ophiolitic igneous rocks, diabases, dolerites etc. In bibliography, they are referred as flint formation. Jurassic age.

Every rock formation of Peonias subzone is found metamorphic at greenschist phase.
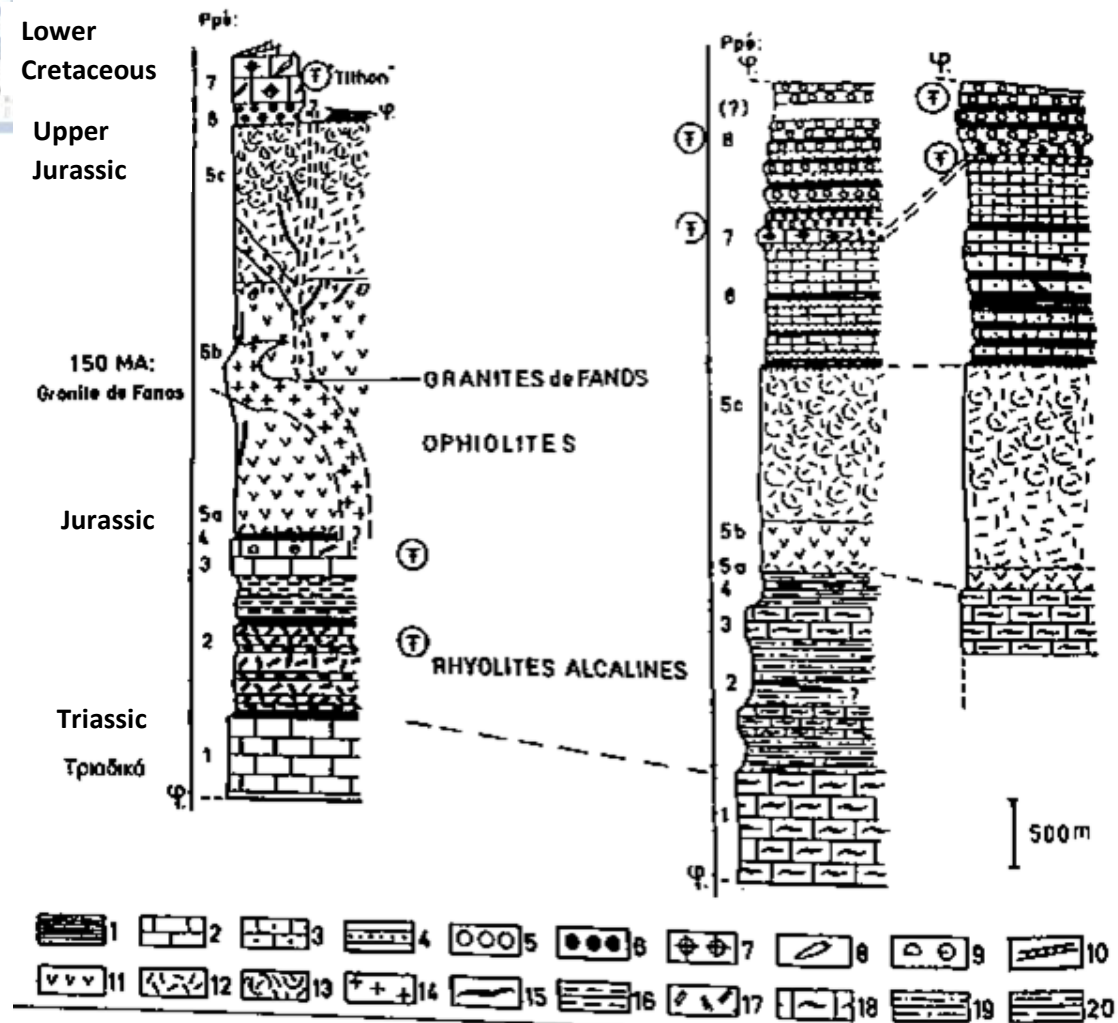
Figure 1.3.2: Gevgeli, Vafeiochori and Artzan units lithostratigraphy. Number explanation: 1: schists and pelites, 2: limestones and marbles, 3: psammitic limestones, 4: sandstones, 5: conglomerates, 6: conglomerates with ophiolitic parts, 7: corals, 8: belemnites, 9: foraminifera, 10: algae, 11: gabbro, 12: dolerites, 13: microlithic ophiolites, 14: granites, 15: pegmatites and granophyres, 16: tuffites, 17: sericitic porphyroid formations, 18: cipollines, 19: metamorphic pyroclastic formations, 20: quartzites (after Mercier 1966).

The lithostratigraphy of **Paikon** subzone, from the oldest to the most recent formation, is (Figure 1.3.3):

- Metamorphic series (alternations among gneisses, mica schists, cipollines, chlorite schists). Paleozoic age.
- Gandatch series: sedimentary metamorphic, mostly carbonate, rocks (marbles, cipollines, crystalline limestones, calc-schists, chlorite-epidotic schists). Triassic – Jurassic age.
- Livadia series: Volcanic-sedimentary rocks of medium metamorphism (chlorite schists, crystalline limestones, sandstones, quartz schists and volcanic (rhyolites, prasinites, metabasites, tuffites) material). Middle – Upper Jurassic age.
- Gropi limestones: carbonate series with fossiliferous marblelike limestones and cipollines. Jurassic age.
- Green schists with sparse limestone intercalations. Jurassic age.
- Spilite – keratophyre sequence of Kromni: marine volcanic rocks (spilites, keratophyres, diabases), volcanic-sedimentary deposits (conglomerates with volcanic cement, quartz conglomerates, sericitic tuffites, pyroclastic breccias) and other marine sediments (psammitic limestones, micro-conglomerates). In the above sequence, High Pressure – High Temperature (HP/HT) metamorphic conditions are observed. Upper Jurassic age.
- Kromni limestones: limestones with fossils of the sponge *Cladocoropsis mirabilis*. Upper Jurassic (Kimmeridgian – Portlandian – Late Tithonian) age.
- Ghrammos formation: Flysch of medium metamorphism (sandstones, conglomerates, pelites, limestones). Lower Cretaceous (Berriasian – Valanginian) age.
- Sea transgression sediments of Middle – Upper Cretaceous age, with no metamorphism:
  - o Dolomites of Upper Albian – Cenomanian age.
  - o Dolomitic limestones of Cenomanian age.
  - o Limestones of Cenomanian – Turonian age.
  - o Clastic series (alternations among sandstones, conglomerates, pelites, squamous limestones, dolomites) of Coniacian – Santonian – Campanian age.
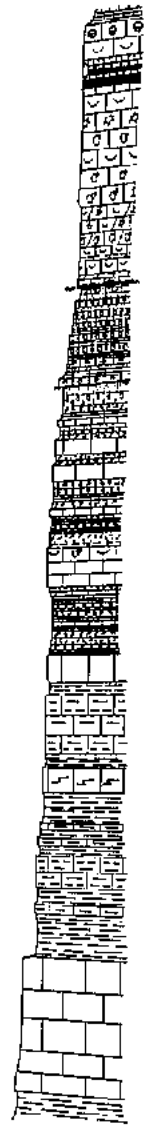

Figure 1.3.3:
Paikon
lithostratigraphy
(after Mercier
1966).

13

    o Grey-black limestones of Maastrichtian age.

    o Psammitic limestones, sandstones, shales (Gola Tsouka Formation) of Maastrichtian age.

Before the Mid-Cretaceous transgression, every formation of Paikon subzone has undergone metamorphism at greenschist phase.

1.4   Geophysical and Geological Surveys in Thermaikos Basin

The company that first did research in Thermaikos basin was Hunt Oil. In 1960, this company conducted aeromagnetic, gravimetric and seismic surveys in the basin, as well as it drilled 3 boreholes (Yannitsa 1, Klidi 1 and Korifi 1). Schlumberger undertook the logging acquisition, and on May – June 1961 worked at Korifi 1 well, on September – October 1961 at Klidi 1 well, and on November 1961 and January 1962 at Yannitsa 1 well. Hunt Oil abandoned Thermaikos basin area in 1962. From 1965 to 1967, the wells Kariotissa 1, Agriosykia 1, Litovoi 1, and Giordino (Agios Athanasios) 1 and 2 were drilled by the Greek State, as they were proposed by the reevaluation of the available data. In 1974, the well Aiginio 1 was drilled by Anschutz company. Later, in 1976, Oikonomou carried out geophysical investigations in the surficial layers of the basin for hydrogeological aim, as mentioned on Sivenas et al. (1997). In 1978, the Greek Public Oil Company (DEP) started its tasks in Thermaikos basin with a wide seismic survey, while in 1979 targeted the survey in Alexandria area. In 1980, another seismic survey was made by Nikex for DEP. The first DEP wells were drilled in 1980 and 1981 (Loudias 1, Alexandria 1) and their logging was made by Schlumberger in 1980. The last seismic survey took place in 1988 by DEP-EKY, and it was completed at 1989 – 1992. At the same year, Xanthopoulos et al. (published at 1990) realized deep VES (Vertical Electrical Soundings) in the northern part of the basin, where the basement is closer to the surface. The next year (1989), Kiriakidis & Brooks, using aeromagnetic and gravimetric data, studied the possible ophiolites' appearances under the basin's sediments. The final until now well (Korifi 2) was drilled by DEP-EKY in 1992, at the end of the 1989 – 1992 survey.

CHAPTER 2

DATA DESCRIPTION

The data of the present Thesis derive from measurements of gravity and total magnetic field that were realized at the area of onshore Thermaikos basin. Moreover, seismic sections, as well as data from boreholes that were drilled on the basin, are, also, used.

The software with which the gravity and magnetic field data were processed is Oasis Montaj and its add-on, GM-SYS Profile Modeling, developed by Geosoft. Also, ESRI's ArcMap (of ArcGIS suite) was used to support processing and presentation of spatial data on their original position at the study area. Finally, MATLAB (of MathWorks company) and Surfer (of Golden Software company) were used for seismic data processing and optical completion of the results.

2.1   Gravity Data

Gravity data of the Greek region, after they were checked for inaccuracies and errors due to obsolescence or use of different geodetic system, were unified and formed a new, updated Gravity Data Bank by Grigoriadis (2009). Thus, the gravity data of Thermaikos basin employed for the present Thesis come from that Data Bank.

First geophysical surveys in Greece were made in 1958, in the mineral exploration framework. Since then, especially after the 1970s, systematic geophysical investigations began in the whole Hellenic region. Gravity surveys were, mostly, conducted by the Greek Institute of Geology and Mineral Exploration (IGME) – now Hellenic Survey of Geology and Mineral Exploration (HSGME) – and other entities, such as Universities and the Hellenic Military Geographical Service (HMGS). HMGS's role in the progress of Potential Field measurements is particularly important, though its main domain is geodetic applications.

At that decade, the first Gravity Anomaly Map of Greece was made by the Hamburg Institute of Geophysics, on behalf of IGME (Makris & Stavrou 1984). The result was the unification and homogenization of every available data of gravity surveys made by different entities (IGME, HMGS etc.) of Greece since then.

In 1987, the creation of a new, modern gravity anomaly map of Greece of 1:500000 scale, was decided, where the most recent gravity measurements made by the Greek Public Power Corporation (PPC), the Greek Public Oil Company (DEP), IGME and Universities (Hamburg and Athens) would be included. As a result, a modern Gravity Data Bank was created at the University of Athens, in collaboration with the University of Edinburg (Lagios et al. 1988), that contained more than 30000 verified gravity stations. This new data bank was named as the "Lagios Data Bank of Gravity Values", from the lead researcher that unified the pre-existing data (Lagios et al. 1994, Lagios et al. 1996). It covers the majority of the continental area of Greece, though it has important deficiencies on the Aegean Sea Islands (Figure 2.1.1). Data from marine areas were collected from Morelli Data Bank (Morelli et al. 1975a, Morelli et al. 1975b). "Lagios" Data Bank contains point gravity and free-air anomaly values, with the corresponding geodetic coordinates at ED50-Greece Geodetic Reference System, projected coordinates at the UTM projection, as well as the orthometric altitude of each point. Due to the different origin and measurements' year of the data, the gravity value accuracy and the exact location of point values and altitudes are not completely known. The measured free-air anomalies are referred to the Geodetic Reference System of 1967 (GRS67), while gravity values to the International Gravity Standardization Network of 1971 (IGSN71).
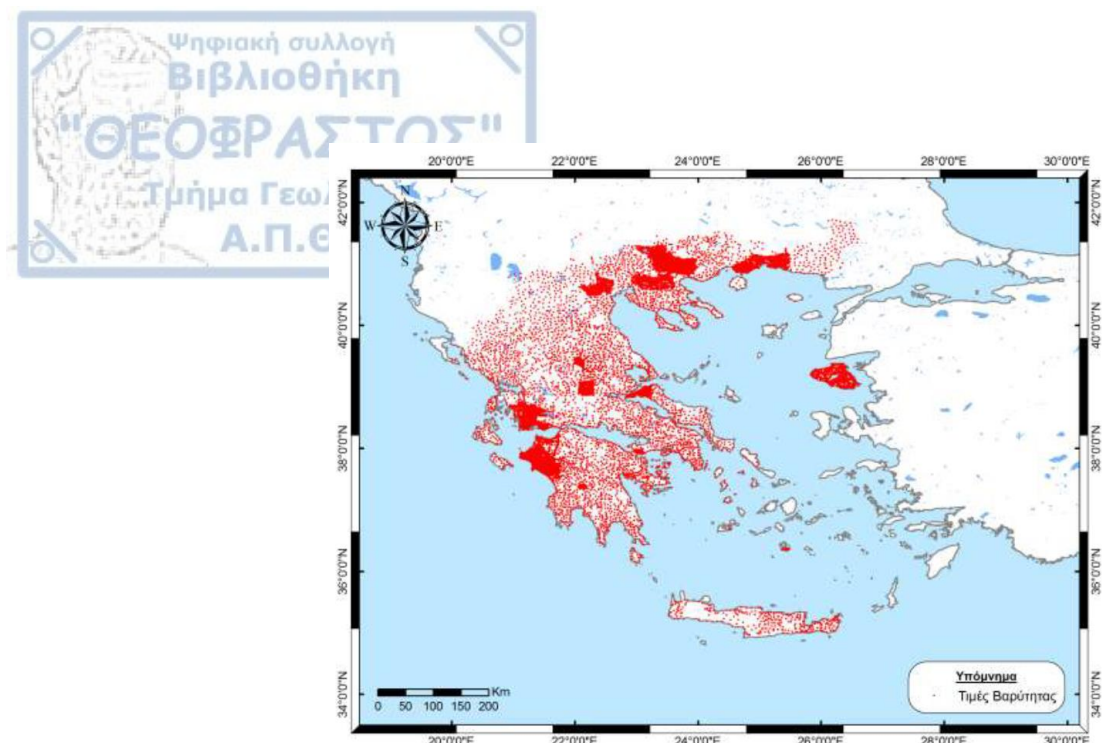
Figure 2.1.1: Gravity values' distribution of "Lagios Data Bank" (after Lagios et al. 1996).

Other sources that include measurements at the onshore Thermaikos basin is HMGS's free-air anomaly point values and Kiriakidis PhD Dissertation (1985). HMGS's point data contain geodetic coordinates, orthometric altitude and free-air anomaly values. Point allocation covers, mostly, the central and north-northwest Greek region. Point coordinates are referred to ED50-Greece Geodetic Reference System, altitudes are referred to Piraeus Tidal Station and free-air anomalies have been calculated at the Geodetic Reference System of 1980 (GRS80). Kiriakidis's data include small areas of the prefectures of Thessaloniki and Chalkidiki. They contain geodetic coordinates, orthometric altitude, free-air anomaly and gravity values. Their Reference System is GRS67.

The Gravity Data Bank of Greece is completed with data from the Bureau of Gravimetric International (BGI) for continental and marine areas, the digitized Morelli's maps (Morelli et al. 1975a, Morelli et al. 1975b, Behrend et al. 1996) and Casten & Makris (2001) data for marine areas, and finally the Tsokas data for Milos (Tsokas, 1996) and Kimolos (Tsokas et al. 1995) islands at the Aegean Sea.

DEP-EKY, former DEP, was developed into the most important entity for gravity survey conduct in the onshore Hellenic region. It conducted surveys in Northern and central Western Greece, as well as in other areas. Northern Greece (including onshore

17
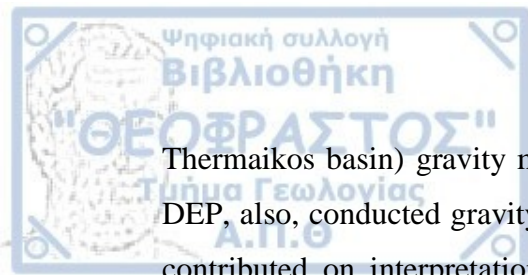
Thermaikos basin) gravity measurements have a density of 1 measurement per km^2. DEP, also, conducted gravity surveys of local scale, mostly on PhD frameworks, that contributed on interpretation of local geology. Kiriakidis's (1985) Dissertation on Thermaikos basin is such an example.

2.2   Aeromagnetic Data

The aeromagnetic data set constitutes a part of a survey that has taken place in 1977 by the Hunting Geology and Geophysics Ltd company, as contractor for the IGME. It was the second campaign of such type that took place in Greece, with the first being that of the year 1966 by ABEM AB company. This first campaign covered areas of Central and Eastern Macedonia and West Thrace. The 1977 survey covered a wider area, including West Macedonia, Thessaly, eastern Central Greece and eastern Peloponnesus. The final product of both surveys was a series of 1:50000-scale contour maps that complied with the corresponding topographic maps of the HMGS and the geological maps of IGME (of 1:50000 scale).

Each of the 1977 survey areas that consists the whole campaign is indicated with a different code name (A1, A2, B, C1, C2a, C2b, C3, D1). The area A1 depicts onshore Thermaikos basin, so these data were used for the present Thesis. For this area, Hunting Geology and Geophysics Ltd used a magnetic field spacing of 200 – 250 m, with a NE-SW flight direction, a 200 km/h airplane speed, a distance between flight lines of 400 m, and 150 m height from ground. Connection tie flight lines were flown at a NE-SW direction and a spacing of 10 km (Chailas et al. 2010).

The IGRF (International Geomagnetic Reference Field) correction value that was added to the magnetic anomaly was 150 nT (constant), following the IGRF model of the epoch (1977.3). In the current Thesis data, the initial IGRF has been removed (Grigoriadis 2009).

The map datum that was used in ArcMap software is the Greek Geodetic Reference System 1987 (GGRS 87 or Greek Grid), whereas the coordinate system is Cartesian and the ellipsoid used is that of the Geodetic Reference System (GRS) 1980.
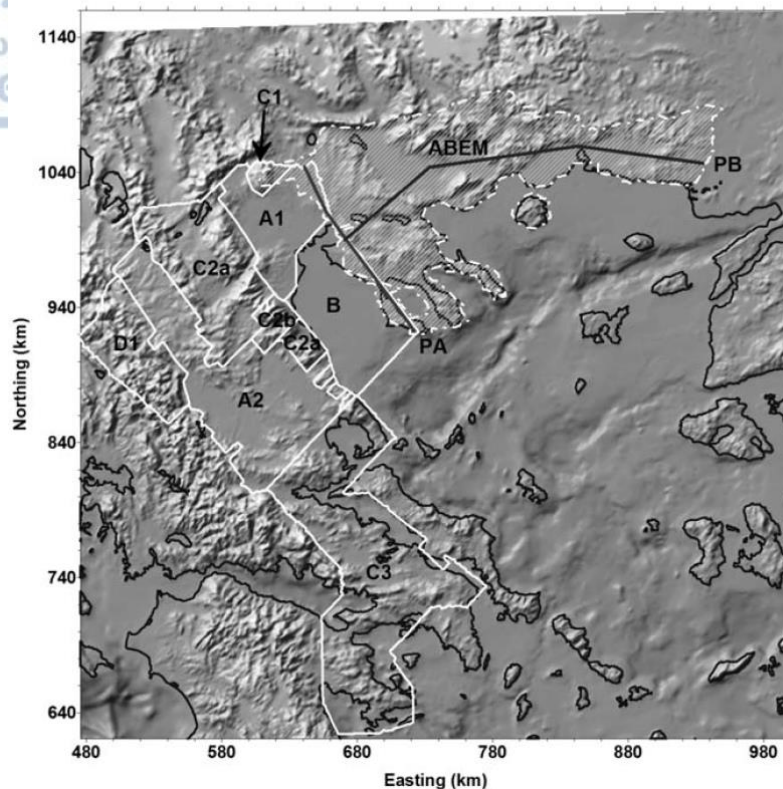
Figure 2.2.1: Area coverage of the aeromagnetic data. Area A1 corresponds to onshore Thermaikos basin (after Chailas et al. 2010).

2.3   Seismic Data

The seismic data set that was used for this Thesis was acquired by DEP-EKY. It is part of the 1978 – 1979, 1980 and 1989 – 1992 seismic surveys. There are two different categories that the available seismic data of onshore Thermaikos basin can be separated (Tsokas et al. 2013).

The first category uses dynamite as the seismic wave source, symmetric or asymmetric split-spread array of source and geophones with 48 channels, source distance of 50 meters and nominal fold of 12 or 24. This category includes the 1978 – 1979 survey by DEP (~ 370 km distance) with the L (3, 5, 6, 8, 9, 11, 14, 15, 19, 23, 25, 27, 29, 33, 88) and AL (1, 2, 4, 7, 10, 12, 13, 16, 17, 21) lines and the 1980 survey by Nikex (~450 km distance) which completed the previous survey, with the rest of the L lines (101, 103A, 104, 105, 107, 111, 112, 114, 115, 122, 124, 126, 128, 129, 130, 132).

19

The second category uses Vibroseis as the seismic wave source, asymmetric split-spread array of source and geophones with 96 channels, distance between sources of 40 meters and nominal fold of 48. This category includes the 1988 (~ 430 km distance) and 1989 – 1992 surveys by DEP-EKY, with the Pieria region PIV (201, 201A, 202, 203, 204, 205, 206, 207, 208, 208A, 209) and Pella region PEV (201, 202, 203, 206, 300, 301, 302, 304, 304A, 402, 403, 405, 406, 407, 500, 501, 503, 504, 505) lines correspondingly.

From the ending of 1980 until the beginning of 1990, the above seismic lines were reprocessed by DEP-EKY. The reprocessing of lines which were obtained using dynamite as wave source, however, caused the destruction of the upper part of the sections. The reprocessing results of seismic lines which were obtained using Vibroseis as wave source have much better quality.

The seismic sections which were used in the Thesis are the lines L8, L9, L88, L105 and PEV203.

2.4 Boreholes in onshore Thermaikos Basin

There are 12 boreholes that were drilled on the area of onshore Thermaikos basin (Figure 2.4.1), 7 of which reached the basement. These wells are: Yannitsa 1, Alexandria 1, Loudias 1, Korifi 1, Korifi 2, Klidi 1, Kariotissa 1, Litovoi 1, Giordino 1, Giordino 2, Agriosykia 1 and Aiginio 1. A description of these wells is given by Sivenas et al. (1997).
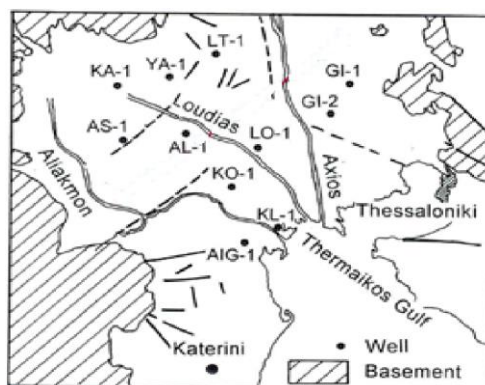
Figure 2.4.1: The locations of drilled boreholes in onshore Thermaikos basin (modified from Sivenas et al. 1997).

Yannitsa 1 (YA-1)

Total Depth: 2607 meters

- From 0 to 831 m, Plio-Pleistocene sediments are encountered, with unconformity above the Upper Miocene sediments. They are described as followed:
    - o 0-104 m: tuffs with intercalations of clays and lacustrine limestones
    - o 104-335 m: lacustrine and sandy-clayed limestones
    - o 335-789 m: clays with sparse intercalations of coarse-grained sandstones
    - o 789-831 m: conglomerates of basic composition with basement's parts
- From 831 to 1131 m, there are sediments of Miocene age, with pseudo-conformity above the Yannitsa Formation. They are consisted of clays with intercalations of coarse-grained sandstones and micro-conglomerates.
- From 1131 to 2607 m, the sediments are of Lower Eocene age. They are described as Yannitsa Formation (Kellogg 1988) and their sequence is, from top to base:
    - o Coarse-grained, clayed sandstones and pelites with sparse limestone and lignite intercalations, with no fossils (1131-1466 m)
    - o Mid- to coarse-grained sandstones with pelite intercalations, with marine fossils (1466-1676 m)
    - o Grey clays with pelite and sandstone intercalations, with few marine fossils (1676-2556 m)
    - o Coarse-grained sandstones, with no fossils (2556-2607 m)

Alexandria 1 (AL-1)

Total Depth: 1706 meters
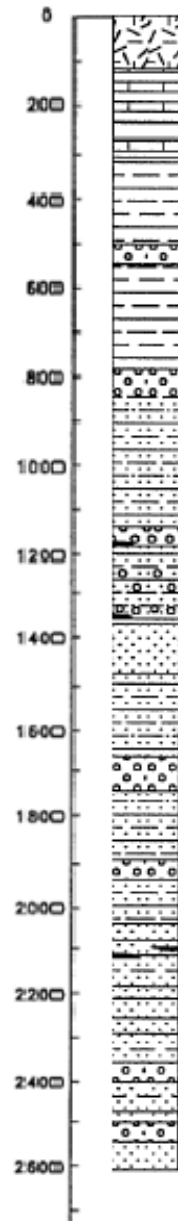
- From 0 to 607 m, Plio-Pleistocene sediments are present, with unconformity above the Miocene sediments. They consist of clays with intercalations of sands and micro-conglomerates, which are more coarse-grained at the lower part.

- From 607 to 918 m, Miocene sediments are encountered, forming of layers of slightly graded sands in lignite clays and mid- to coarse-grained sandstones with porosity between 15 and 30 %.

- From 918 to 1595 m, there are Paleogene formations, which are made of:

  o 918-1305 m: turbidites of Upper Eocene – Lower Oligocene (clays and pelites with thin intercalations of fine-grained, calcareous sandstones)

  o 1305-1595 m: coarse-grained sandstones and conglomerates with abundant lignite (Yannitsa Formation)

- From 1595 to 1706 m, the well drills the basement, which is consisted of ophiolites.

Loudias 1 (LO-1)

Total Depth: 3086 meters
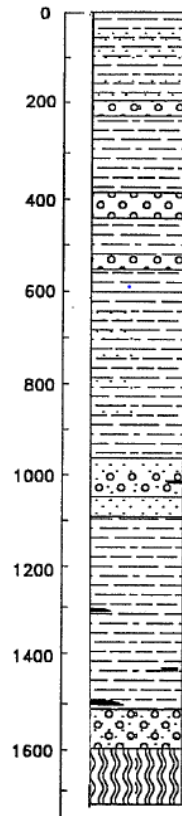
- From 0 to 725 m, Plio-Pleistocene sediments are encountered. They are clays with intercalations of fine- to coarse-grained sands, micro-conglomerates and limestones. The intercalations are thicker in the lower part.
- From 725 to 1510 m, there are Miocene sediments, with unconformity above Paleogene turbidites:
  - 725-1051 m: clays transforming to pelites, with intercalations of fine- to coarse-grained sands and sandstones with high porosity (30-50 %) and thickness
  - 1051-1510 m: slightly graded conglomerates and sandstones with clay cement, with clay and lignite intercalations
- From 1510 to 2885 m, Paleogene sediments are present, which are consisted mainly of turbidites. In the lowest 35 meters above the Cretaceous limestone, there are basic conglomerates of Lower Eocene, which are considered as part of the Yannitsa Formation.
- Above the basement, there is a limestone of slight metamorphism of Cretaceous age, with a thickness of 75 m (2885-2960 m).
- From 2960 to 3086 m, the basement is drilled, which consists of chlorite schists and quartzites.

23
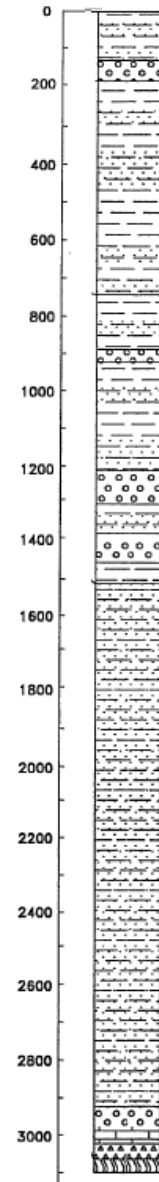
Korifi (KO-1 and KO-2)

Total Depth of KO-1: 3129 meters

Sivenas et al. (1997) describe only one well, with the name Korifi 1.

- From 0 to 840 m, there are Plio-Pleistocene sediments, which are consisted of clays and clayed sandstones of possible shallow marine origin with thin intercalations of clayed sands (from 0 to 100 m) and limestones (from 100 to 220 m) of continental origin.

- From 840 to 1764 m, Miocene formations are encountered, with unconformity above the Paleogene turbidites. They are marls, clays and slightly graded sandstones above 1485 m and conglomerates, sandstones and clays below 1485 m.

- From 1764 to 3129 m, Paleogene sediments are present:
  - 1764-2925 m: turbidites of Upper Eocene – Oligocene age
  - 2925-3129 m: coarse-grained sandstones and micro-conglomerates (part of the Yannitsa Formation)
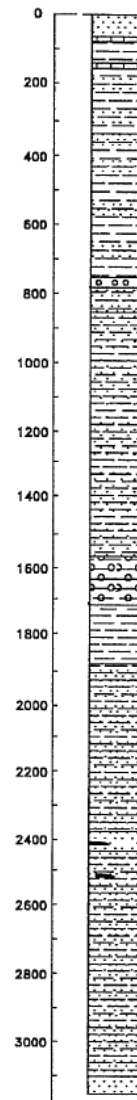
Klidi 1 (KL-1)

Total Depth: 4055 meters

- From 0 to 975 m, there are Plio-Pleistocene sediments, with pseudo-unconformity above the Miocene formations. They consist of clays with few intercalations of sands and sandstones with clay cement and some limestone intercalations below the depth of 200 m.
- From 975 to 2441 m, Miocene deposits are encountered, which are alternations among clays, sandstones and micro-conglomerates. They are laying with pseudo-conformity above the turbidites.
- From 2441 to 4055 m, the geological formations are described as turbidites and they date on Paleogene.
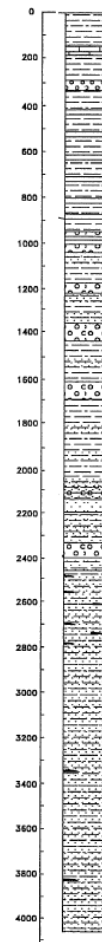
Kariotissa 1 (KA-1)

Total Depth: 690 meters

- From 0 to 669 m, there are Plio-Pleistocene sediments, which are deposited straight above the basement rocks:
  - 0-324 m: alterations among clays, marls and fine-grained sands
  - 324-669 m: coarse-grained sands
- From 669 to 690 m, the basement is drilled. The rocks encountered are mica schists and quartzites.

25
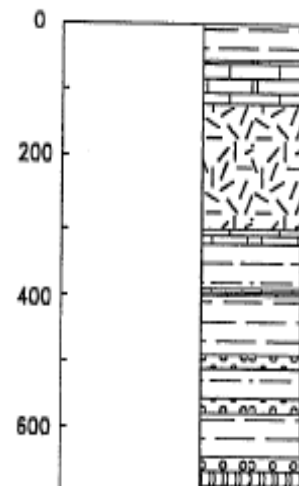
Litovoi 1 (LIT-1)

Total Depth: 1910 meters

- From 0 to 783 m, there are Plio-Pleistocene sediments, in the following sequence:
    - o 0-140 m: tuffs with intercalations of limestones
    - o 140-783 m: coarse-grained conglomerates with basement's parts, which are covered with thick layers of clay with intercalations of fine- to coarse-grained sands
- From 783 to 1880 m, Miocene deposits are encountered, which consist of coarse-grained conglomerates with thin intercalations of clays. They indicate a continental and a coastal depositional environment.
- From 1880 to 1910 m, the basement is present, with amphibolites and ultrabasic rocks. Paleogene formations are completely absent from this well.
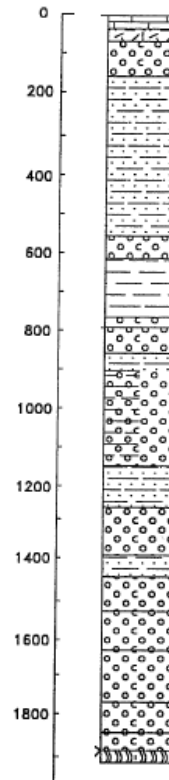
Giordino (Agios Athanasios) 1 (GI-1)

Total Depth: 666 meters

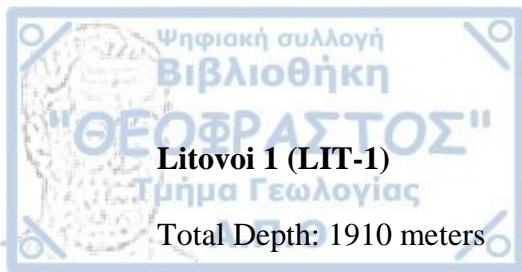- From 0 to 600 m, there are Plio-Pleistocene sediments, deposited straight above the basement. They are made of clays with intercalations of sands, which are thicker in the lower part.
- From 600 to 666 m, the basement is drilled. It consists of grey clays and quartz sandstones of medium metamorphism.

26
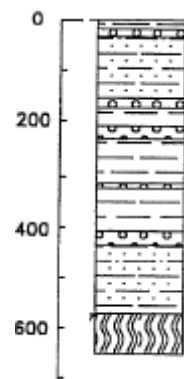
Giordino (Agios Athanasios) 2 (GI-2)

Total Depth: 2092 meters

- From 0 to 579 m, there are Plio-Pleistocene sediments, consisted of clays with sand intercalations.
- From 579 to 1593 m, Miocene deposits are encountered, with unconformity above the Paleogene turbidites. They are sandstones and conglomerates in alterations with thin layers of clay, indicating a continental to brackish water depositional environment.
- From 1593 to 2087 m, Paleogene formations are present:
    o 1593-1972 m: turbidites (sequence of clays and pelites with thin intercalations of fine-grained calcareous sandstones)
    o 1972-2007 m: limestone of possible coastal origin, with no fossils
    o 2007-2087 m: breccia formation
- From 2087 to 2092 m, the basement was drilled, which is consisted of amphibolites and gneisses.
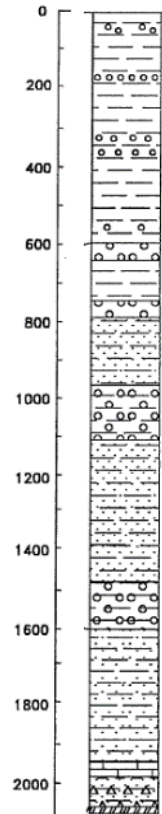
Aiginio 1 (AIG-1)

Total Depth: 2744 meters

- From 0 to 300 m, Plio-Pleistocene sediments are present, with angular unconformity above the eroded formations of Miocene.
- From 300 to 1119 m, Miocene deposits are encountered, which are made of basic conglomerates with intercalations of marls, sandstones and clays. At the lower part, intercalations are absent.
- From 1119 to 2744 m, the formations belong to Lower Paleogene and they are, probably, turbidites.

27

Agriosykia 1 (AS-1)

Total Depth: 1524 meters
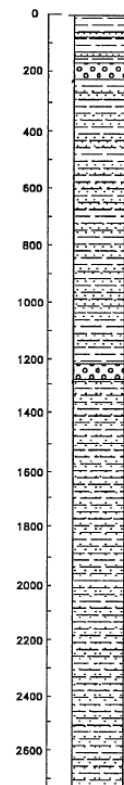
- From 0 to 690 m, Plio-Pleistocene sediments can be observed:
    - 0-131 m: loose sands and clays with thin intercalations of layers of limestones
    - 131-262 m: tuffs
    - 262-690 m: sandstones, clays, marls and thin layers of lacustrine limestones in the upper part, basic conglomerates in the lower part
- From 690 to 1051 m, Miocene sediments are present. They consist of clays with intercalations of thick layers of conglomerates with argillic cement (from 950 to 1051 m, conglomerates are coarse-grained and consolidated).
- From 1051 to 1495 m, the Paleogene Yannitsa Formation is drilled, dating at Lower Eocene, consisted of coarse-grained sandstones and grey clays with lignite intercalations and microfossils. In the lower part, it consists of lignitic clays.
- From 1495 to 1524 m, the basement is encountered with quartzites, mica schists and diabases.
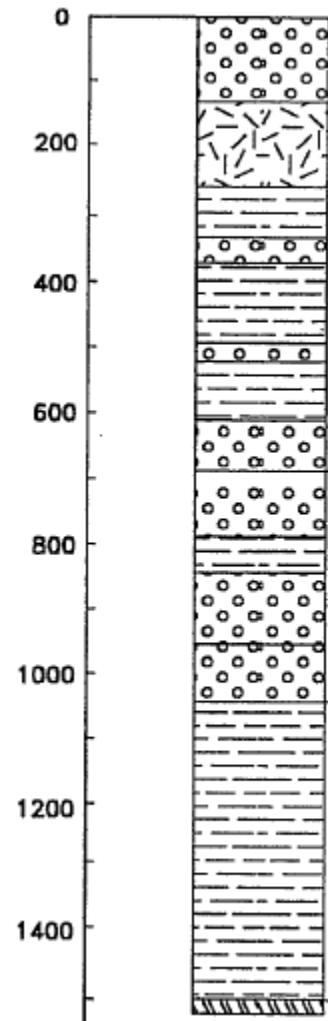
2.5 Table of Measurements

Measurements of thickness, two-way vertical travel time and velocity which were used for the present Thesis are gathered in the following Table 2.5.1 (modified from Tsokas et al. 2013):

Well (position at seismic line)	Estimated Parameters	Plio-Pleistocene	Miocene	Paleogene (Eocene-Oligocene)
AL-1 (11th km of L8)	Thickness (m)	620	350	630
	Interval two-way time (ms)	620	280	330
	Velocity (m/s)	**2000**	**2500**	**3818**
YA-1 (0th m of L8)	Thickness (m)	870	290	-
	Interval two-way time (ms)	615	265	-
	Velocity (m/s)	**2829**	**2189**	**-**
KO-1 (750th m of L88)	Thickness (m)	800	925	-
	Interval two-way time (ms)	680	720	-
	Velocity (m/s)	**2353**	**2569**	**-**
LO-1 (7th km of L23)	Thickness (m)	760	760	1520
	Interval two-way time (ms)	770	420	830
	Velocity (m/s)	**1974**	**3619**	**3663**
LO-1 (3.2nd km of PEV203)	Thickness (m)	760	760	1520
	Interval two-way time (ms)	820	520	680
	Velocity (m/s)	**1854**	**2923**	**4471**
KL-1 (12.5th km of L88)	Thickness (m)	915	1485	-
	Interval two-way time (ms)	800	1020	-
	Velocity (m/s)	**2288**	**2912**	**-**
Velocity – Mean value (m/s)		**2216**	**2785**	**3984**
Velocity Used (m/s)		**2200**	**2800**	**4000**

Table 2.5.1: Thicknesses, two-way travel times and velocities of onshore Thermaikos basin's formations (after Tsokas et al. 2013).

29

2.6   Formation Density Logging

Geophysical logging is called the constant recording of the variation of a physical rock parameter (density, electric resistivity, spontaneous potential etc.) along the length of a borehole and can be achieved with the descending of specific tools, called logging sondes, inside the well.

Bulk density of geologic formations can be estimated with the use of gamma ray density logging, which relies on gamma-gamma scattering. The Compensated Neutron Formation Density (FDC) log is, actually, a graph that shows density changes in accordance with depth. It was initially developed in the 1950s and was already in use by the hydrocarbon industry by the 1960s. It measures, via detectors, the gamma ray radiation that is scattered by the formations due to medium-energy gamma ray emission from a radioactive source of known intensity that is found inside the logging sonde. That scattering interaction is known as Compton scattering, according to which medium-energy gamma rays lose a part of their energy due to consecutive collisions with the formation electrons. The number of collisions depends on the electron density (the number of electrons in a volume unit). The source is, usually, Co^{60} or Cs^{137} (it sends out gamma rays of 0.66 MeV intensity). The density tool uses two (or more) detectors (the near and the far detector) of different penetrative ability, at progressively longer distances from the source. The distance between the detectors sets the vertical resolution of the instrument (a typical distance is approximately 10 inches). Detectors can be Geiger-Müller counters or scintillators.

The intensity of the secondary gamma radiation that is produced by the geologic formations is, approximately, inversely proportional with the electron density in the formation (Dobrin & Savit 1988). The electron density depends directly, but not perfectly, on the bulk (formation) density, so an estimation of the second can be achieved, by making certain corrections, which depend on the formation's characteristics (that are usually small, excluding some formations, like evaporites), the mudcake (created by the drilling fluid) effect and the sonde standoff. Bulk density can be estimated from an empirical equation that links together formation and electron density. The above logging can create dense measurements of density (every 20 cm or less). The depth of investigation of density logging decreases with increasing rock density and almost always measures the invaded zone. Bulk density is usually measured

at g/cm^3, while gamma radiation is given at API units. According to the Schlumberger Oilfield Glossary (https://www.glossary.oilfield.slb.com), American Petroleum Institute (API) units measure radioactivity, based on an artificially radioactive concrete block at the University of Houston, USA, that is defined to have a radioactivity of 200 API units, twice the radioactivity of a typical shale. The formation is the primary standard for calibrating gamma ray logs.

Clay	1.63 - 2.60		Slate	2.70 - 2.90
Silt	1.80 - 2.20		Phyllite	2.68 - 2.80
Soil	1.20 - 2.40		Schist	2.39 - 2.80
Sand	1.70 - 2.30		Gneiss	2.59 - 3.00
Sandstone	1.61 - 2.76		Granulite	2.52 - 2.73
Shale	1.77 - 3.30		Amphibolite	2.90 - 3.04
Limestone	1.93 - 2.90		Eclogite	3.20 - 3.54
Dolomite	2.28 - 2.90			
Chalk	1.52 - 2.60			
Halite	2.10 - 2.60			
Gypsum	2.20 - 2.60			

Table 2.6.1: Density values (in g/cm^3) for the most common sedimentary and metamorphic rocks (taken from: https://gpg.geosci.xyz/content/physical_properties/tables).

Density logging gives valuable information that can be used in the interpretation of gravity and seismic data and it is further used for the estimation of formation's porosity, which can be, also, calculated with sonic logging and neutron porosity logging. Density logging can be, further, used in combination with sonic logging for the calculation of the formation's mechanical characteristics.

Density logging tools can, also, rely on Photoelectric Absorption (PE), where the low-energy region of the scattered gamma ray spectrum is analyzed separately. Photoelectric Absorption is controlled by the atomic number (Z) of elements, which is strongly correlated with formation's lithology and rock type. Photoelectric Absorption Index, which is the measure of PE of a geologic formation and depends on the rock type, porosity and the fluid type that fills the rock voids, is estimated with the aid of Litho-Density Tool (LDT). LDT contains a radioactive source of monochromatic gamma radiation of 662 keV and two detectors that measure gamma rays of 0-662 keV energy.

The sound waves loggings (CVL, Continuous Velocity Logs) can give an estimation of the sound (seismic) waves' speed movement at the formations' interior. This speed is connected with the formation density. The relation of that speed with density is presented by using curves. This logging results in accurate speed measurement, but its values are approximate.

Besides well logging, there are three more geophysical methods for estimating rock density: Nettleton method, Parasnis method and realization of underground measurement of the gravity field intensity in two different depths by using specially designed gravimeters (Dobrin & Savit 1988).

Nettleton (1939) described a method where gravity profiles for various given values of underground formations' density are calculated and the one that makes the profile less correlated with the topographic section is selected. Parasnis (1952) proposed a similar method for calculating rock density, though on this method no topographic events related with erosion were needed, in contrast with Nettleton's method.

Concerning well logging on Thermaikos basin, important work has been made by providing data for the underground geological regime of the area. Especially for density measurement, in Alexandria 1 well, the Public Petroleum Corporation conducted Compensated Neutron Formation Density Logging, measuring bulk density, porosity (measured in the % of matrix) and gamma ray absorption of the formations, while DEP-EKY made the same measurements in Loudias 1 well.

NAME:	ALEXANDRIA 1 22 26 09 N 40 41
LOCATION:	29 E
DATE:	5 DEC 1980
DEPTH:	1706m

1	SONIC LOG	0-1706m	SINGLE TIME(sec)		INTERVAL VELOCITY (m/sec)	
2	SIMULTANEOUS COMPENSATED NEUTRON FORMATION DENSITY	300-1706m	CALIPER (hole diameter in inches)	GAMMA RAY (api units)	NEUTRON POROSITY % (LS matrix)	BULK DENSITY (g/cm3)
3	SIMULTANEOUS INDUCTION RESISTIVITY SONIC (ISF -SONIC)	0-1706m	SPONTANEOUS POTENTIAL (millivolts)	GAMMA RAY (api units)	RESISTIVITY (ohm m)	INTERVAL TRANSIT TIME Δt (μsec/ft)
4	FOUR-ARM-HIGH RESOLUTION CONTINUOUS DIPMETER	300-1706m	ORIENTATION (Azimuth, Relative Bearing, Deviation)		CORRELATION CURVES	

Table 2.6.2: Logging in Alexandria 1 well (after Tsokas et al. 2013).

NAME: **LOUDIAS 1**
LOCATION: 22 34 48.4 N   40 04 53.5 E
DATE: 20 OCT 1980
DEPTH: 3086m

1	SIMULTANEOUS COMPENSATED NEUTRON FORMATION DENSITY	230-1520m	CALIPER (hole diameter in inches)	GAMMA RAY (api units)	NEUTRON POROSITY % (LS matrix)	BULK DENSITY (g/cm3)
2	SIMULTANEOUS COMPENSATED NEUTRON FORMATION DENSITY	1500-2165m	CALIPER (hole diameter in inches)	GAMMA RAY (api units)	NEUTRON POROSITY % (LS matrix)	BULK DENSITY (g/cm3)
3	SIMULTANEOUS INDUCTION RESISTIVITY SONIC (ISF -SONIC)	0-300m	SPONTANEOUS POTENTIAL (millivolts)	GAMMA RAY (api units)	RESISTIVITY (ohm m)	INTERVAL TRANSIT TIME Δt (μsec/ft)
4	SIMULTANEOUS INDUCTION RESISTIVITY SONIC (ISF -SONIC)	240-1520m	SPONTANEOUS POTENTIAL (millivolts)	GAMMA RAY (api units)	RESISTIVITY (ohm m)	INTERVAL TRANSIT TIME Δt (μsec/ft)
5	SIMULTANEOUS INDUCTION RESISTIVITY SONIC (ISF -SONIC)	1520-2165m	SPONTANEOUS POTENTIAL (millivolts)	GAMMA RAY (api units)	RESISTIVITY (ohm m)	INTERVAL TRANSIT TIME Δt (μsec/ft)
6	SIMULTANEOUS INDUCTION RESISTIVITY SONIC (ISF -SONIC)	1520-2200m	SPONTANEOUS POTENTIAL (millivolts)	GAMMA RAY (api units)	RESISTIVITY (ohm m)	INTERVAL TRANSIT TIME Δt (μsec/ft)
7	FOUR-ARM-HIGH RESOLUTION CONTINUOUS DIPMETER	1500-2200m	ORIENTATION (Azimuth, Ralative Bearing, Deviation)		CORRELATION CURVES	
8	GEOLOGICAL MUD LOG	320-2200M	DRILLING RATE (min/m)	ppm HYDROCARBONS IN MUB	LITHOLOGICAL DESCRIPTION (samples every 8m)	

Table 2.6.3: Logging in Loudias 1 well (after Tsokas et al. 2013).

The following Table contains geologic formations' densities in Alexandria 1 and Loudias 1 wells, according to well logging.

Alexandria 1			Loudias 1		
Depth (m)		Density	Depth (m)		Density
from	to	(g/cm³)	from	to	(g/cm³)
300	875	2.15	0	350	2.00
875	960	2.25	350	1360	2.10
960	1150	2.45	1360	1500	2.20
1150	1320	2.20			
1320	1700	2.45			

Table 2.6.4: Formation Density in Alexandria 1 and Loudias 1 wells (after Vafidis 2018, personal communication).

In Yannitsa 1 and Klidi 1 wells, the W. H. Hunt company measured Spontaneous Potential (in milliVolts), electric resistivity (in Ohm·m), gamma ray and neutron absorption (in API units). W. H. Hunt, also, measured Spontaneous Potential, resistivity and interval transit time (in microseconds per foot, measured through Sonic Logging)
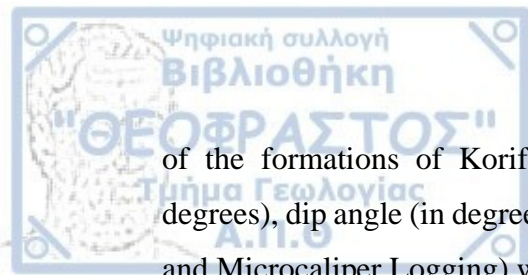
of the formations of Korifi 1 well. Measurements of temperature (in Fahrenheit degrees), dip angle (in degrees) and hole diameter (in inches, measured through Caliper and Microcaliper Logging) were made, as the usual technique recommends.

The available logs for the present Thesis include Yannitsa 1, Klidi 1 and Korifi 1 logs, along with Simultaneous Compensated Neutron Formation Density Logs of Alexandria 1 and Loudias 1 boreholes, in Tagged Image File Format (TIFF) and Portable Document Format (PDF), correspondingly.

34

CHAPTER 3

GRAVITY AND MAGNETIC DATA PROCESSING

A potential field is an area where forces act at every point. It can be defined as every naturally-occurring field that satisfies Laplace's Differential Equation: $\nabla^2\varphi = 0$. The physical meaning of that equation is that there are not extreme values at the area of a potential field, provided that there are no sources or locations where the field is discontinuous (called sinkholes) at this area. If such locations exist, the Laplace's Equation is transformed into Poisson's Equation: $\nabla^2\varphi = f$.

Potential fields are vector fields. Gravity, magnetic and static electric field are examples of such fields.

Historically, potential field methods were used in combination with seismic methods in order to construct an integrated earth model within dependent geophysical information. Furthermore, aeromagnetic surveys are considered as a primary tool for providing full coverage over large geographical areas.

3.1   Measurement of Potential Fields

Generally, there are two ways for measuring gravity field: the measurement of the absolute gravity value and the measurement of the relative gravity value (Tsokas 1999). The absolute gravity value is measured at laboratories and reference stations, using pendulums and dropping weights. The set of the reference stations creates the International Gravity Standardization Network (IGSN), in which the relative gravity values taken on field are interfered. Relative gravity value is the one used more often during field measurements. It is, practically, the gravity variation among the measurement points. Gravity measurements are made in units of force (e.g. Newton), but it is more common to measure gravity in units of acceleration or field intensity (Gal – named after the Italian physicist, astronomer and engineer Galileo Galilei – and its

35

subdivisions: milliGal – mGal – 10^{-3} Gal and microGal – μGal – 10^{-6} Gal). It should be noted here that: 1 Gal = 1 cm/s^2.

Gravity is measured with instruments called gravimeters. Until the 20th century, gravity acceleration measurements were realized using torsion balances (Cavendish and Eötvos balances) and old-type pendulums. After World War I, the progress of geophysical research led to the development of more practical methods for calculating relative gravity with appropriate instruments. Modern gravimeters were developed in 1936 by Lucien LaCoste and Arnold Romberg. Traditionally, the more commonly used gravimeters contain springs that follow Hooke's Law, which are used to counteract the force of gravity pulling on an object. The change in length of the spring may be calibrated to the force required to balance the gravitational pull. The majority of modern gravimeters, though, uses specially-designed metal or quartz "zero-length springs". Zero-length springs do not follow Hooke's Law, as there is an initial force that holds the spring's spirals in contact. The spring's length change is proportionate to the gravity field strength. Another important parameter of every gravimeter is its spring sensitivity. These instruments can detect vibrations and gravity changes caused from human activities. Depending on the interests of every survey, that can be counteracted by integral vibration isolation and signal processing.

Gravimeters can be separated into two main categories: stable and unstable (or astatic) type. This separation comes from the fact that in almost every gravimeter there is a mobile system, usually a phalanx, that is in stable or unstable balance. Askania, Boliden, Hartley, Gulf, Nörgaard and Scintrex CG are examples of stable gravimeters, while LaCoste-Romberg, Thyssen, Worden and Sodin consist the most common unstable gravimeters. Especially, LaCoste-Romberg gravimeter (Figure 3.1.1) is used in the majority of field surveys and ground stations, as it provides an accuracy of 0.01 mGal. LaCoste-Romberg gravimeter contains a zero-length spring.

Gravimeters are used in petroleum and mineral exploration, seismology, geodesy, metrology and geophysical surveys.

Figure 3.1.1: A LaCoste-Romberg gravimeter (taken from: http://docplayer.net/47902417-Lacoste-romberg-instruction-manual-model-g-gravity-meter-g-a-summary-of-clausthal-de-java-grav-gdmanual.html).

During first geophysical surveys, the instruments that were used for the magnetic field record were the magnetic variometers, such as Schmidt magnetometer and torsion magnetometer, which are no longer used as they have been replaced by modern instruments. Today magnetometers can be divided into two main categories: the total field (or scalar) magnetometers that calculate only the total strength of the magnetic field and the vector magnetometers that can calculate the vector components of the magnetic field on specific directions. Magnetometers that are used nowadays are: fluxgate magnetometers, proton magnetometers, optical magnetometers, Superconducting Quantum Interference Devices or SQUIDs and magnetic gradiometers (they can be separated at axial and planar gradiometers, according to the placement of the magnetometers they carry). Magnetometers can, also, be steady, portable (or mobile), laboratory and survey, according to their use.

3.2   Bouguer Anomaly

Bouguer anomaly is a gravity anomaly, where corrections concerning topographic effect and measurements' elevation have been made. When the only correction made is that for the elevation effect, the free-air gravity anomaly results. Bouguer anomaly was

named after Pierre Bouguer (1698-1758), a French mathematician, geophysicist, geodesist and astronomer (Figure 3.2.1), who proved that gravitational attraction decreases with elevation.


Figure 3.2.1: Portrait of Pierre Bouguer (taken from: https://en.wikipedia.org/wiki/Pierre_Bouguer).

Bouguer anomaly is related to the observed gravity value at a field with the following equation:

$$\Delta g_B = g_{obs} - (g + g_{fa} + g_b - g_T + g_i)$$

where g_{obs} is the observed gravity value at the point of measurement, g is the latitude correction, g_{fa} is the free-air correction (that compensates for heights above sea level, assuming there is only air between the measurement station and the sea level), g_b is the Bouguer correction (the correction for the gravity attraction at the reference station due to Earth's rocks and sediments density), g_T is the topographic correction and g_i is the isostatic correction (that depends on the survey's extent and can be dispensed). Consequently, Bouguer anomaly (Δg_B) is the remaining value of gravitational attraction.

A Bouguer map shows horizontal differences in the gravity acceleration. As a result, only horizontal changes in density produce anomalies and purely vertical changes in density produce the same effect everywhere and result in no anomalies.

38
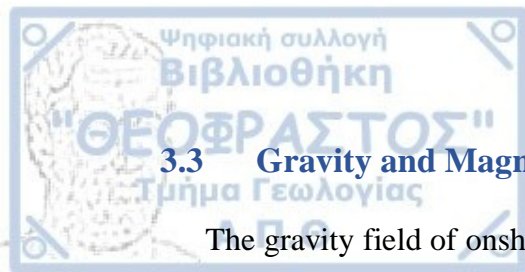
3.3 Gravity and Magnetic Fields of Thermaikos Basin

The gravity field of onshore Thermaikos basin is depicted at Figure 3.3.1, with the form of Bouguer anomaly. By studying that image, two areas with high values of Bouguer anomaly can be distinguished at the northern and southern parts of the basin. Also, high values of the anomaly are found at the easternmost part, where the city of Thessaloniki lies. On the contrary, small Bouguer anomaly is found at the areas where the ophiolitic basement of the basin reaches the surface, creating hills that surround the basin at the westernmost part. Finally, the center of the basin is characterized mostly by lower values of the anomaly, due to the large thickness of the underground sediments.

At this point, it should be mentioned that since the distance between the gravity measurements is relatively large (approximately 4 km), the resulting maps of the gravity field do not show great detail concerning the anomalies' variations.

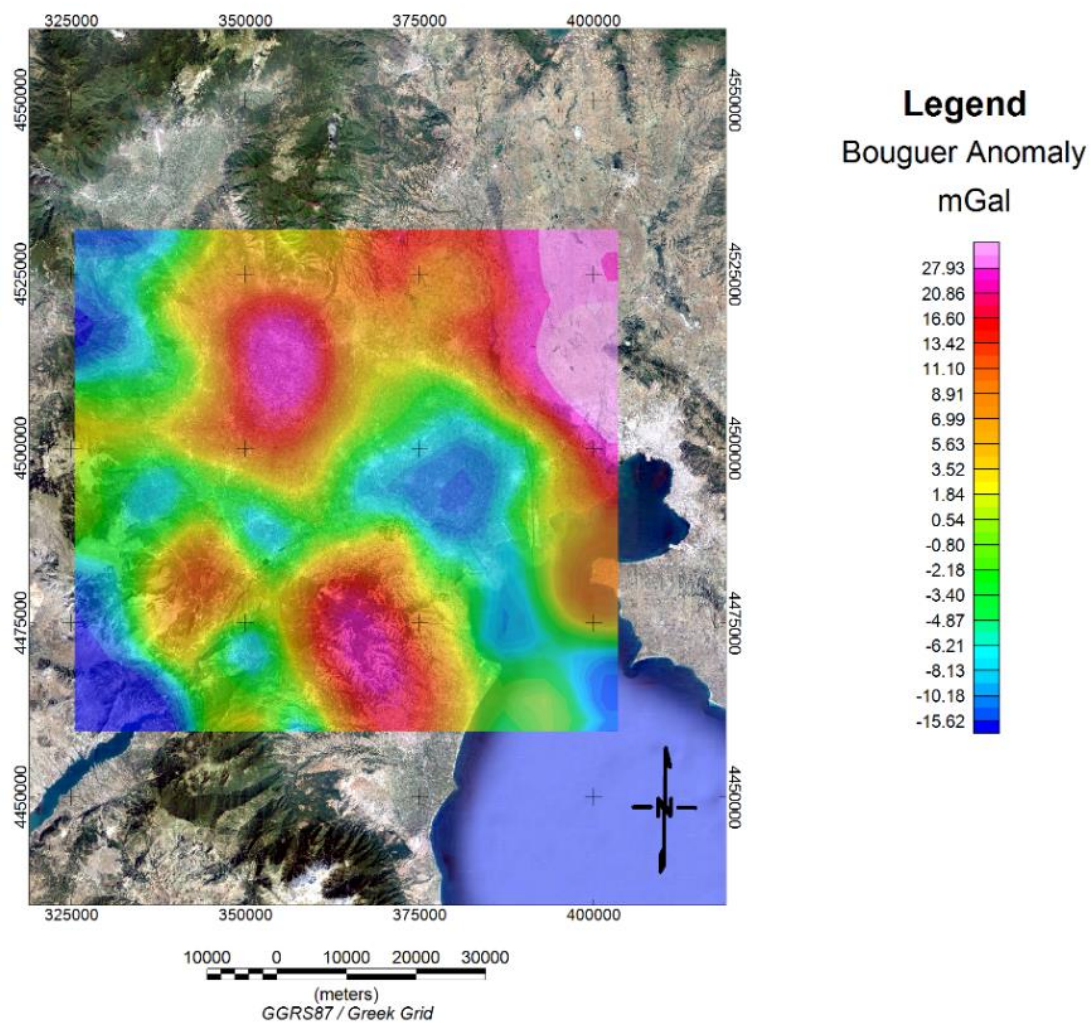**Gravity Field**

Onshore Thermaikos Basin

Figure 3.3.1: Bouguer anomaly of onshore Thermaikos basin.

In regions where sedimentary basins are found, like the onshore Thermaikos basin area, magnetic contours are normally smooth and variations are small, reflecting the basement's depth rather than near-surface structures. The larger anomalies are caused by magnetic susceptibility variations rather than the basement's relief. Consequently, anomaly magnitude is not of much value in finding basement's depth and depth calculations are usually based upon anomaly shape measurements, especially sharpness. Regions where igneous or metamorphic rocks predominate usually exhibit complex magnetic variations. Deep features are often camouflaged by higher frequency magnetic effects originating nearer the surface.

On Figure 3.3.2, the magnetic field of the study area is depicted. Large magnetic anomalies can be observed at the western and southern boundaries of the basin, where ophiolites reach the surface. The central part of the basin appears, mostly, with lower anomaly values, especially at its northern part, with some local exceptions at the areas of Pella and Anatoliko (see Figure 1.1.1 on Chapter 1), where the anomaly' values are higher. Onshore Thermaikos basin is generally prevailed with low magnetization values, a typical situation for a sedimentary basin, because of the large sediments' thickness.
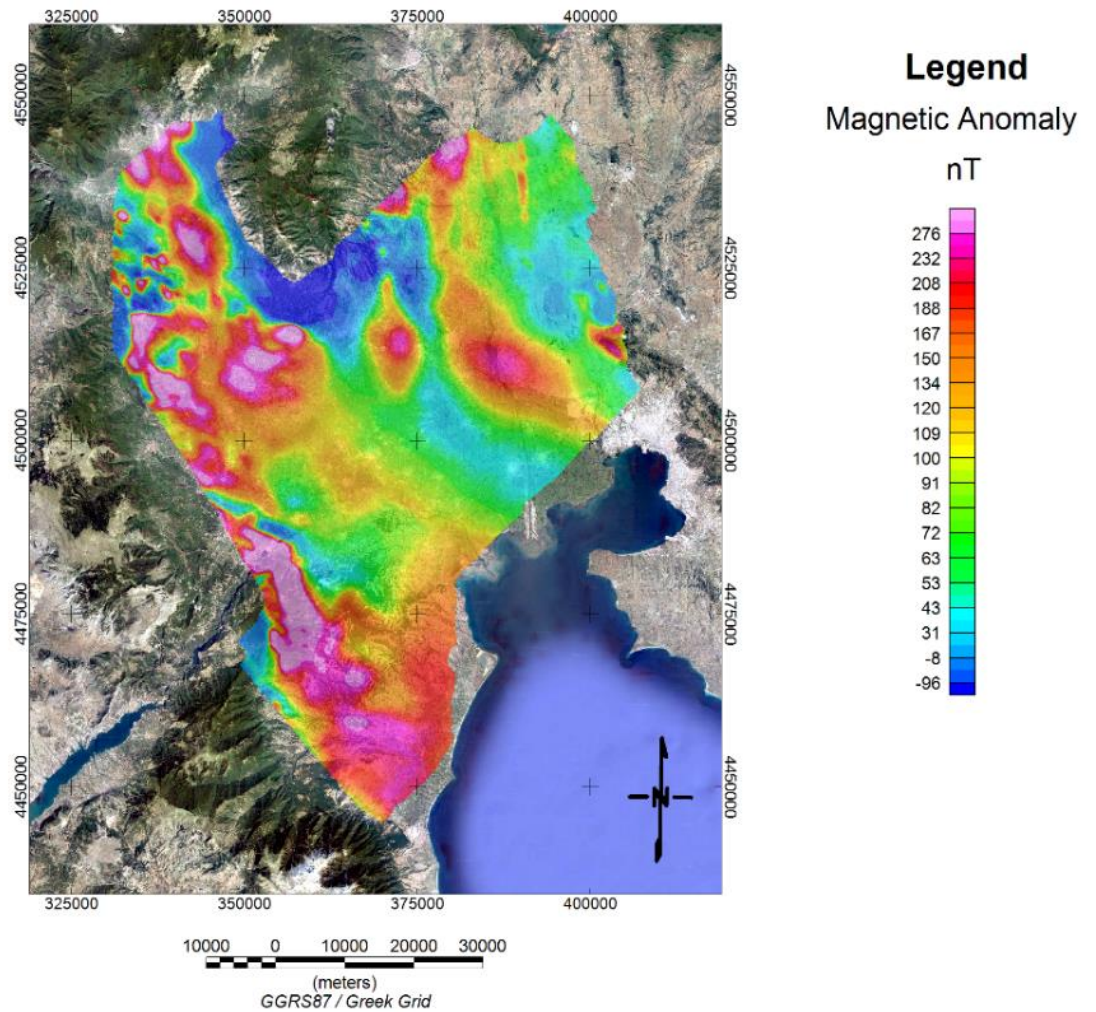
Figure 3.3.2: Magnetic field of onshore Thermaikos basin.

3.4 Transformations of Potential Fields

The ultimate goal of every geophysical survey is the detection of the underground target (the source of the anomaly) and, consequently, to draw conclusions regarding its shape, burial depth and composition (the source's characteristics). The target's detection is realized at the moment where its disturbance on gravity, magnetic or both fields or on other geophysical records that have been conducted in the area will be noticed; a disturbance that disrupts the upper Earth's crust layers' homogeneity. However, the finding of the target's (the source of the disturbances) properties constitutes the final survey stage. This stage is, traditionally, called as interpretation.

There is a number of methods that show different source characteristics and aid interpretation importantly. They all rely on the geophysical measurement transformation into a new form, that's why they are named as "transformations of potential fields".

Most of these transformations are applied after the geophysical data have been displayed as spatial wavenumber functions. The mean for this display is the Fourier Transformation. Fourier Transformation properties are the ones that facilitate transformation operations. That is the reason why the growth of this particular domain was rapid after the introduction of Fast Fourier Transform (FFT) and the computer development in the early 1980's. Transformation that are made using Fourier analysis can, also, be realized with different manners; the use of FFT, though, can facilitate the whole process significantly.

3.5 Field Continuation

If the field over a surface is completely known, the field over any other arbitrary surface can be determined, due to the fact that potential fields obey Laplace's Equation. No other mass must be present between these two fields, though. This process is called continuation. The term "field continuation" describes the calculation of the potential field in a different level than the one that the measurements were made. The measurements' surface can be flat or floating.

Upward Continuation

According to Henderson and Zietz (1949), the potential field strength value at a point that is found at a level $z_0 - \Delta z$ above the measurement level z_0, since the measurement surface is flat, is given by the equation below:

$$U(x, y, z_0 - \Delta z) = \frac{\Delta z}{2\pi} \int_{-\infty}^{\infty} \int_{-\infty}^{\infty} \frac{U(z', y', z_0)}{[(x - x')^2 + (y - y')^2 + \Delta z^2]^{3/2}} dx' dy'$$

where x', y' are the coordinates of points at the level of measurement. This relation is, also, known as the integral of upward continuation. It permits the calculation of the gravitational acceleration anywhere in free space from a knowledge of its values over the surface.

The transformed field at the new highest level is attenuated in comparison with the field at the initial level. Upward field continuation acts as a low-pass filter for wavenumbers. Low wavenumber (or long wavelength) anomalies that remain after transformation have the same form as the anomalies of the initial level, but they are presented effectively smoothed, since short wavelength anomalies would have been reduced or eliminated.

Upward continuation is of no important use in gravity analysis, but in aeromagnetic interpretation allows the comparison of measurements made at different flight elevations. It is, also, used to suppress anomalies of small-scale features near the surface, in cases where the depth of interest is found deeper underground. Lastly, upward continuation reduces topographic effects in ground magnetic surveys.

Downward Continuation

Downward continuation transformation, first described by Peters (1949), lies on the fact that if the calculation of the gravity or magnetic field over a surface closer to an anomaly source is made, then the anomaly should be sharper and less confused by the effects of deeper features. At this method the gravity values and derivatives of a shallower surface are used in order to calculate gravity value at depth. Since derivatives involve differences, the above calculation enhances uncertainties in the newly downward-continued field, though.

Downward continuation transformation strengthens high wavenumbers and emphasizes high frequencies. Consequently, data errors from measurements or from previous processing are, also, strengthened. Moreover, minor noise is increased in the measured field, a fact that may outweigh the benefit of the sharper anomalies. This method is used to detect the target's limits, but should be used with precaution, as well as it must not exceeds the target's burial depth. Moreover, it is not suitable at areas of complex shallow magnetized structures, a characteristic of regions with mineral exploration. Although this method is not used widely for that purpose, downward continuation can aid at the estimation of the sediments' thickness in hydrocarbon surveys.

3.6   Residual and Regional Fields

Apart of the anomalies that are of interest, Bouguer map, also, includes anomalies caused by deeper or shallower sources. Such anomalies usually overlay the ones that interest the survey, while the map shows the final picture. However, in order to study the geologic plays of interest and reach to conclusions, their anomalies have to be depicted in clean form.

The effects of shallow masses are usually of short wavelength and they can be largely removed by smoothing short-wavelength anomalies. They are called as near-surface noise. The effects of deep anomalies constitute the regional field (or, simply, regional). The field after the removal of near-surface noise and regional field is called residual field (or residual) and consists of the anomalies that are caused by the structures of interest. At the Bouguer map, the regional, the residual and the near-surface noise coexist and they are represented at every calculated Bouguer anomaly value at measurements' stations.

The field source's anomaly tends to reduce its amplitude as the distance between the measurements' points and the source increases. Simultaneously, a larger area is affected by the results of the anomaly, i.e. the anomaly wavelength increases. Therefore, the anomalies smoothness is the main criterion for their distinction as regional or residual.

The depth range we wish to emphasize depends on the objectives of the interpretation. Shallow anomalies are of interest in mineral exploration, but are usually regarded as undesirable noise in hydrocarbon exploration. The most useful factor in interpretation is the knowledge of the local geology.

The major problem in interpretation is separating anomalies of interest from the overlapping effects of other features. Residualizing attempts to remove the regional field from measurements in order to emphasize the residual field. There is a number of methods in order to succeed it and they can be divided into categories, which include: surface-fitting, graphical, empirical gridding, second vertical derivative and wavelength filtering (by using Fourier Transform) residualizing methods. However, both residual and regional are distorted by the effects of each other.

In order to remove the regional field from Thermaikos basin data the polynomial surface-fitting method was applied. According to this method, the regional field is approximated by a polynomial fitted to the observed field, which is strongly influenced by the residual field (Beltrão et al. 1991). The residual field originates after the subtraction of the regional from the observed field.

By studying the residual gravity field of onshore Thermaikos basin (Figure 3.6.1), large Bouguer anomaly can be observed at two areas, at the northwestern and southern parts of the basin, in similar way as in the total gravity map in Figure 3.3.1. At the same time, the central part of the basin is characterized by low values of the anomaly.
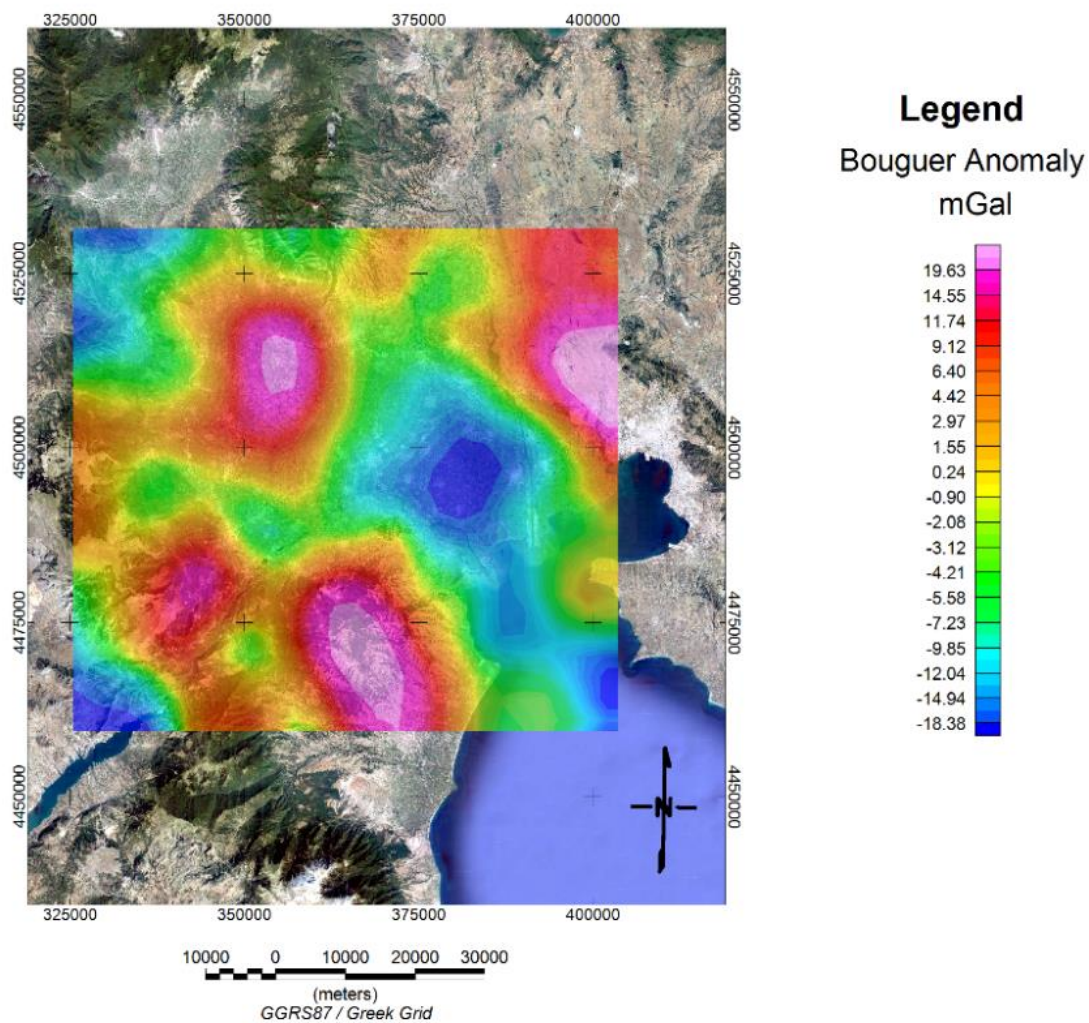
Residual Gravity Field

Onshore Thermaikos Basin

Figure 3.6.1: Residual gravity field of onshore Thermaikos basin.

The residual magnetic field (Figure 3.6.2) demonstrates high values across the western basin's boundary, while lower values are found on the central part, with an exception on the central-eastern part where high values are present. The lowest values of the magnetic anomaly are located at the northern part of the basin.
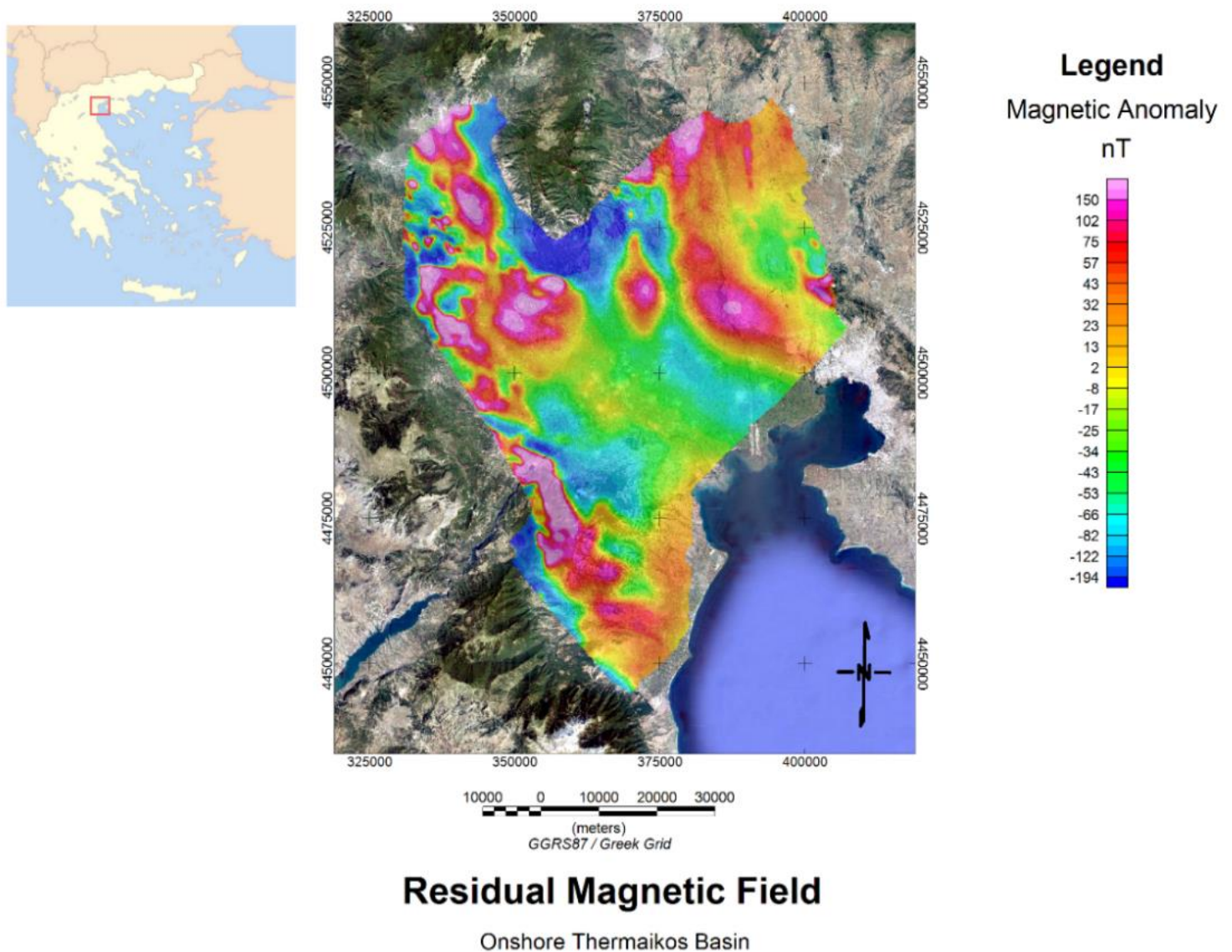

Residual Magnetic Field

Onshore Thermaikos Basin

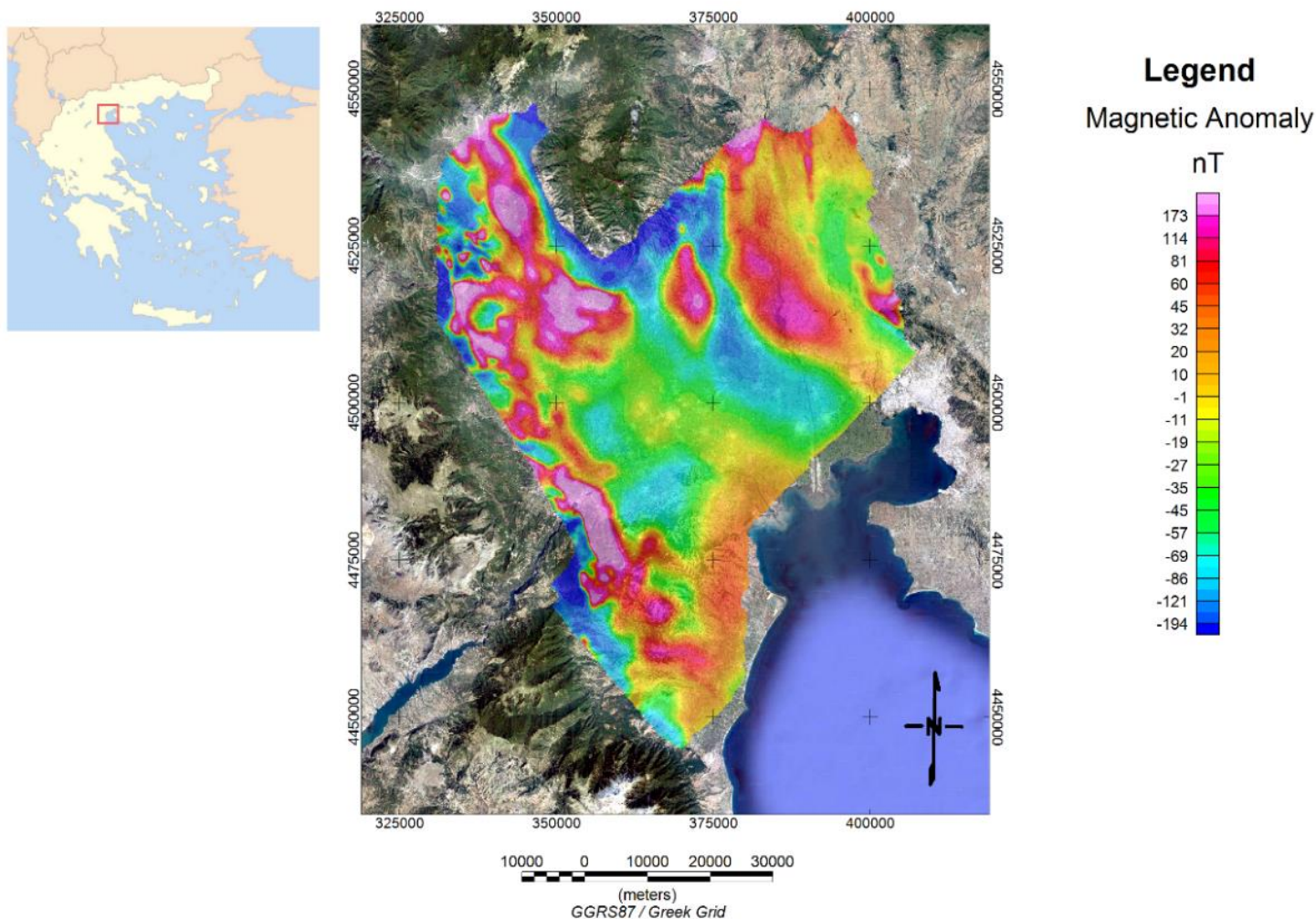Figure 3.6.2: Residual magnetic field of onshore Thermaikos basin.

3.7   Reduction to the North Magnetic Pole

The Earth's total magnetic field anomalies caused by underground structures and bodies, that can be simulated as simple geometric shapes, are depicted as lobes, the polarity of which depends on whether the contrast in magnetization between the structure and its surrounding formations is positive or negative. They, also, depend on the magnitude distribution and direction, as well as the Earth's normal magnetic field direction at the area where the measurements are made. As a consequence, the magnetic anomaly shape of the same structure will be different when the measurements take place at different areas on Earth, e.g. the Geomagnetic Equator, the North Magnetic Pole, an average geomagnetic latitude.

Anomaly complexity is minimum at the North Magnetic Pole, since the anomaly presents one peak at the vertical that passes through the structure's center. At average latitudes the anomaly presents two lobes, one positive and one negative.

The Reduction to the North Magnetic Pole is applied at the magnetic measurements in order to simplify total-field maps and their interpretation. This operation changes the actual inclination to the vertical direction and it is made easier at high latitude areas. As the measurements are made at latitudes near the Magnetic Equator, the process becomes more difficult.

The reduced-to-Pole magnetic field of the study area (Figure 3.7.1) is very similar to the residual magnetic field, with high anomaly values at the western part and lower values at the central part of the basin. At that point, it should be mentioned that the onshore Thermaikos basin is found at a latitude of approximately 40º38' N.

49

Reduced-to-Pole Magnetic Field

Onshore Thermaikos Basin

Figure 3.7.1: Reduced-to-Pole magnetic field of onshore Thermaikos basin.
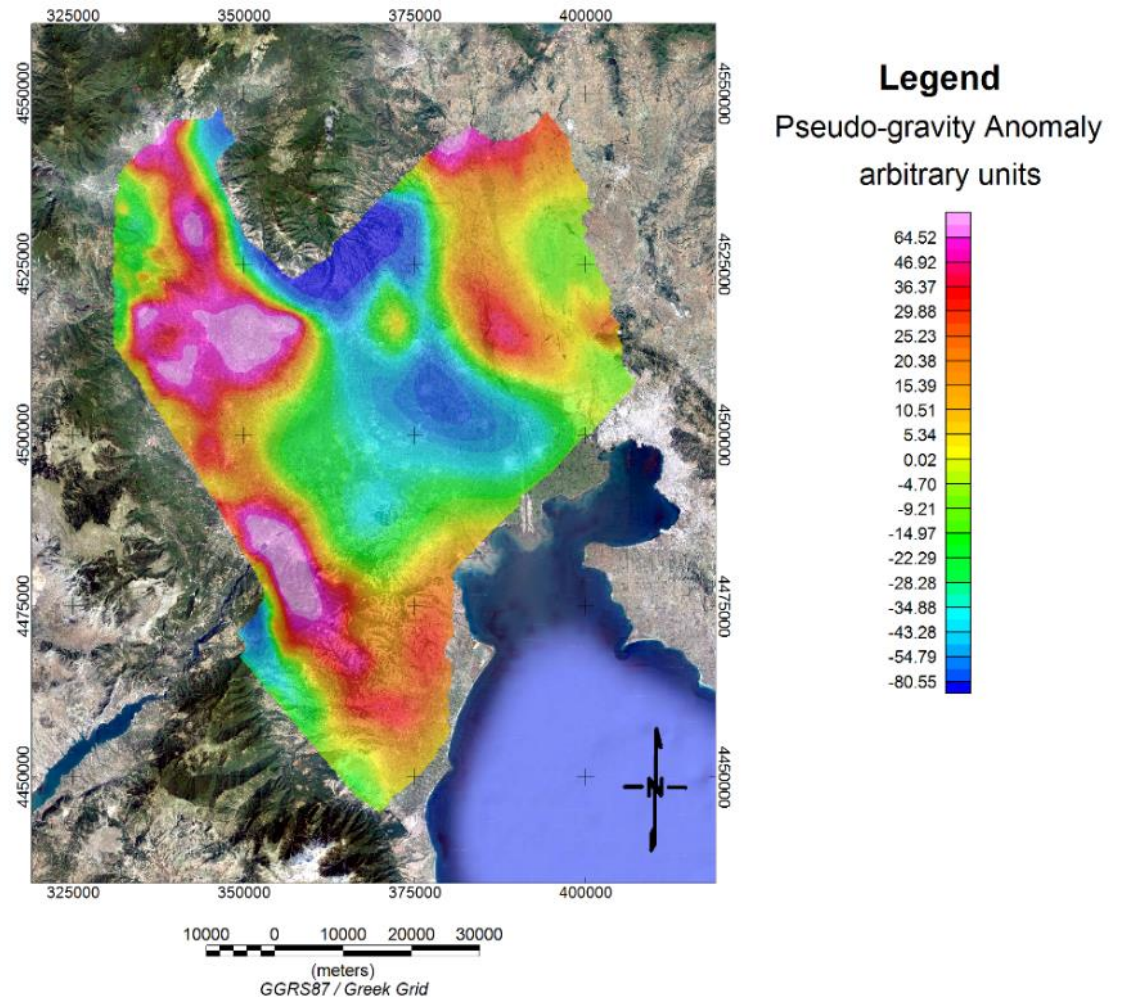
3.8 Pseudo-gravity Transformation

Poisson's Equation associates magnetic potential, V(P), with the gravity field strength on the direction of magnetization, g_m, since the source of both fields has uniform magnetization and density. This equation is the following:

$$V(P) = -\frac{C_m M}{G\rho} g_m$$

where M is the value of the uniform magnetization, ρ is the uniform density and G is the gravitational constant (approximately equal to 6.674×10^{-11} $m^3 \cdot kg^{-1} \cdot s^{-2}$). C_m is a constant of the CGS (Centimetre – Gram – Second) system of units, equal to $\mu_0/4\pi$ (or 10^{-7}) henry/m in SI (Système International, in French) system of units (μ_0 is called vacuum permeability or magnetic constant). Baranov (1957) used the above equation aiming to transform the magnetic anomalies into a form where a large percentage of asymmetry due to magnetic inclusion will have been canceled. This transformation was named by the same researcher as "pseudo-gravity transformation" and its result as "pseudo-gravity". It's called so because the magnetic field is being treated in analogy to a gravity field, so pseudo-gravity is another manner to represent magnetic data.

Pseudo-gravity transformation converts the bipolar magnetic field into unipolar form. The resulting anomalies can be compared with the Bouguer anomalies that are caused by the same structures, as the two anomalies resemble each other. Quantitative conclusions concerning structure's size and shape can be obtained by the transformation result, as the edges of anomalies are well defined.

In Figure 3.8.1, the pseudo-gravity field of onshore Thermaikos basin is presented. The anomalies' boundaries are clear in the western part of the basin, where the ophiolitic basement is closer to the surface. At the northern and central parts of the basin, pseudo-gravity anomaly is smaller due to the large sediments' thickness.
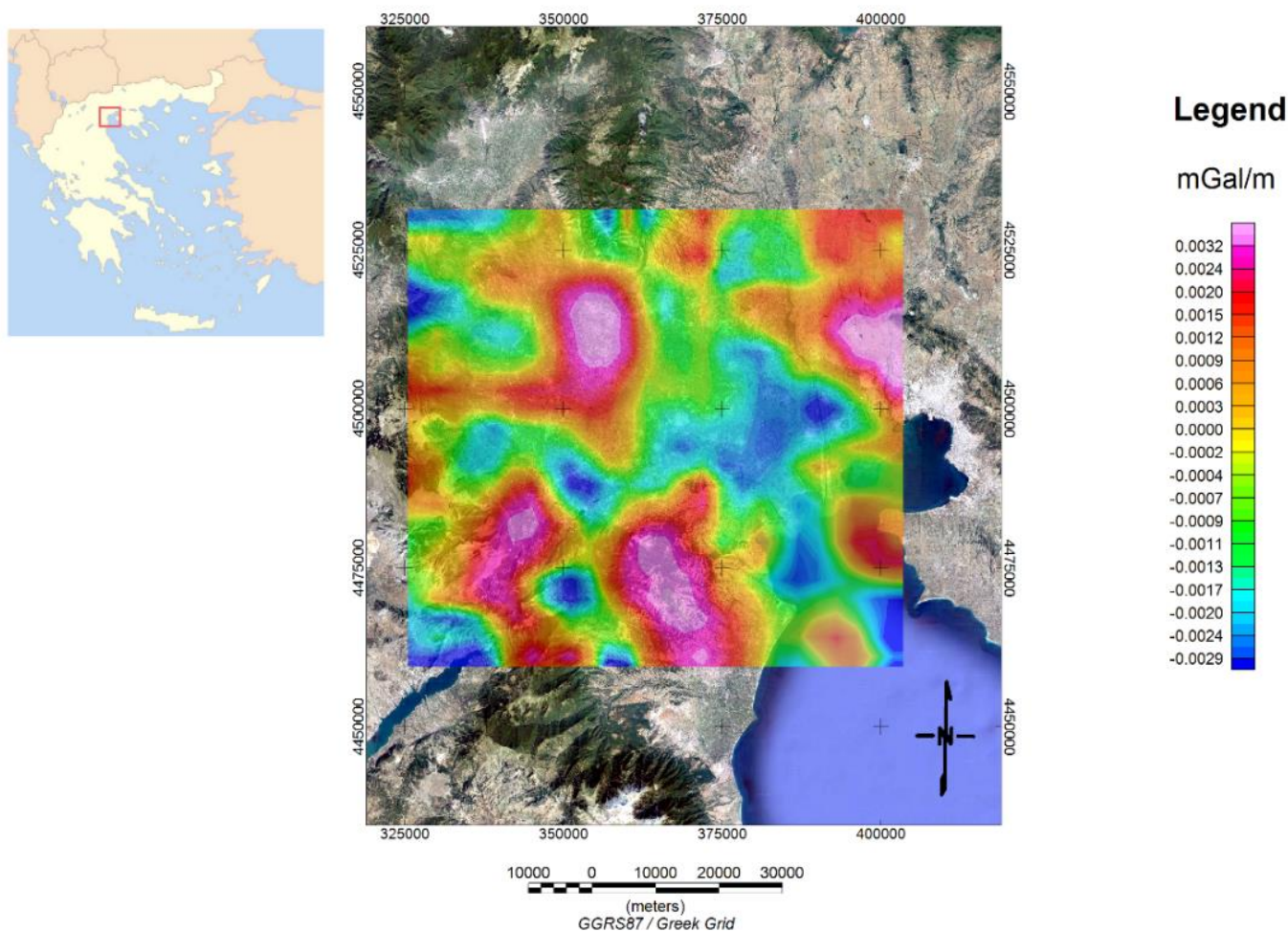
Figure 3.8.1: Pseudo-gravity field of onshore Thermaikos basin.

3.9 Derivatives

The use of derivatives lies in the sharpening of edges of anomalies and the enhancement of the signal of shallow formations and bodies. The calculation of the first and the second derivative is often, which comes with the construction of the corresponding maps. The first derivative can be, also, calculated by the gradiometers.

The second derivative analysis creates curvatures that indicate the presence of shallow anomalies caused by small-scale features near the surface. This is particularly useful in mineral prospecting. Since hydrocarbon traps are, usually, found on large depths, the second derivative calculation was not useful for this Thesis's purposes. The second vertical derivative can be obtained from the horizontal derivatives, though.

The 1st vertical derivative map of the magnetic field of the study area (Figure 3.9.2) depicts the anomalies' edges clearer than the pseudo-gravity map, since the locations of the anomalies' sources (basement rocks) are demonstrated in detail. In similar manner, gravity anomalies' locations (Figure 3.9.1) are clearly visible and they are separated from the rest of the gravity field.

1st Vertical Derivative of the Gravity Field

Onshore Thermaikos Basin

Figure 3.9.1: 1st vertical derivative of the residual gravity field of onshore Thermaikos basin.
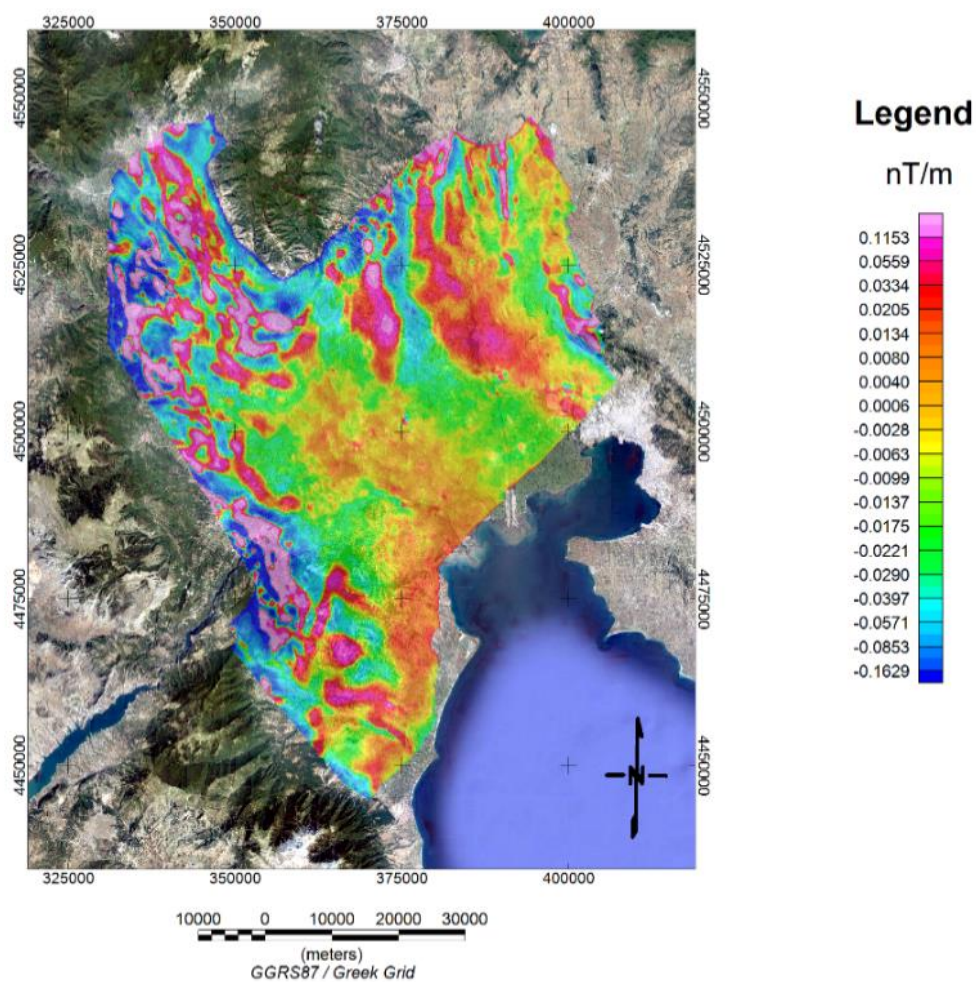
1st Vertical Derivative of the Magnetic Field

Onshore Thermaikos Basin

Figure 3.9.2: 1st vertical derivative of the reduced-to-Pole magnetic field of onshore Thermaikos basin.

3.10 Horizontal Gradient

The horizontal gradient of a potential field is defined as the absolute value of the resultant of the horizontal derivatives. It is used to successfully image the subsurface structure of an area, as it can locate the formation boundaries due to density or magnetization contrast from gravity and magnetic data, correspondingly. The maximum values of the horizontal gradient (Horizontal Gradient Maxima) appear at points where the boundaries of the formation causing the potential field display at the earth's surface, under specific conditions. These boundaries have to be vertical, whereas the potential field must be that of the Bouguer anomaly or the pseudo-gravity transformation of the magnetic field.

The greatest advantage of the horizontal gradient method is that it is least susceptible to noise in the data; it requires only the calculation of the two first-order horizontal derivatives of the field and the horizontal gradient filter. The amplitude of the horizontal gradient, as described by Cordell and Grauch (1985), is expressed as the following equations:

$$HG(x,y) = \left[\left(\frac{\partial g}{\partial x} \right)^2 + \left(\frac{\partial g}{\partial y} \right)^2 \right]^{\frac{1}{2}}$$

$$HG(x,y) = \left[\left(\frac{\partial H}{\partial x} \right)^2 + \left(\frac{\partial H}{\partial y} \right)^2 \right]^{\frac{1}{2}}$$

where $(\partial g/\partial x)$ and $(\partial g/\partial y)$ are the horizontal derivatives of the gravity field in the x and y directions, while $(\partial H/\partial x)$ and $(\partial H/\partial y)$ are the horizontal derivatives of the magnetic field in the x and y directions, respectively.

The importance of the horizontal gradient maps in the interpretation of magnetic and gravity data is great, since the horizontal location of the anomalies' source and its depth can be identified easily. It is commonly used in addition to the Analytic Signal method.

56

3.11 Terracing Transformation

Terracing is applied for the study of the spatial distribution of a natural quantity (density or magnetization) which provokes an anomalous field. It consists an inversion method, as it calculates specific source's parameters. Terracing was proposed by Cordell and McCafferty (1989) and it is depended on the sign of the local field curvature (2nd derivative).

Field curvature in a central point i along a route on an x axis, is given by the following equation:

$$C_i = \frac{\Delta g_{i+1} + \Delta g_{i-1} - 2\Delta g_i}{2\Delta x}$$

where Δx is the sampling step and Δg_i, Δg_{i+1}, Δg_{i-1} are the Bouguer anomaly values at three successive points of the route, considering that a parabola is adjusted at these three points. Subsequently, the sign of the C_i quantity is checked. The new value for the Bouguer or magnetic anomaly of the central point is the smallest (whether the sign is positive) or the largest (whether the sign is negative) value of the three values. If curvature equals to 0, the anomaly value is not changed.

The transformation result is the field segregation into terraces, each of which depicts an area where the natural quantity remains constant (as long as the geological formations are characterized by constant values of the natural quantity which causes the anomalous field).

Terracing transformation is, usually, applied in magnetic data that have been previously transformed into pseudo-gravity data and it gives an estimation of the magnetic susceptibility's spatial distribution, but it can be, also, applied in reduced-to-Pole magnetic data.

Figure 3.11.1 corresponds to the terracing field that was created from the residual gravity field map. In this map, four terraces of high anomaly values are present, one at the southern (Aiginio region, see Figure 1.1.1), the second at southern-western (Veria region, see Figure 1.1.1), another at the northern-central (Skidra – Galatades region, see Figure 1.1.1) and the fourth at the easternmost (Thessaloniki region, see Figure 1.1.1) parts of onshore Thermaikos basin. Moreover, there is one terrace of low anomaly value, at the central part of the basin, in Chalastra – Katerini region. At that region,

lower values exist due to large sediments' thickness. Due to the large distance between gravity measurements that have been conducted at the area, the maximum values of the horizontal gradient do not give a clear picture on where to find an important underground structure. Figure 3.11.2 correlates the geology of the basin with the terracing field, showing that high values are gathered in areas where sediments are mainly present. It is possible that underground structures, such as anticlines, are found there.

In analogy, on Figures 3.11.3 and 3.11.5 depict the terracing field that was created from the reduced-to-Pole magnetic field and the pseudo-gravity field. These maps show an existence of terraces with high anomaly values at the western part of the basin, while lower values' terraces are found at northern and central parts. High values characterize regions where ophiolites and other metamorphic rocks of the basement are found closer to the surface. This can be, also, observed on Figures 3.11.4 and 3.11.6, which depict the correlation between geology and maximum values of the horizontal gradient for the reduced-to-Pole and pseudo-gravity field. The maximum values of the horizontal gradient show clearly the boundaries of the formations of high magnetization values.
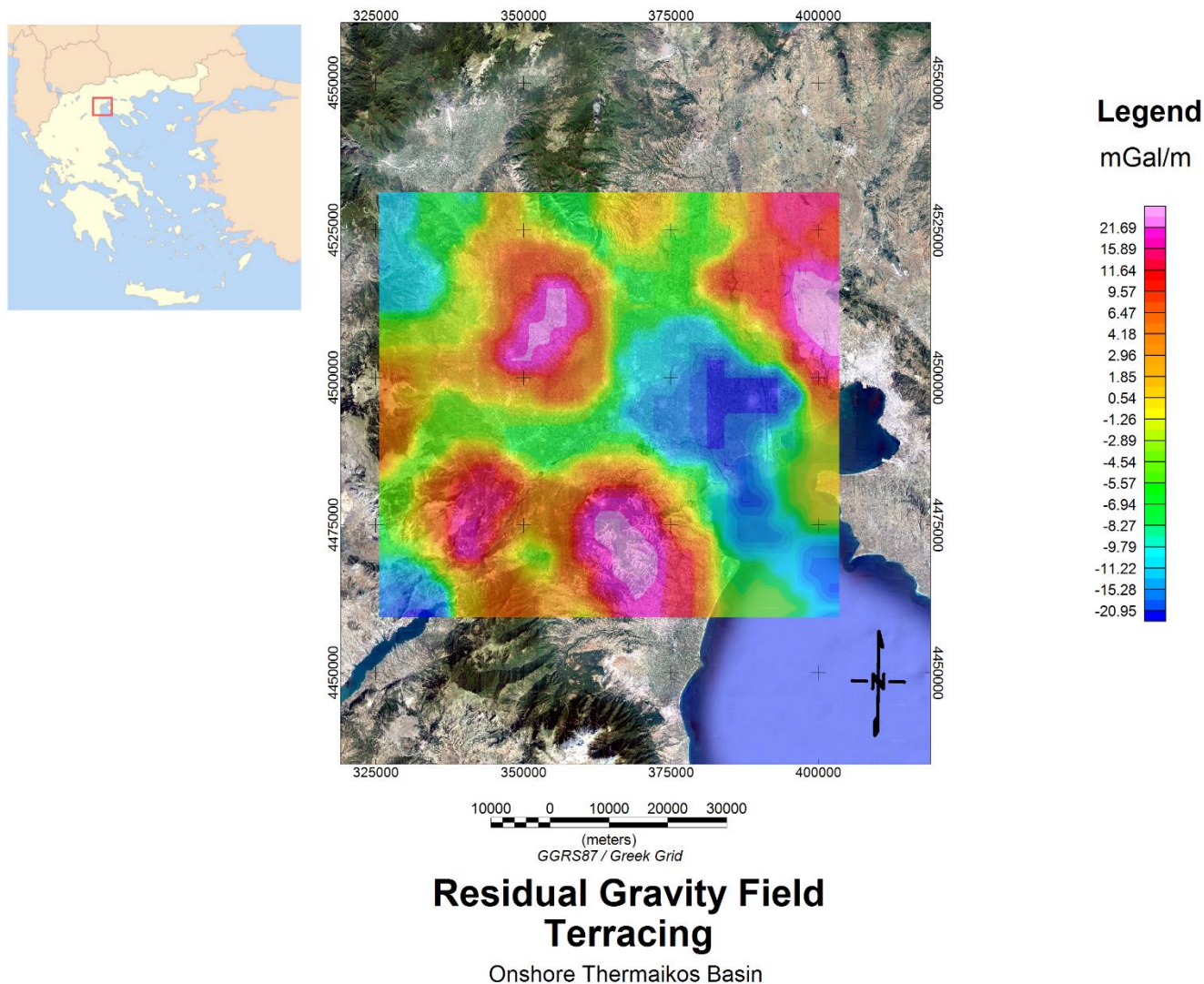
Figure 3.11.1: Terracing field, created from the residual gravity field map.
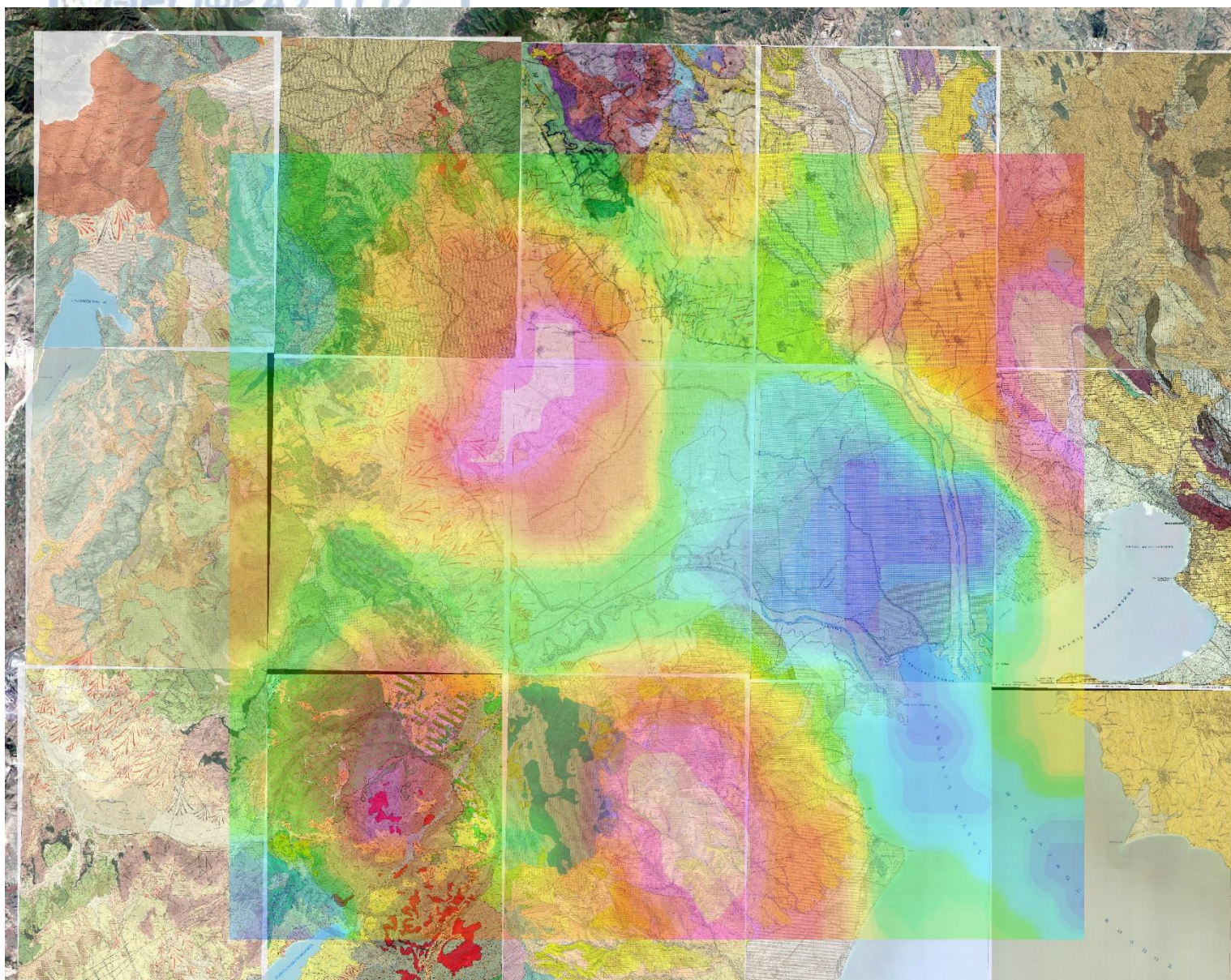
Figure 3.11.2: Terracing of the gravity field overlaying the geologic maps of Thermaikos
basin.
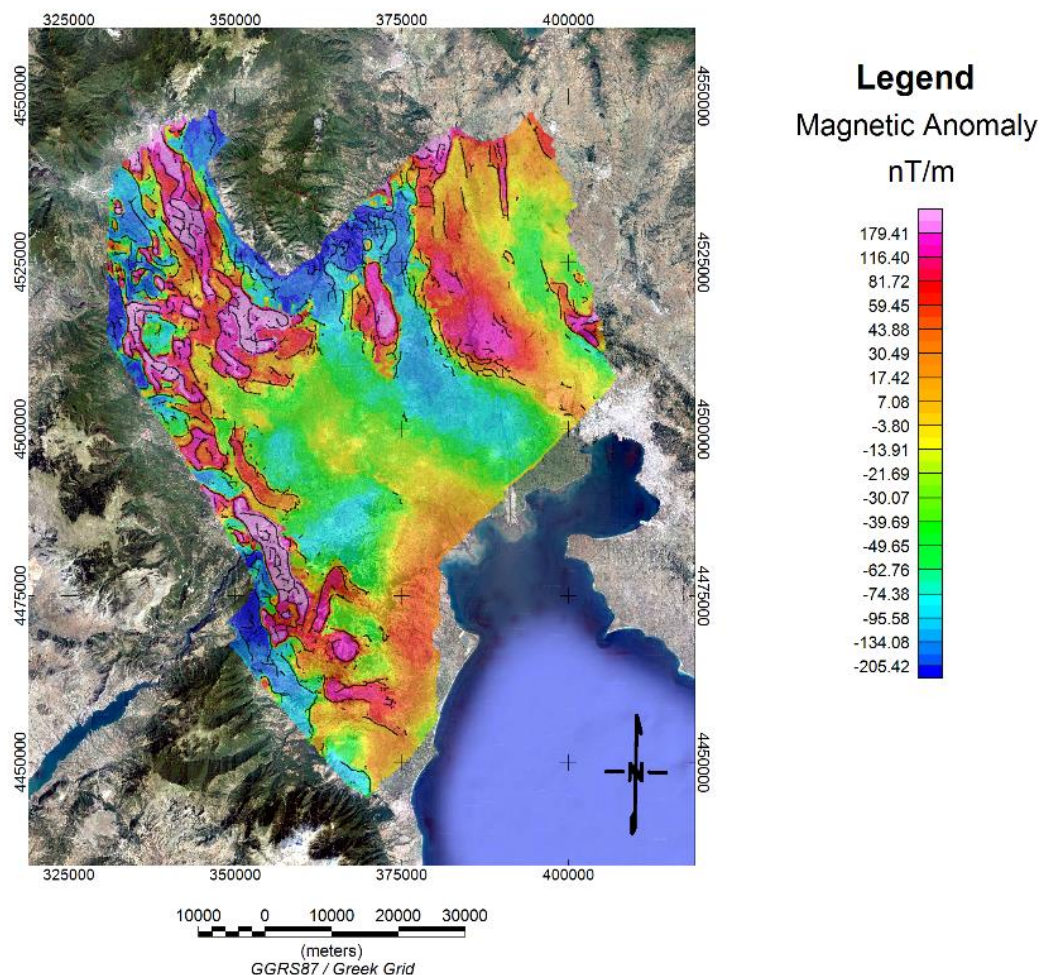
Reduced-to-Pole Magnetic Field
Terracing and Horizontal Gradient Maxima
Onshore Thermaikos Basin

Figure 3.11.3: Terracing field, created from the reduced-to-Pole magnetic field map.
Maximum values of the horizontal gradient are presented as black dots.

Figure 3.11.4: Horizontal gradient maximum values of the reduced-to-Pole magnetic field overlaying the geologic maps of Thermaikos basin.
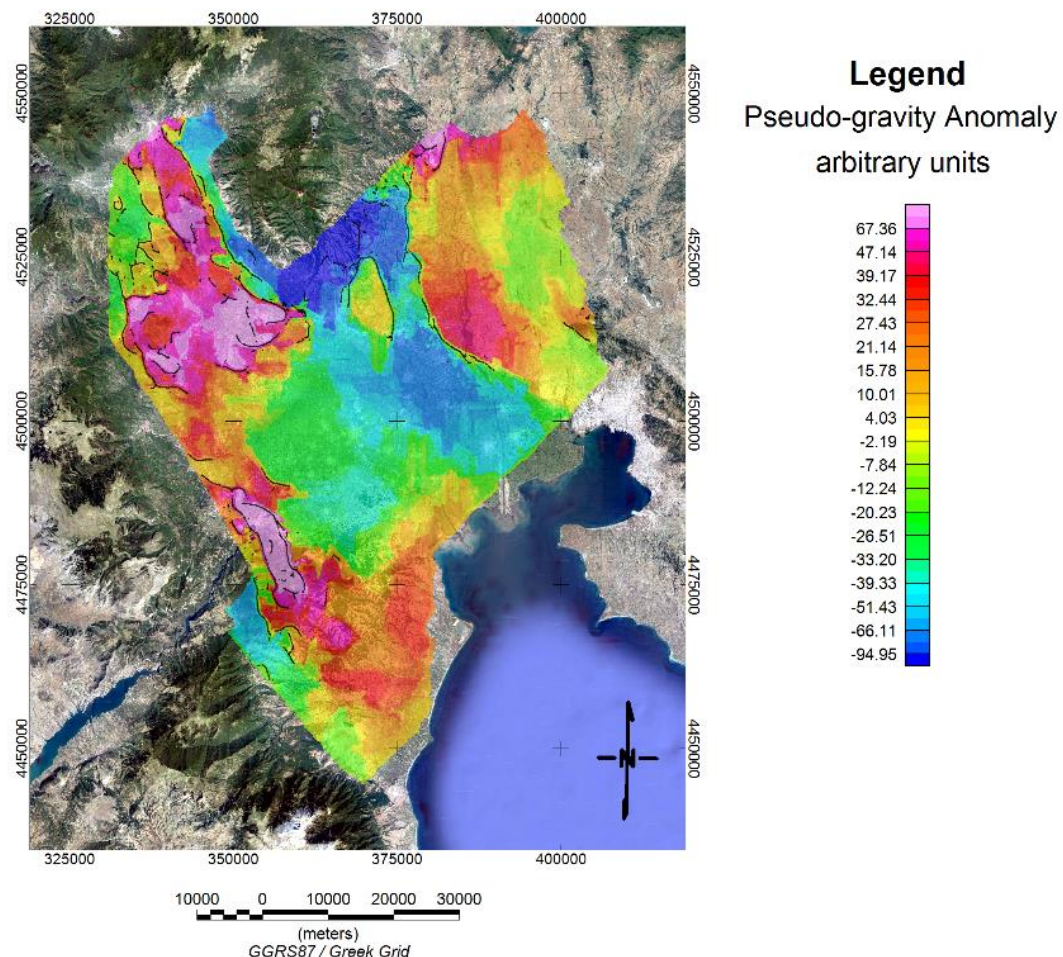
Pseudo-Gravity Field
Terracing and Horizontal Gradient Maxima
Onshore Thermaikos Basin

Figure 3.11.5: Terracing field, created from the pseudo-gravity field map. Maximum values of the horizontal gradient are presented as black dots.

Figure 3.11.6: Horizontal gradient maximum values of the pseudo-gravity field overlaying the geologic maps of Thermaikos basin.

3.12   Gravity and Magnetic Interpretation Theory

During interpretation stage, it is possible to calculate one or more parameters that quantify the source's properties. In each case, though, the results of other geophysical surveys on the area, its geology and every other relevant information should be taken into account.

Since the interference effects of other features have been significantly removed from the data, the interpretation problem concerning target recognition will evoke, i.e., in most cases, the mass distribution that causes the residual anomaly. Finding the characteristics of the anomalous field source or sources, though, is a relatively difficult process. One way for succeeding at this, for gravity data, is using a method, introduced by Bhattacharyya (1978), called iterative modeling (the direct problem solution as mentioned later on text).

Comparing the residual anomalous field with anomalies caused by simple shape masses is a technique still useful in some interpretation cases though, since gravity anomaly is not especially sensitive to minor changes in the shape of the anomalous structure and the results are close enough to reality. Also, the gravity effect of simple shapes gives valuable information on determining what aspects of an anomaly indicate the burial depth, shape, total mass, density contrast etc.

The potential field anomalies can be provoked by different mass or magnetization distributions. As a result, the existence of an enormous number of solutions leads to the introduction of limitations at the problem. These limitations could stem from the knowledge of geologic and tectonic conditions at the study area, from the data of a borehole made in the area, or from the use of another geophysical method. All that information should be taken into account at every stage of processing and much more of interpretation of anomalous fields. For instance, the knowledge of the wider geologic regime will indicate the correct form of the regional field that needs to be removed in order to isolate the anomalies of interest. On the other hand, that knowledge will lead, also, to the correct consideration of underground structures' characteristics and the confinement of the infinitude of possible models.

For gravity data, there are two general approaches for the solution of that subject, which are the direct (or forward) and the inverse approaches. The direct problem solution consists of the calculation of the effects caused by a model that looks like the

65

observed anomaly source. This synthetic field is compared with the observations. After, by correcting the model parameters, it is tried to achieve identification of the synthetic and the observed fields through a process of constant approaches. The initial selection of a model is made based on the geological information and the interpreter experience. Therefore, the direct problem approach leads to unique solution. On the contrary, the inverse problem approach involves determining the geometry and physical properties of the source from measurements of the observed field, without simply selecting a model and determining the parameters that match its anomaly approximately. As a result, its solutions are practically countless. It is obvious that in both approaches some simplifications are necessary, especially in what is called as problem customization, i.e. the mathematic description of the problem through some parameters. Multiple techniques have been developed for the solution of both the direct and the inverse problems (e.g. the least-squares method).

Last but not least, during interpretation of gravity anomalies, caution should be given to the burial depth of the anomaly source, as there are maximum-depth rules applying (Smith 1959), the effect the overburden layers may have at the measurements (especially if their thickness is significant) and the mass of the source itself, as it may be greater or lesser than initially estimated.

Magnetic survey results are displayed as a set of profiles or as a magnetic contour map. Magnetic anomalies are, generally, more numerous, more erratic, less persistent and of larger magnitude than gravity anomalies, with the exception of some large sedimentary areas where the two kinds of anomalies are similar. As a result, regional – residual field separation is more complex in magnetic data and interpretation is often only qualitative.

Magnetic features are frequently directly related to surface outcrops. Furthermore, the connection between magnetism and topography, or buried geologic structures (especially in mineral exploration areas) is often. Cases of remanence, however, should be treated cautiously, as it can produce significant effects and lead to incorrect interpretation results. Unlike gravity interpretation, depths are determined by semiempirical depth rules or techniques, like Werner deconvolution or matched filtering.

66

CHAPTER 4

SEISMIC DATA PROCESSING AND DEPTH MODELS
OF ONSHORE THERMAIKOS BASIN

The objective of the seismic data processing is the creation of seismic sections as close to the sub-surface's reality as possible, by removing all noise and distortions introduced by the seismic acquisition method, that can be interpreted, in order to create a depth model of the basin. A depth model is necessary in cases where intense tectonic events (obductions, diapirs, faulting etc.) have taken place in the study area, so the seismic time sections give a twisted image of the underground regime (Grigoriou et al. 1988). The process consists an inversion method that aims to the actual placing of the interpreted seismic reflections.

At the present Thesis, where the time horizons were created from stacked seismic sections, the inversion is based on the depiction of normal incidence rays. That technique demands the depiction of seismic rays on the underground with their travel time being equal with the reflection time, which is given by the seismic section. After the initial determination of the ray angle, its travel route depends on the velocity model. The process starts with the determination of the first geologic formation's seismic velocity, a layer that starts from the surface and reaches to the first reflector, where the formation changes. The corresponding rays of seismic waves are, then, depicted and form a guide for the reflector determination at the depth model. The same process is repeated for the finding of the rest of the reflectors, until the depth model is completed.

The seismic velocities of the geologic layers that are necessary for the construction of the depth model can be obtained either from borehole measurements, or from the processing of seismic sections, or from combination of information from the above methods (the most usual case). The final velocity values are the mean values of a specific formation and have to be the same for every depth model where the corresponding formation appears, in order for the models to be consistent among them.

Since the introduction of digital recording, a routine sequence in seismic data processing has evolved (Yilmaz 2001). There are three main steps in seismic data processing: deconvolution, stacking, and migration, usually applied in that order, though migration can be applied before (pre-stack migration) or after (post-stack migration) stacking. Other important procedures are velocity analysis, statics corrections, normal moveout and dip-moveout correction. Figure 4.1 is a flowchart of the processing steps.

Field Tapes and Observer's Log

(1) **Preprocessing:**
- **Demultiplexing**
- **Reformatting**
- **Editing**
- **Geometric Spreading Correction**
- **Setup of Field Geometry**
- **Application of Field Statics**

(2) **Deconvolution and Trace Balancing**

(3) **CMP Sorting**

(4) **Velocity Analysis**

(5) **Residual Statics Corrections**

(6) **Velocity Analysis**

(7) **NMO Correction**

(8) **DMO Correction**

(9) **Inverse NMO Correction**

(10) **Velocity Analysis**

(11) **NMO Correction, Mnting and Stacking**

(12) **Deconvolntion**

(13) **Time-Variant Spectral Whitening**

(14) **Time-Variant Filtering**

(15) **Migration**

(16) **Gain Application**

Figure 4.1: A conventional seismic processing flowchart (after Yilmaz 2001).

4.1   Seismic Data Acquisition

The acquisition of seismic data is made with a specific purpose: the sub-surficial 'target' that has to be imaged, i.e. the geologic structure of interest that is possible to

68

act as a trap for hydrocarbons. Most of the survey parameters (geographic location, fold, shooting direction etc.) are closely related to the geometry and burial depth of that structure.

Before the seismic acquisition procedures, the area or location of the exploration activities is surveyed and the seismic lines are accurately marked out, with the use of Global Positioning System (GPS) and total stations. Along these lines, the seismic wave sources, the receivers and the cables for recording are laying in order to complete the seismic array. The location where the seismic data will be acquired is called seismic survey area.

The seismic source is a device that produces acoustic energy that is recorded at the receivers. Onshore seismic surveys mostly use an explosive energy source, like dynamite, or vibrators (widely called Vibroseis), devices that provide energy by shocking the Earth's surface. Shots from air shooting is another method, less frequently used. Dynamite is placed in holes below the weathered layer of the earth, which is characterized by low velocity and its detonation is usually referred to as the 'seismic shot'. Each seismic shot position is numbered and its coordinates and elevation are accurately mapped, forming the 'shot points'. The energy released in a shot depends on the size of the explosive material, the depth of the shot hole and the local ground conditions. The shape of the source wavelet generated from an explosive is a minimum-phase wavelet (it has no amplitude before a definite start time and the greatest amount of its energy is at time zero), while the shape of the Vibroseis source wavelet is a zero-phase wavelet (it has amplitude at the start time and it is symmetrical about the time zero, with energy at negative time). For the offshore seismic acquisition, air-guns are used as the energy sources.

For the recording of the acoustic energy provided by the seismic source, specific electromagnetic instruments are used, called receivers. The receivers detect that energy in the form of ground motion or a pressure wave in fluid and transform it to an electrical impulse. Onshore (and sea-bed) receivers are named as geophones, while offshore receivers are known as hydrophones, having almost the same function and characteristics. They are laid out at regular intervals around or to one side of a shot point and are connected by wire to a recording unit found on a truck or a ship. The distance between the source and the receiver is called offset. Geophones detect ground

69

motion only in the vertical direction, therefore a number of geophones is grouped together in an array around the central receiver position, creating a channel, also improving the total signal output, and finally 'tuning' the geophones so that energy from deep is enhanced and energy from sides (e.g. ground noise) is attenuated.

Changes in sound velocity or density of the geologic formations cause reflection and refraction of the seismic waves, as a result a part of the energy produced by the source is sent back towards the surface.

Figure 4.1.1 illustrates the seismic data acquisition process during a land survey.
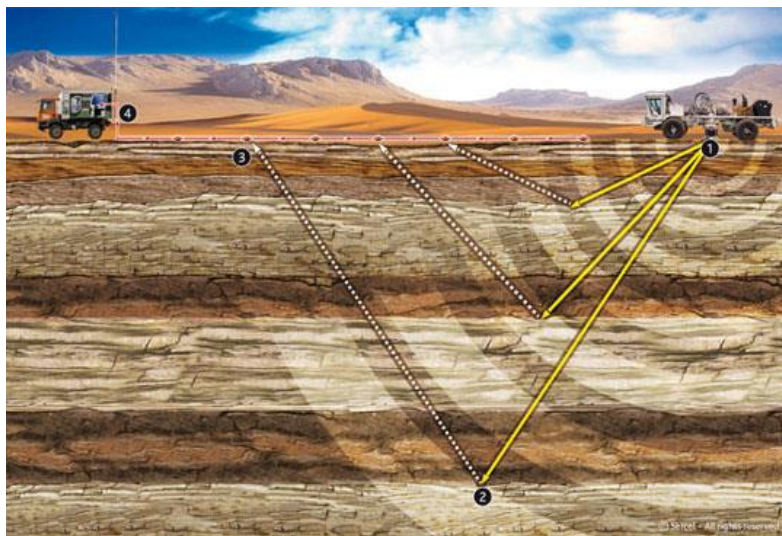

Figure 4.1.1: Acquisition of seismic data on land. Number explanation: 1: Energy source (Vibroseis) 2: Geologic formation (sedimentary layer) where the energy is reflected 3: Receiver (geophone) that records the reflected energy 4: Recording unit (truck) that gathers the recorded signal of every receiver (taken from: https://www.argas.com/land-data-acquisition/).

The seismic traces are data recorded as functions of time from one shot point at one receiver's location. This time, measured in seconds or milliseconds, is the time needed for the seismic wave to travel from its source into the subsurface, reflect and return to a receiver at the surface, so it is called as 'two-way travel time'. The seismic field record (Figure 4.1.2) contains every seismic trace recorded from one shot point. Its horizontal scale is the receiver distance from the source, measured at feet (or miles) or meters (or kilometers), while the vertical scale represents the two-way travel time. The final seismic section that gives an idea for the subsurface structure is created by the display of many seismic traces by side in their correct spatial position. The term nominal fold (or full fold or, simply, fold) of a 3-D seismic survey corresponds to the fold of coverage

70

for the maximum offset, which is the number of seismic traces that are located within a bin and will be stacked. A bin is a square or rectangular area that contains all traces of the same Common Mid-Point (CMP).
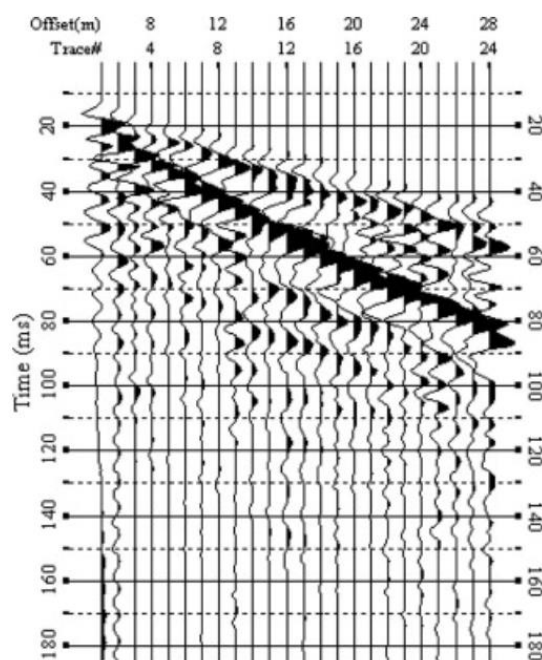

Figure 4.1.2: Raw data of a seismic field record (taken from: https://www.researchgate.net/figure/The-raw-data-of-the-surface-waves-seismogram-records-left-panel-after-applying-the_fig2_259169858).

Seismic field data are recorded digitally as a sampled data at regular time interval. In order to process the data, they are initially amplified at the pre-amplifier and may pass through analogue low-cut-off (or high-pass) filter, so that frequencies less than the cut-off frequency are attenuated. After that, the data are filtered by an analogue high-cut-off (or low-pass) filter, for the attenuation of frequencies above the cut-off frequency, usually the Nyquist frequency, i.e. the maximum frequency beyond which aliasing occurs. Aliasing is the distortion of frequency, resulting in ambiguity between the seismic data and noise, as seismic signal with higher frequencies is reconstructed in the form of seismic signal with lower frequencies. Then, the data are amplified again.

71

4.2   Pre-processing

After the acquisition of seismic data, the survey parameters that will be used in processing are identified and written down. Important parameters are, also, the sample interval (the time or distance between data points), the sample rate (the number of measurements per time units) and the sampling frequency (the number of sample points in a time unit). For the onshore Thermaikos basin survey, these parameters are described on Chapter 2.

Field data are recorded in a multiplexed mode, using a certain type of format. These data are demultiplexed, so they can be read as seismic traces at different offsets with a common shot point. The conversion of analogue to digital information to a known readable format that will be used throughout processing (a procedure known as transcription) follows and the data are stored in tapes. Although every processing contractor and oil company has a preferred format for data storing and processing, usually the SEG-Y or the SEG-D formats (established by the Society of Exploration Geophysicists) are used. The SEG-Y is a trace-sequential (or demultiplexed) format, widely used for data exchange. Thermaikos basin seismic data that were processed include stacked and migrated sections, which are saved in the SEG-Y format.

Trace editing is, also, included in pre-processing. During trace editing, high amplitude anomalies, traces with transient glitches and mono-frequency signals are deleted, while polarity reversals (changes to correct polarity) are corrected and horizontal seismic waves that travel along the water surface in shallow marine data are zeroed. Polarity is the manner that seismic data are recorded and displayed, usually the standard specified by the Society of Exploration Geophysicists (SEG) according to which normal polarity data have compressional wave from positive reflection coefficient boundaries recorded as a negative number on tape and displayed as a trough. A negative reflection has the same shape but reversed (Figure 4.2.1).

Figure 4.2.1: Polarity representation according to geology and acoustic impedance log (after Onajite 2014).

Swell and cable noise (more often in marine data), which are present with high amplitudes, can be removed by a low-cut filter application. In order to correct for the amplitude effects of spherical wavefront divergence, a gain recovery function, that depends on the seismic wave travel-time, is applied. Automatic Gain Control (AGC) system controls the increase in the amplitude of an electrical signal from the original input to the amplified output and is used to improve the visibility of seismic data that have been amplitude-decayed due to attenuation or spherical divergence.

Afterwards, field geometry is merged with the seismic data. On land data, based on survey information, the geographic coordinates of source and receivers' locations for all traces are stored on trace headers and elevation statics are applied to reduce travel-times to a common datum level, correcting for the near-surface weathered layer (that has low but variable horizontal and/or vertical seismic velocity and thickness) and differences in elevation of source and receivers. In order to remove the effect of variation in the weathered layer and any changes in the near-surface formations that cause trace-to-trace time difference, bulk time shifts are applied, called statics corrections. They are based on up-hole data, refractions, first breaks, or reflection event smoothing.

4.3   Deconvolution

In seismic data acquisition, the produced acoustic wave is quickly distorted due to absorption and attenuation (the loss of energy or amplitude of waves as they pass through rocks) that occur in the subsurface. Moreover, the presence of multiple and 'ghost' reflections make is difficult to determine which reflectors gave the recorded reflections. In order to construct a clear and easy to interpret seismic section, a process called deconvolution is applied to the data, that removes all of the above-mentioned unwanted effects. Deconvolution is applied as early as possible during the seismic processing sequence to stabilize the frequency content of the data and to remove multiple reflections prior to velocity analysis. Usually, it is applied to pre-stack data, trace-by-trace, but it can be applied to all the traces of a shot record, as well. This process can improve the resolution of the seismic section by restoring high frequencies of the seismic signal that are attenuated due to absorption during its travel through the subsurface, and produce a broad bandwidth with high frequencies, that is a more accurate representation of the subsurface.

There are two types of deconvolution: spiking and predictive deconvolution. In spiking deconvolution, the earth's reflectivity and the source wavelet are separated and the source wavelet embedded on the seismic trace is compressed to a signal as short as possible, called spike, in order for the seismic trace to contain only the reflectivity. Spikes (short pulses) have large bandwidth and their arrival time is easy to be measured. The frequency content and the temporal resolution of the data are significantly improved and the reflection event can be seen clearly and with finer detail on the seismic section. In predictive deconvolution, short-period multiple reflections, that modify the frequency spectrum of the data by adding information in each primary reflection, are eliminated, while the rest of the seismic trace is left untouched. The reflection continuity is improved and the reflection events are easier to trace. Deconvolution techniques are based on optimum Wiener filtering.

After deconvolution application, the data often need filtering with a wide band-pass filter, as both high- and low-frequency noise and signal are enhanced, as well as trace balancing in order to bring the data to a common Root-Mean-Squared (RMS) level is often applied (Yilmaz, 2001).

74

4.4   Common Mid-Point (CMP) Sorting

A seismic trace may contain hundreds to thousands of samples, with each seismic shot generating 24 or 48 traces. A number of traces consists a shot gather and many shot gathers consist a seismic line. A seismic line will, therefore, contain several millions of samples (Onajide, 2014). The term shot (or field) record is used to describe the gather of all traces associated with one shot. It is possible to sort a subset of traces from an entire set of several shot records, in various ways.

While seismic data acquisition with multifold coverage is done in shot-receiver (s, g) coordinates, seismic data processing uses midpoint-offset (x, y) coordinates. The transformation needed is achieved by sorting the data into Common Mid-Point (CMP) gathers. CMP gather refers to a group of all traces that fall into the same midpoint (Figure 4.4.1). Based on field geometry, each trace is assigned to a midpoint between the associated source and receiver locations. The traces of a common midpoint differ in move-out, offset and the receivers and source's locations. They are used as input to later stages of processing, such as velocity analysis and CMP stacking after the Normal (and Dip) Move-Out (NMO and DMO) corrections. Common Depth Point (CDP) gather is used as a synonym of CMP gather, but these two terms are equivalent only in cases where the reflectors are horizontal and velocities do not vary horizontally. In cases of dipping reflectors, only the term CDP gather should be used.
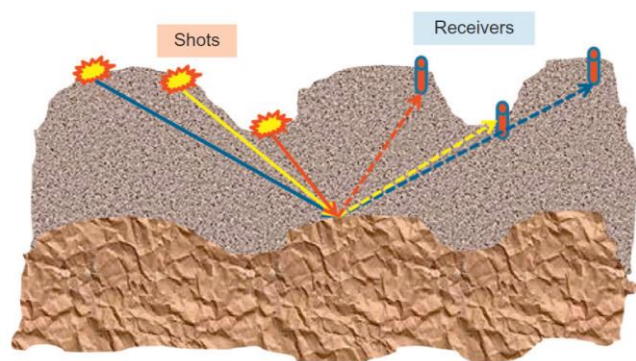

Figure 4.4.1: Representation of common midpoint (CMP) reflections (after Onajide, 2014).

Stacking charts are diagrams that are constructed during the CMP sorting procedure and are useful at the reprocessing of a seismic line, since missing shots or receivers that may negatively affect the midpoints can be easily identified.

Except of the CMP gather, seismic data can be sorted in a number of different other ways:

- Common Offset Gather, that is created by all traces with the same shot-receiver offset. Traces differ in receivers, source and reflection points' locations.
- Common Shot Gather, that contains all traces recorded from a single shot. Traces differ in move-out and offset, whereas receivers may differ in dip.
- Common Receiver Gather, that contains all traces recorded in the same station during the survey and it is useful in identifying bad traces, but it is not commonly used in seismic processing.

4.5   Residual Statics Correction

Due to often near-surface velocity irregularities, the moveout in CMP gathers does not always conform to a perfect hyperbolic trajectory. Lateral velocity variations caused by a complex overburden structure can cause negative moveouts, when reflections arrive at long-offset traces before the short-offset traces (Yilmaz, 2001).

Residual statics corrections are applied to the moveout corrected CMP gathers, in order to improve stacking quality. Source and receivers' locations are the only parameters that time shifts depend on, while the ray paths among them are of no importance. However, small errors in statics corrections may be present after the procedure, which are characterized by trace-to-trace time differences. The processed gathers are stacked to form a new stacking section.

4.6   Velocity Analysis

In a seismic record, copies of the primary reflections are generated by long-period multiples. These unwanted reflections are removed by the velocity discrimination process, since their travel path is much larger than primary reflections and, also, their velocities are lower. During velocity analysis, the velocity that flattens the reflection

76

hyperbola on a CMP (or CDP) gather or group of gathers (stacking or seismic velocity) and derives from the seismic data is determined. This velocity gives the optimum CMP (or CDP) stack output after applying Normal Move-Out (NMO) corrections. Although stacking velocity is not the real velocity of the rock, at shallow depths the two velocities are close. Rock velocities generally increase with depth due to higher pressure and compaction, as a result the velocity function (velocities picked at various CMP or CDP locations of the seismic line) also increases. The result is a table of numbers that measure the signal coherency, as a function of velocity versus two-way zero-offset travel time. In order to determine the stacking velocity, the Velocity Analysis Techniques are applied, i.e. the Constant Velocity Gathers (CVG), the Constant Velocity Stack (CVS) and the Semblance procedures. Multiple reflections appear as fake semblance peaks among the primary reflections.

For Thermaikos basin data, the average formation velocity of longitudinal waves was calculated by the stacked sections (two-way travel times) and the formations' thicknesses, taken from well core description (Sivenas et al. 1997). These velocities were verified by the available sonic loggings of AL-1, YA-1 and LO-1 wells. The above measurements are represented at Table 2.5.1 on Chapter 2.

In velocity analysis, stacking velocities are picked at selected locations along the seismic section and the results are linearly interpolated from one analysis location to the other, on condition that the reflector and the reflection time are the same (Onajide, 2014). A quality control of the picked velocities for their spatial consistency is made afterwards, often by examining the iso-velocity contours (represent velocity functions with the same value) along the seismic line. The picked velocities are finally used to construct a 3-D volume of the velocity field. For each CMP or CDP gather or group of gathers, a velocity field is created. At the velocity spectra that represents the velocity field, the horizontal axis depicts the scanned velocity, while the vertical axis depicts the two-way zero-offset travel time. Figure 4.6.1, shows the velocity field constructed for the L8 seismic line of Thermaikos basin. Red color indicates high velocities, while blue color corresponds to low velocities.
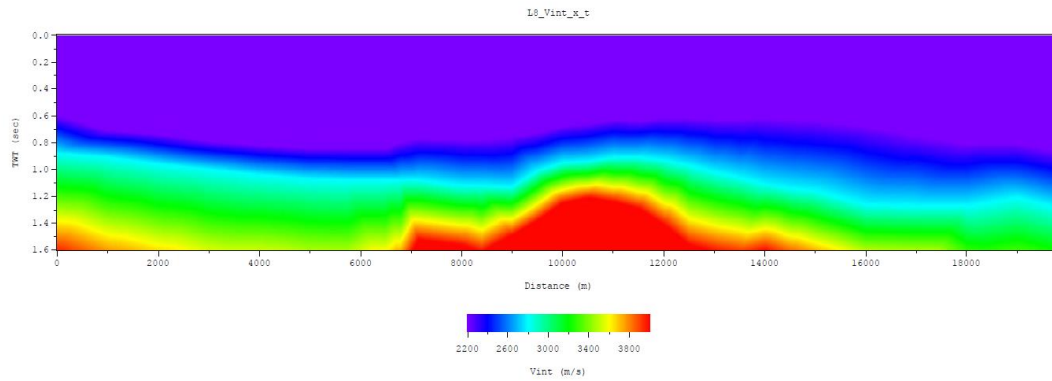
77

Figure 4.6.1: Velocity field of L8 seismic section (after Tsokas et al. 2013).

4.7   Normal Move-Out (NMO) Correction

The Normal Move-Out (NMO) correction is applied in CMP gathers after the velocity analysis, as it is strongly depended on the layer velocities. This dynamic correction is a time-variant operation that is applied to each seismic trace of a CMP or CDP gather and removes the move-out effect (hyperbolic distortion of reflection events) which appears on reflection times, resulting in all traces from a reflector being equal in time. Before NMO correction, primary and multiple reflections always appear as hyperbolic curves due to the distance between the shot and the receiver (offset), as shown on Figure 4.7.1.
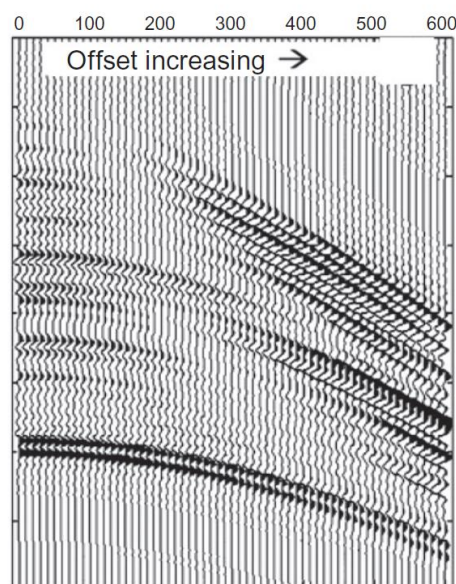
Figure 4.7.1: Hyperbolic curves due to offset increase (taken from: tle.geoscienceworld.org).

78

However, after applying the NMO correction, the offset effect is completely removed from time, primary reflections are mostly flattened across the offset range and multiple reflections are all under-corrected. The seismic traces are stretched in a time-varying manner, causing their frequency to gain lower values, a distortion that increases at shallow times and large offsets. The amplitudes of shallow events are, therefore, muted before stacking. After the NMO correction processing, in each CMP or CDP gather, seismic traces are summed to form a stacked trace at each midpoint location.

4.8   Multiple Attenuation

Multiple reflections are events that reflect more than once in layers of the subsurface with strong acoustic impedance, the seabed, the water-bottom interface, or the air-water interface (for marine seismic data), in contrast to primary reflections that are created by the energy reflection once, at a single reflector. In marine data, sequences of strong reverberation can be caused by the air-water and water-bottom interfaces. Time delay of the multiples from the primary reflections characterizes multiples as short- or long-period multiple reflections. Short-period multiples appear as copies of primary reflections, while long-period multiples appear as separate reflection events. Multiples obscure the primary reflections and make the interpretation of the seismic section very difficult, as they appear as distinct events on it. In Figure 4.8.1, the different types of multiple reflections are analyzed.
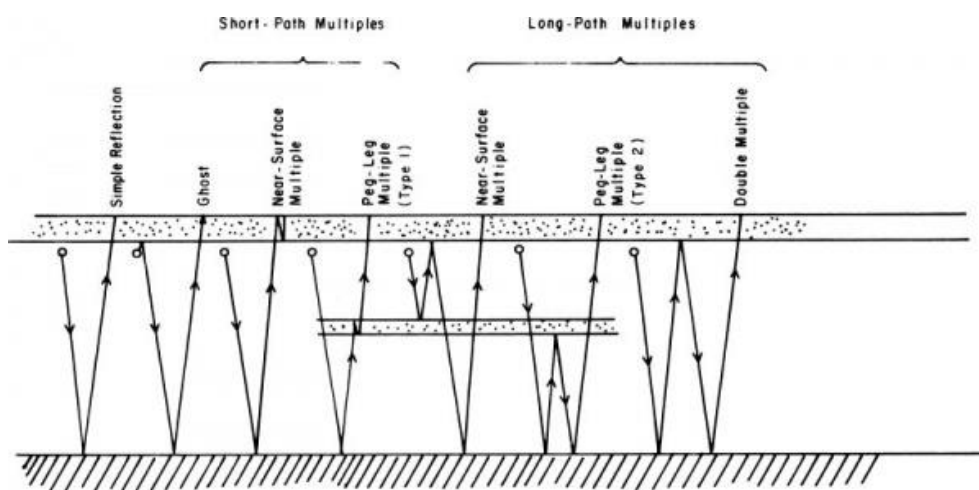

Figure 4.8.1: Different types of multiple reflections (taken from: https://wiki.seg.org/wiki/Dictionary:Multiple).

Multiple reflections and reverberations are attenuated using techniques applied to data in various domains (including CMP domain) based on their periodicity or differences in move-out velocity between multiple and primary reflections. Deconvolution is one method of multiple attenuation, as it can remove a significant amount of energy associated with short-period multiple reflections and reverberations (Yilmaz, 2001).

4.9   Dip Move-Out (DMO) Correction

If dipping reflectors exist within the seismic section, the seismic data will not be recorded at their correct spatial position, as the reflection points move 'up-dip' away from the nominal CMP and the actual points are different for different offsets. Velocities obtained from the CMP gathers will be incorrect, also. Dip Move-Out (DMO) correction is necessary in order to correct for the dip effect on stacking velocities and preserve reflections with conflicting dips during the process of CMP stacking. By applying DMO correction, the data are repositioned, so that only one common reflection point exists for all traces in the (newly created) CDP gather, while noise and mis-positioned data are cancelled out and signal is kept. DMO correction is directly proportional to the trace offset and the angle of dip, but inversely proportional to the stacking velocity.

DMO correction is approached with the following equation:

$$\Delta T = \frac{X^2 \sin^2 \varphi}{V^2}$$

where X is the trace offset, φ is the angle of dip for the subsurface interface and V is the velocity of the overlying layer. With the velocity increasing with depth, the correction is smaller.

Figure 4.9.1 shows a seismic section before and after DMO correction. After DMO, random noise is reduced and some details are enhanced due to the velocity stabilization and the correction from CMP to CDP.

80

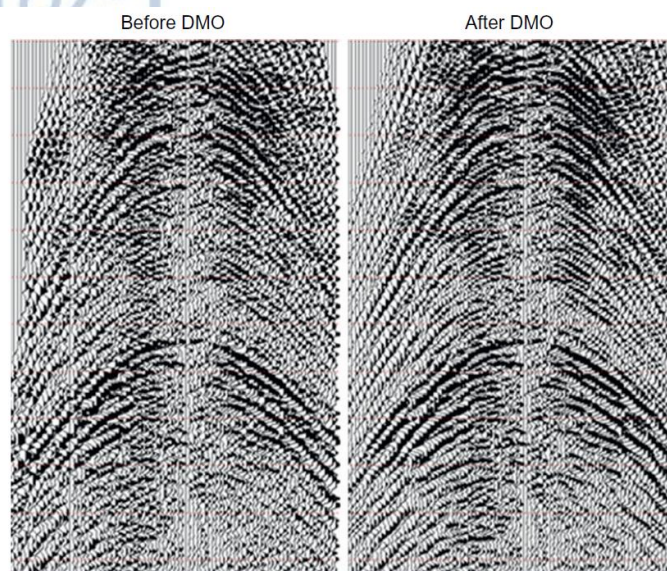Before DMO   After DMO

Figure 4.9.1: A seismic section before (left) and after (right) DMO correction (taken from: inter-geo.org).

After DMO correction, the Inverse Move-Out correction follows and velocity analysis at closely spaced intervals continues, before applying CMP/CDP stacking. During this second velocity analysis, super gathering technique is applied, which is a method of improving signal-to-noise ratio of the seismic data, where several CDP gathers are examined at once. Moreover, the mute technique can be applied, in order to remove the longer offsets and to eliminate noise and the NMO stretch. Mute simply zeroes (replace the traces with zeroes) everything above a chosen time and is used to be applied after NMO and DMO corrections.

4.10   CMP/CDP Stacking

After the application of NMO and DMO corrections, all pre-stack seismic traces from different shot records with a common reflection point, such as CMP data, are added together in order to give a single, zero-offset trace that could have been recorded at that midpoint location. The display of these stack traces creates a stack seismic section. By stacking, noise is reduced or attenuated by a factor equal to the square root of the fold and the signal-to-noise ratio is improved, while the overall seismic data quality is generally improved. Noise in the seismic record is random and is picked up

81

by the receivers at the surface, together with the reflected seismic traces. Noise can be created both onshore (from passing vehicles, wind, recording instruments etc.) and offshore (waves, noise on boats etc.).

The amount of data is reduced during stacking by a factor known as the fold of coverage (or the fold of stack or, simply, the fold). Fold is, also, the number of traces that have been added together during stacking. The fold of coverage (n_f) is given by the following equation:

$$n_f = \frac{n_g \Delta g}{2\Delta s}$$

where n_g is the number of recording channels and Δg and Δs are the receiver group and source intervals, correspondingly. According to Yilmaz (2001), by using the above equation, the following rules can be established:

- The fold does not change when alternating traces in each shot record are dropped.
- The fold is halved when every other shot record is skipped, whether or not alternating traces in each record are dropped.

The following Figure 4.10.1 shows a representative stacked section of onshore Thermaikos basin seismic data.
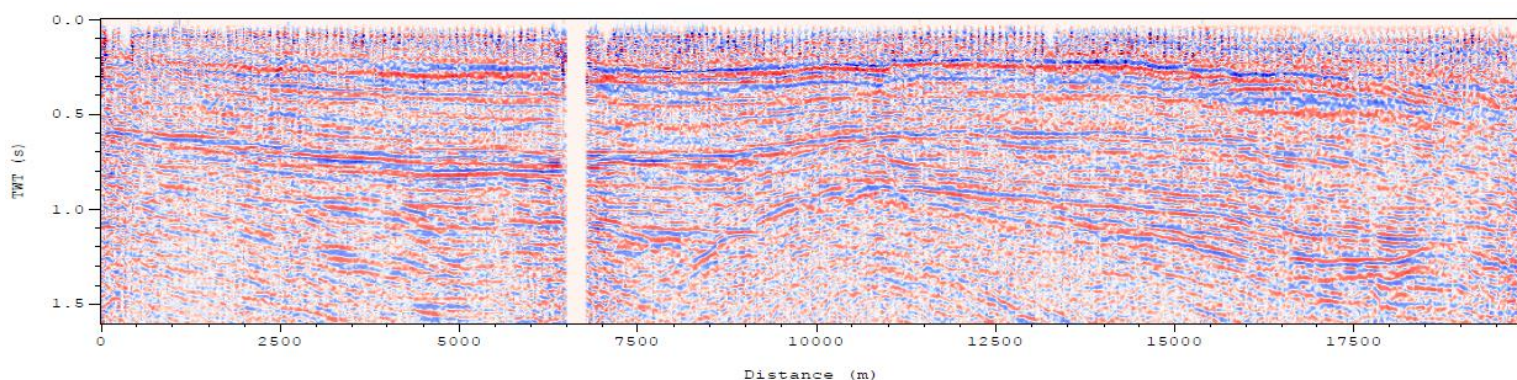

Figure 4.10.1: The L8 stacked seismic section from Thermaikos basin data (after Tsokas et al. 2013).

For the seismic data stacking, there are three different techniques to apply. The weighted stack can be used for the attenuation of multiple reflections and the removal of any AVO (Amplitude Variation with Offset – variation in reflection amplitude with

82

change in distance between source and receiver) effects. Median and Min-Max stack are used to eliminate the highest and/or lowest amplitudes, while they, also, eliminate spikes and noise burst.

4.11   Instantaneous Envelope

Signal analysis is useful for the extraction of important information from time-series (e.g. seismic data). One such example is the clearer representation of strong reflectors after applying the instantaneous envelope methodology.

Complex seismic trace analysis results to separation between amplitude and phase of a waveform. These two parameters are called attributes. Instantaneous envelope consists the only complex characteristic of a trace, which is used in lateral variations' detection at reflectors. The equation that describes instantaneous envelope is the following:

$$E(t) = \sqrt{x(t) + x^*(t)}$$

where x(t) is the time-series of a seismic trace, while x*(t) is the 90° phase shift of x(t) (Taner et al. 1979).

The stacked sections of Table 4.11.1 were reprocessed by Tsokas et al. (2013). The same researchers applied the instantaneous envelope depiction methodology to the new stacked sections in order to achieve better depiction of stacked data, an example of which is presented on Figure 4.11.1.

Area	Seismic Lines	Wells
Alexandria	L8, L15	AL-1, YA-1
Platy	L9, PEV302	KO-1
Loudias	L23, L120, PEV203	LO-1
Klidi	L88, L105, PEV403	KL-1

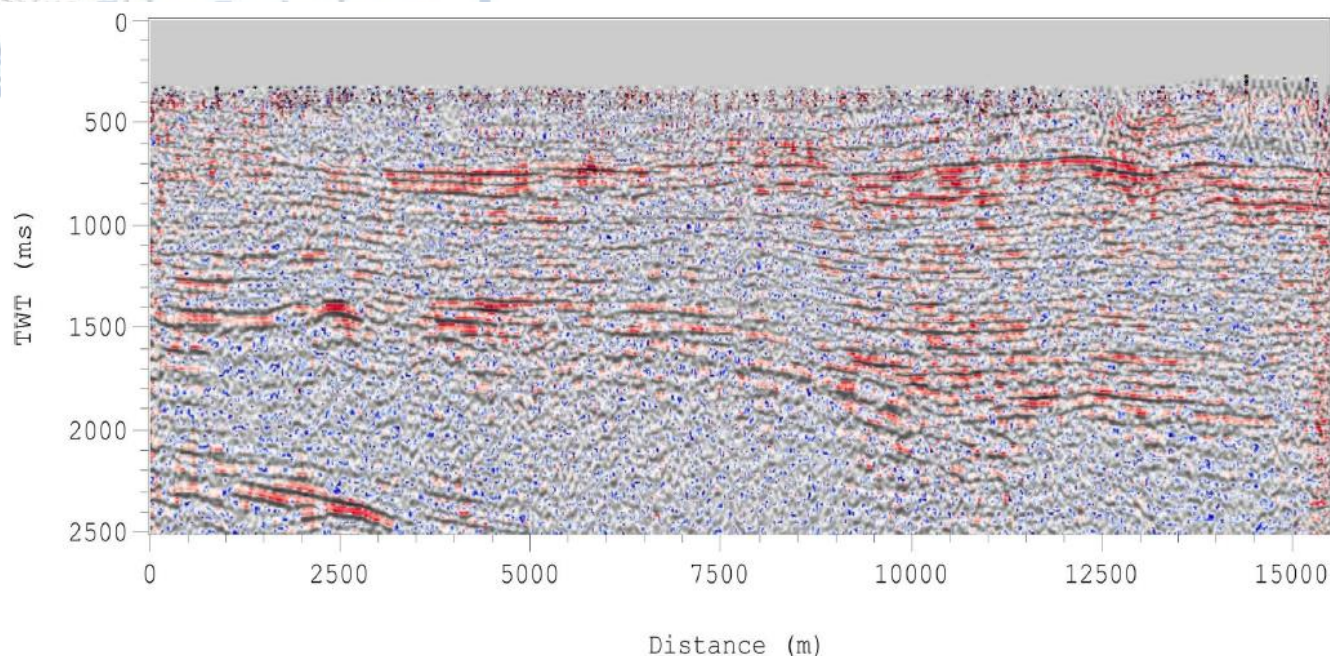Table 4.11.1: Onshore Thermaikos basin data used by Tsokas et al. (2013).

Figure 4.11.1: Overlay of the Instantaneous Envelope section over the stacked section. Figure represents the L88 seismic section of Thermaikos basin (after Tsokas et al. 2013).

4.12 Spectral Balance

A decline in time domain resolution with depth is observed at the seismic sections due to seismic waves' depreciation, which is more obvious at high frequencies. Spectral balance is applied to waveforms for the correction of the above phenomenon. Waveforms' amplitudes are enhanced in time – frequency (t – f) domain. In order to be effective, spectral balance is applied at every seismic trace in small duration time 'windows'.

The upgrade of spectral identity of data visibly enhances the recording quality and increases resolution in time domain, especially in stacked sections. Consequently, layers of thinner thickness are more easily observed.

84

After stacking and instantaneous envelope depiction, Tsokas et al. (2013) further applied the spectral balance methodology to depict clearer the spectral identity of data of the L8 seismic section, as shown on Figure 4.12.1.
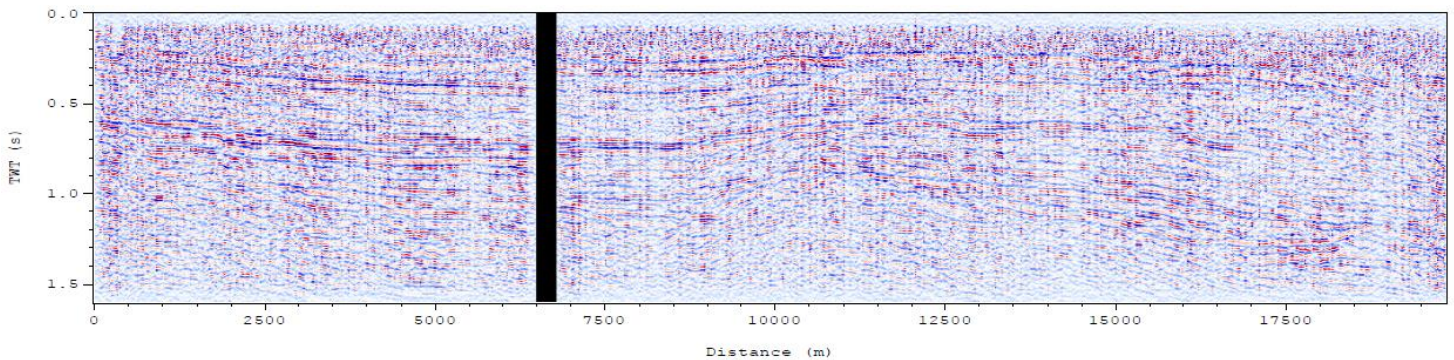

Figure 4.12.1: The L8 stacked seismic section after the application of Spectral Balance methodology (after Tsokas et al. 2013).

4.13   Migration

In seismic exploration, the reflection point lies at the midpoint between the source and the receiver only in case where the reflector is horizontal. If the reflector is inclined, the reflection point is located not at the midpoint, but up-dip of the source – receiver offset. As a result, reflections from dipping reflectors are depicted in the wrong place. In order to reposition them in their (expected) true subsurface position, the migration process is applied to the stacked (or pre-stacked) data. By migration, diffractions are, also, removed. The migrated section represents the geological cross-section along the seismic line traverse. In Figure 4.13.1, a comparison is made between the representation of the same seismic data before and after migration.

Knowledge of the velocity model (lateral and vertical seismic waves' velocity variations) is crucial for migration application. The velocity that optimizes the energy repositioning to the true reflection point is called migration velocity. The creation of the new velocity field for migration is, usually, based on stacking velocities. If migration velocity is too low, the data will be under-migrated, whereas if migration velocity is too high, the data will be over-migrated.
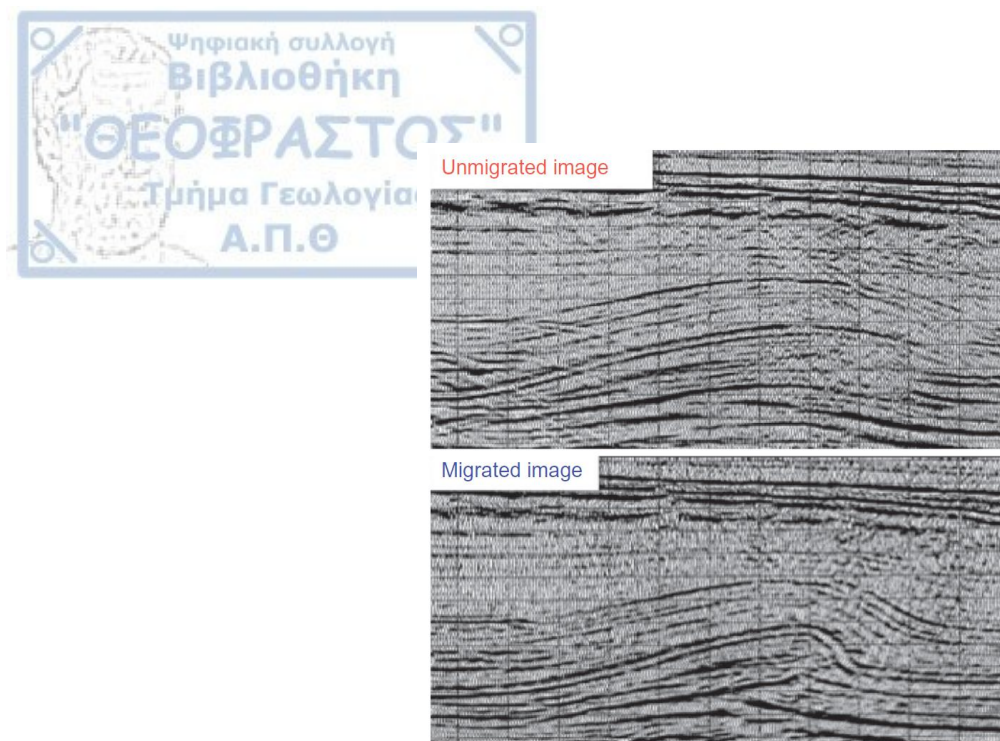
Figure 4.13.1: Unmigrated (top) and Migrated (bottom) seismic section (taken from: AAPG Slide Resource - The Seismic Method by Fred Schroeder. Courtesy of ExxonMobil).

There are two categories of migration, applied to both pre- and post-stack data: time and depth migration. Time migration repositions the reflected seismic data from their apparent location on a midway between the source and the receiver to their true reflection point in space and time. It is based on three principles, each one creating a different migration method: Kirchhoff migration, finite-difference migration and Fourier transform migration. Although, since time migration is represented in time scale, depth model's accuracy is confined and the migrated section is difficult to be compared with the previous stacked section.

Depth migration includes modified techniques of Kirchhoff migration and other wave equation methods that can locate the origin points of reflections by studying the 'bending' of seismic rays by refraction within the subsurface. Input data is unmigrated seismic data in time domain, while the output is migrated data in the depth domain. The precise calculation of average velocity (which is derived from stacking and interval velocity) is of high importance. There are three methods in depth migration: finite-difference migration, ray-theoretical migration and image-ray tracing migration. However, depth migration requires greater computer time to process than time migration, a fact that leads to greater data processing cost. Consequently, migration results are often displayed in time (time migration), being equally acceptable as in depth (depth migration) displays, at least for the most of the researches and companies.

86

Pre-stack time (PSTM) and pre-stack depth (PSDM) migrations use all of the seismic data as input, in cases of geological structures that is impossible to stack correctly without first migrating the data before stack. PSTM gives a good image of the subsurface if velocity field varies only slightly laterally, while PSDM achieves clear image when velocity varies rapidly laterally (Onajide 2014). In cases of almost flat layers with small variations in velocity, post-stack migration is applied. Pre-stack migration is often used in areas with complex geology, providing much better imaging, but requires more computer time and cost in contrast with post-stack migration. A comparison between the results of pre- and post-stack migration methods is presented in Figure 4.13.2.
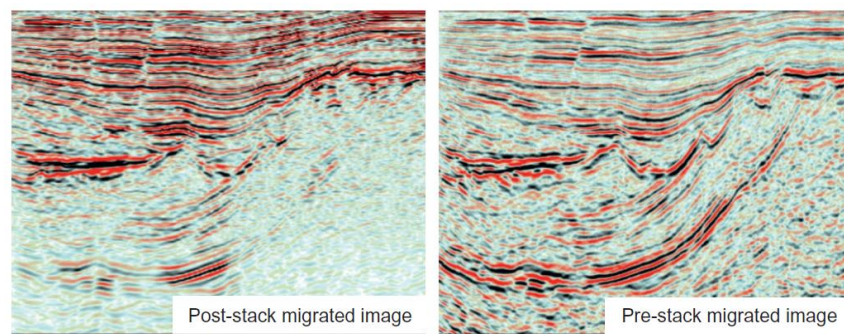
Figure 4.13.2: Post-stack (left) and pre-stack (right) migrated section (taken from: www.geomega.hu).

Tsokas et al. (2013) applied three migration methods at the reprocessed stacked sections of Table 4.11.1 (except of PEV403): Kirchhoff migration (Schneider, 1978) in two different seismic traces' windows (for the total number of traces and for 50 traces), finite-difference (or downward continuation) migration (Claerbout, 1985) and phase-shift (or Gazdag) migration (Gazdag, 1978). At each one of the created migrated sections, they later applied Instantaneous Envelope depiction.

Kirchhoff migration method is based on the fact that a seismic wave's reflection to a point causes diffraction. Diffracted waves are found on diffraction curves (hyperbolas). During Kirchhoff migration, the amplitudes that belong to a hyperbola are summed, in order to give the amplitude of the corresponding point at migrated section, consequently every point of unmigrated section is considered as a part of diffraction. Kirchhoff migration is, also, widely used in cases of consecutive reflectors, on condition that they can be described from the interference of successive reflected waves originating from closely-located point targets (Sheriff & Geldart 1995). One important parameter in applying Kirchhoff migration is the aperture width, which is related to the diffraction curve. The shape of the diffraction curve varies with time and distance. A sufficient number of traces must be included in the processing window in order to completely define the diffraction curve and avoid the curve's collapsing and the incorrectly migrated data (Onajide 2014). The result of Kirchhoff migration's application at the L105 seismic section of Thermaikos basin data is given on Figure 4.13.3. The aperture width value of this section is 50 traces, while the maximum dip angle of Kirchhoff migration application is 90º.
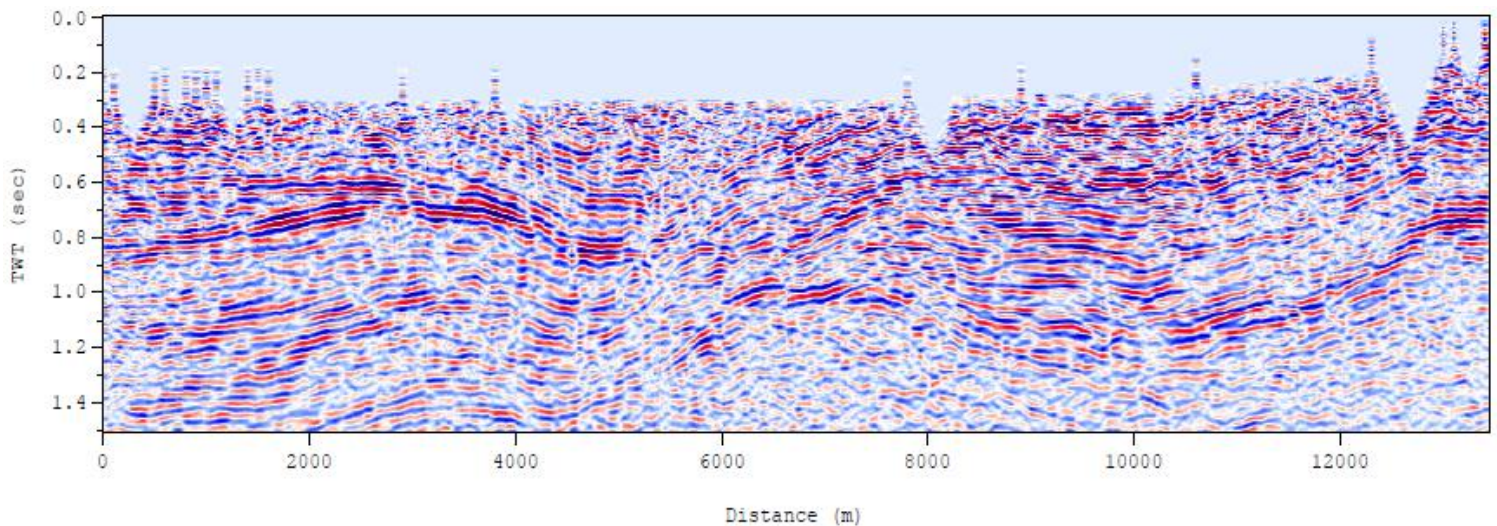

Figure 4.13.3: The L105 migrated section of Thermaikos basin after Kirchhoff migration (after Tsokas et al. 2013).

In finite-difference migration method, the seismic wave field at the earth's surface is known, the wave equation is solved with finite-difference method and the field is successively calculated for greater depths. This method of migration is paralleled with the geophone positioning at the reflector's depth and is, also, called downward wave field continuation. Lateral velocity variations are more easily handled with this method. One important parameter of finite-difference migration is the step length in time of wavefield extrapolation. If that interval is too small, under-migration will occur and the seismic events will be repositioned far enough up-dip (Onajide 2014). Finite-difference migration method's result, as applied on L105 seismic section, is shown on Figure 4.13.4. The step length in time of this section is 4 ms, while the maximum dip angle of finite-difference migration application is 90°.
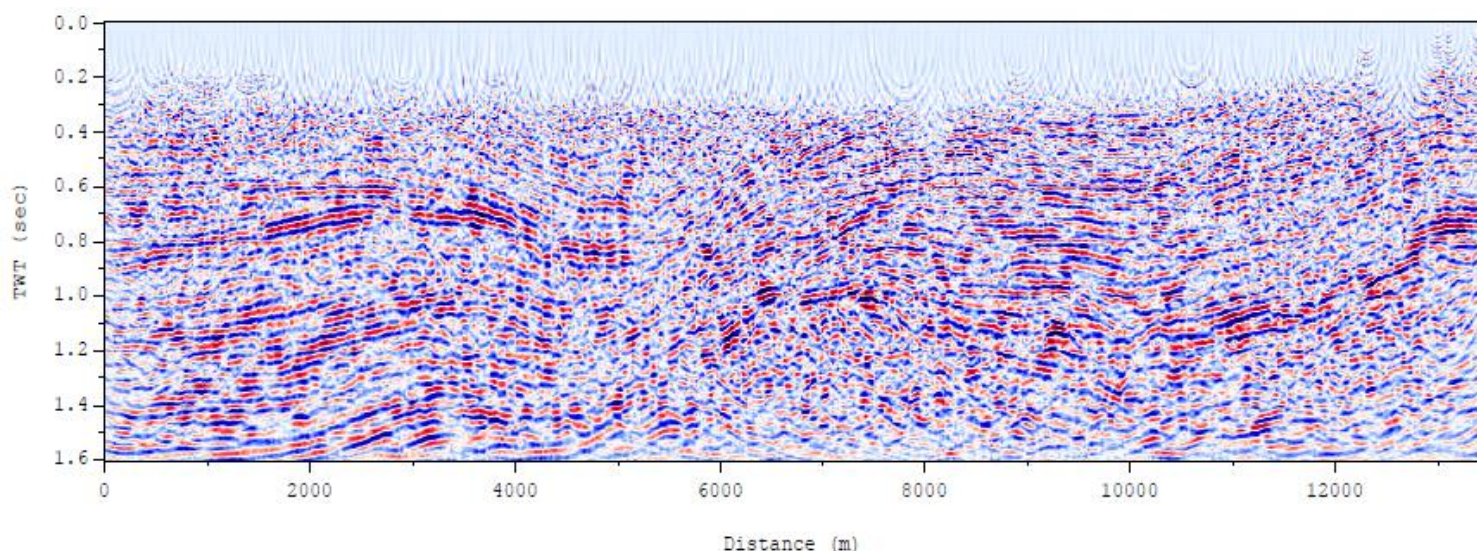

Figure 4.13.4: The L105 migrated section of Thermaikos basin after finite-difference migration (after Tsokas et al. 2013).

Phase shift (or Gazdag) migration is applied to frequency – wavenumber (f – k) domain. This method is based in the phase shift that occurred during downward continuation of the wavefield. A depiction of Gazdag migration's result on L105 seismic section is given on Figure 4.13.5. The maximum dip angle of Gazdag migration application is 90°.
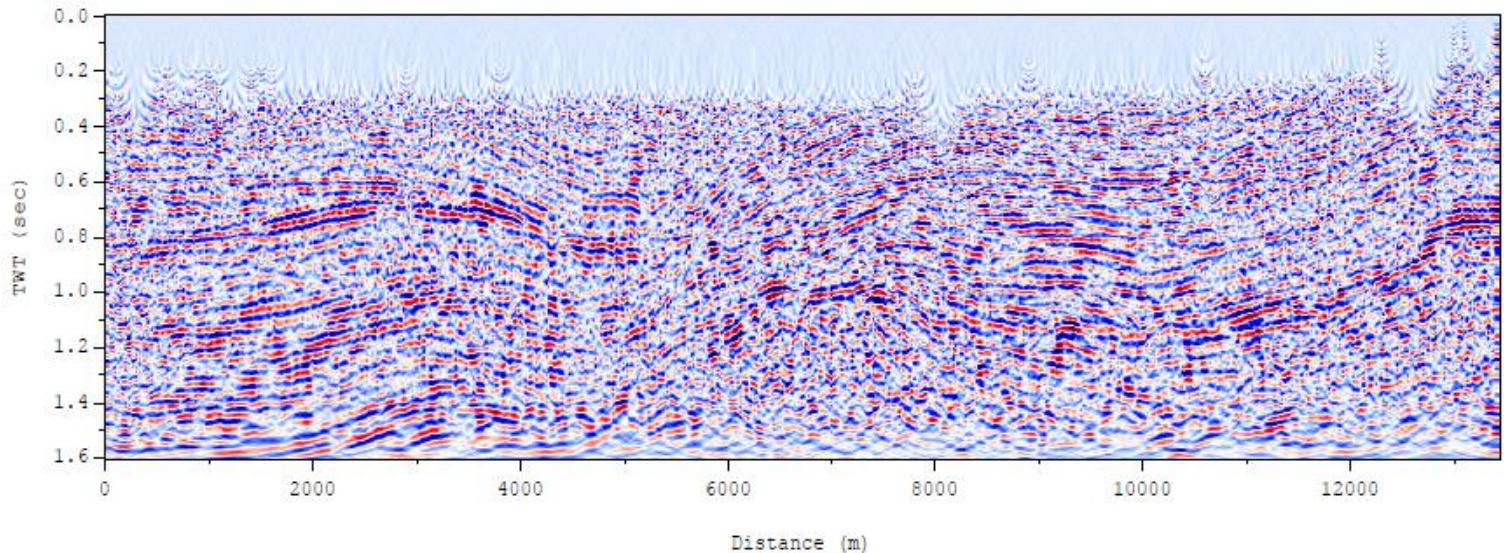
89

Figure 4.13.5: The L105 migrated section of Thermaikos basin after phase shift migration (after Tsokas et al. 2013).

Structural complexity caused by faulting and/or folding generally produces problems in stacking and representing the subsurface as follows (Yilmaz, 2001):

- Fault surfaces and salt flanks cause steeply dipping reflections, which conflict with gently dipping and near-flat reflections associated with the less undisturbed strata during stacking. In order to solve this, pre-stack time migration or dip-moveout correction followed by post-stack time migration is applied.

- Travel-time and amplitude distortions during stacking are produced by non-hyperbolic moveout due to strong lateral velocity variations, since the hyperbolic moveout assumption made on this processing step does not apply in these cases. The velocity variations are associated with complex overburden structures, like salt and overthrust tectonism. Pre-stack depth migration is applied at the above situations.

- Both of the above cases do exist as 3-D problems in nature, which are solved with 3-D migration process.

In unmigrated seismic sections, anticlines appear wider than they are, crossing through the reflection points, following the 'rule': the higher their dip is, the wider they appear. After migration, these structures appear compressed, making possible the estimation of hydrocarbon reserves they could contain (Figure 4.13.6). Incorrect migration velocities, though, may lead to wrong imaging, making the structure

90

narrower or wider than its original geometry, while lateral and vertical uncertainties may rise when using the data to well-to-seismic tie during seismic interpretation.
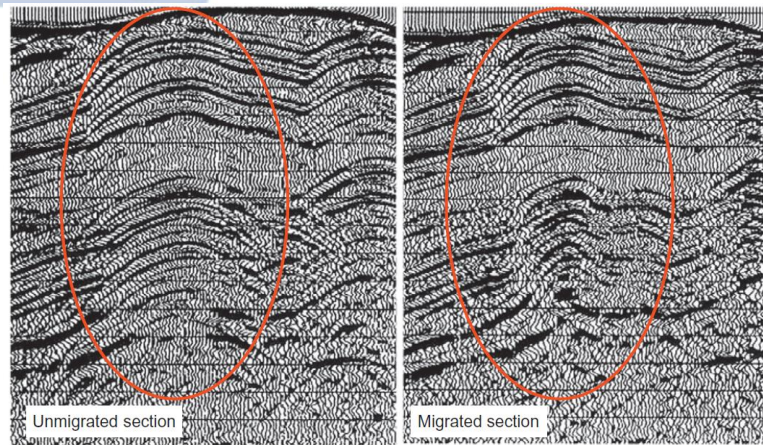

Figure 4.13.6: An anticline in unmigrated (left) and migrated (right) section (after Onajide 2014, taken from: Geophysical Methods by Larner et al.).

Faults affect seismic imaging in two ways (Onajide 2014):

- Due to the dip of the fault plane, the reflections are located at a point up-dip on the fault plane, so the fault acts as an inclined surface that needs to be repositioned.

- They cause abrupt termination of formations, producing diffraction curves that look like anticlines in the seismic section (Figure 4.13.7), as the distance from the formation termination point increases. The apex of the diffraction curve is called the diffraction point and is located at the true reflection point. All the reflection events of the diffraction curve can be attributed to this point. Migration is applied in order to restore abruptness to the faulted reflection and to make the fault apparent to the migrated seismic section.
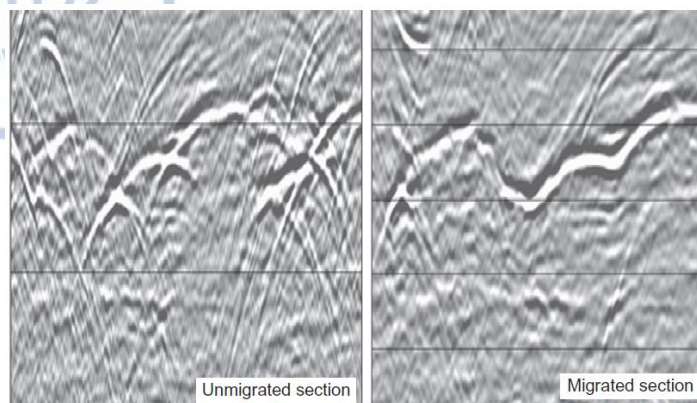
91

Figure 4.13.7: Diffraction curves created by a fault in unmigrated (left) and migrated (right) data (after Onajide 2014, taken from: Shell E&P Learning).

4.14   Post-stack Processing

To the end of data processing, various filters are applied to the final stacked or migrated seismic section. In cases where noise dominates over the signal, band-pass or time-variant frequency filters are used to reduce or attenuate frequency components. A post-stack processing often includes the following procedures (Yilmaz, 2001):

- Deconvolution after stack in order to restore high frequencies attenuated by CMP stacking and to suppress reverberations and short-period multiple reflections.

- Time-variant, spectral whitening for further flattening of the spectrum and accounts for the time-variant character of the source waveform. A time-variant filter uses multiple frequencies along the seismic section, so that the best signal-to-noise ratio is provided according to the circumstance.

- Time-variant band-pass filtering, so that noise at the high- and low-frequency end of the signal spectrum will be removed. A band-pass filter rejects frequencies below its low-cut-off and above its high-cut-off frequencies, while it passes a range of frequencies within its limits unaltered.

- Attenuation of random noise uncorrelated from trace to trace.

- Display gain for the stack data, usually application of a slow time-varying gain function that amplifies weak late reflections without destroying the previous processes' results.

4.15   Depth Models of Onshore Thermaikos Basin

Depth models of the onshore Thermaikos basin were created from the migrated seismic sections, with the aid of well data. These models are useful for the simulation of wave propagation on the underground formations, while they provide a clear picture of the underground geologic regime.

Five cross-sections were drawn at the basin's area, in order to construct the depth models. These cross-sections are depicted on Figure 4.15.1, on the basis of the residual gravity field map, whereas they can be studied in detail on Figure 4.15.2.
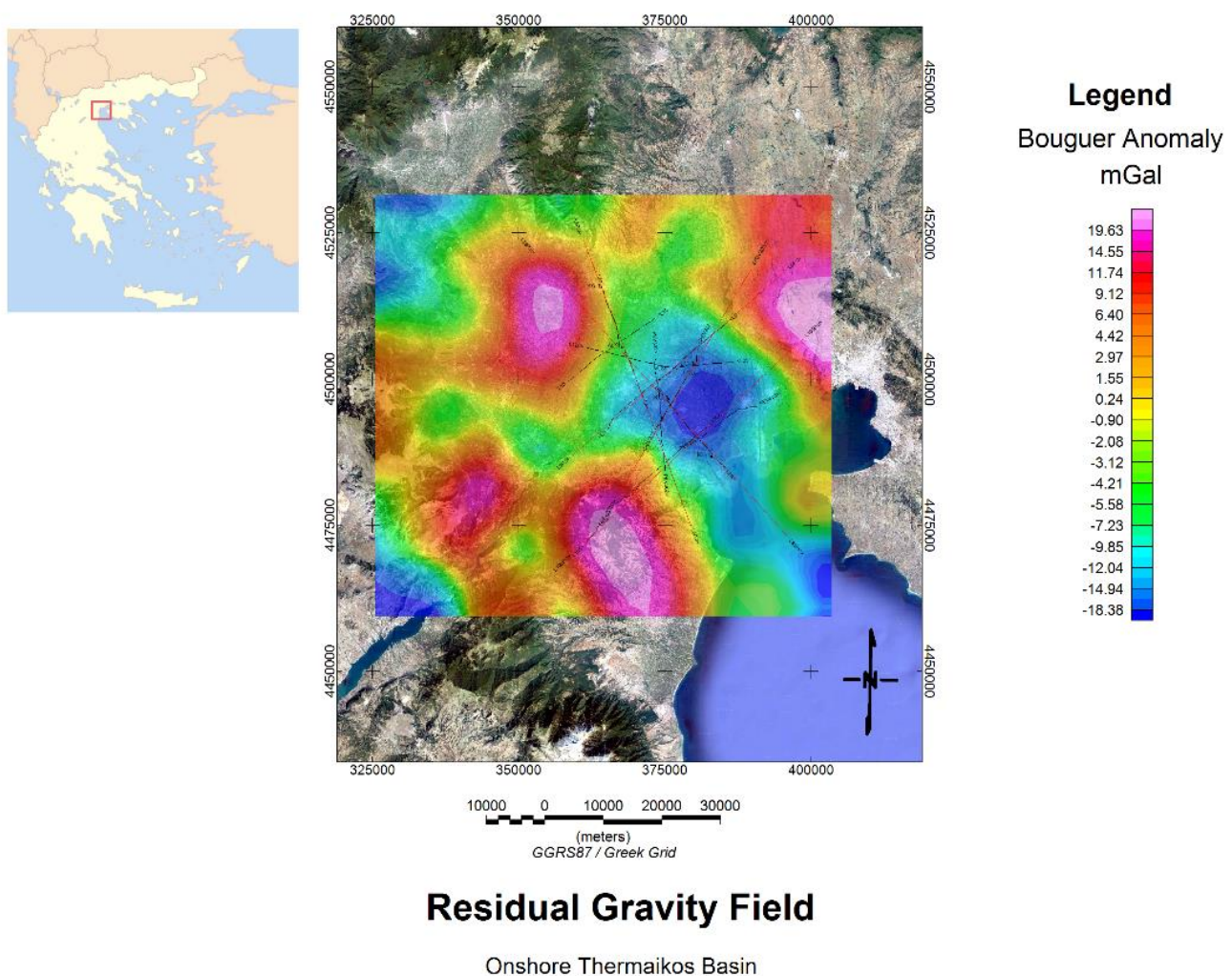

Residual Gravity Field

Onshore Thermaikos Basin

Figure 4.15.1: Cross-sections that were drawn in onshore Thermaikos basin.

Figure 4.15.2: Detail of Figure 5.5.1.

For the creation of each of the depth profiles, the velocity model, calculated from the seismic data as written on Table 2.5.1 at Chapter 2, was imported on Oasis Montaj add-on, GM-SYS Profile Modeling. Afterwards, density values were calculated from velocity values using Gardner's equation and with the aid of Table 2.6.4 at Chapter 2.

Gardner et al. (1974) proposed the following equation for the calculation of density (ρ), when only internal velocity of P-waves (V) is known:

$$\rho = \alpha V^{\beta}$$

where α and β are empirically derived constants, depended on geology.

94

Small changes were made at the two-way travel time section, according to the corresponding seismic section, in order to satisfy the gravity data. Finally, the time section was converted for the creation of the final 2-D depth model.

The following Figures (4.15.3, 4.15.4, 4.15.5, 4.15.6 and 4.15.7) contain the results of GM-SYS modeling. Their structure is the following:

- Planar view of the cross-section.
- Magnetic field variations, calculated by Oasis Montaj software.
- Gravity field variations, calculated by Oasis Montaj software.
- 2-D depth model.
- Travel time section, used for the creation of the depth model.

The locations of any existed well along the cross-sections are, also, pointed out, both on depth model and on planar view.

On Table 4.15.1, the legend of these Figures is contained.

The L8P section (Figure 4.15.3) has a total length of 52.56 km and is found in a NW-SE direction. It contains the L8 seismic section (length: 19.5 km), as well as the YA-1 and the projection of AL-1 boreholes.

The L88P section (Figure 4.15.4) has a total length of 64.42 km and is found in a NW-SE direction. It contains the L88 seismic section (length: 15.7 km), as well as the projections of AL-1, KO-1 and KL-1 boreholes.

The L9P section (Figure 4.15.5) has a total length of 48.212 km and is found in a SW-NE direction. It contains the L9 seismic section (length: 27.6 km) and no borehole.

The SPEV203 section (Figure 4.15.6) has a total length of 45.46 km and is found in a SW-NE direction. It contains the PEV203 seismic section (length: 16.2 km), as well as the LO-1 and the projection of KO-1 boreholes.

The L105P section (Figure 4.15.7) has a total length of 53.66 km and is found in a SW-NE direction. It contains the L105 (length: 29.3 km) and the projection of PEV403 (length: 11 km) seismic sections and no boreholes.

95
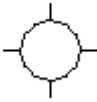
Symbol	Meaning	Symbol	Meaning
▭ (yellow)	Plio-Pleistocene formations	☉ (filled bottom)	Well with hydrocarbon indications
▭ (green)	Miocene formations		
▭ (red)	Oligocene-Eocene formations	○	Dry well
▭ (dark green)	Basement formations		

Table 4.15.1: Legend of Figures 4.15.3, 4.15.4, 4.15.5, 4.15.6 and 4.15.7.

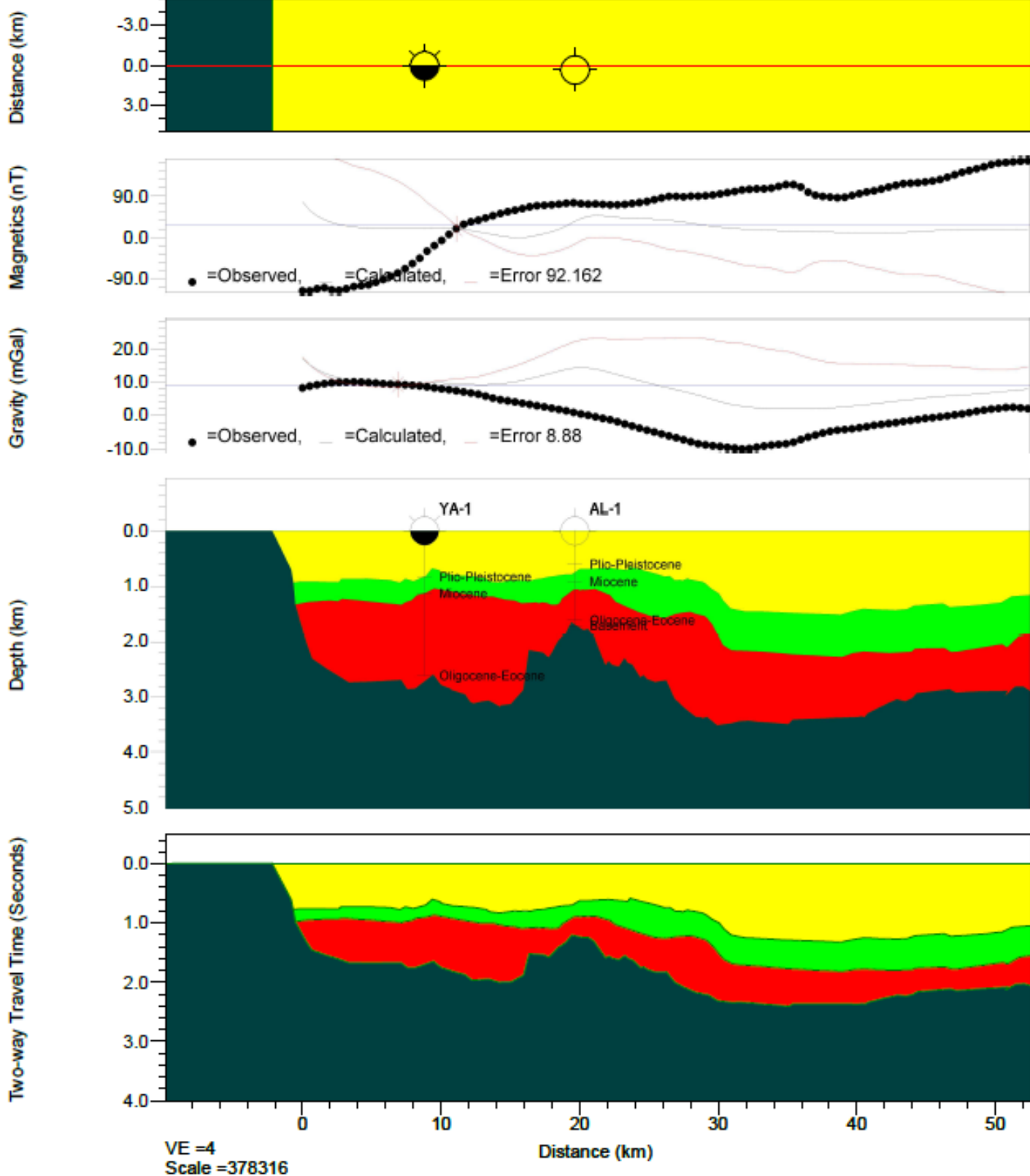# L8P Profile
Generated with GM-SYS

Figure 4.15.3: The L8P section analysis.
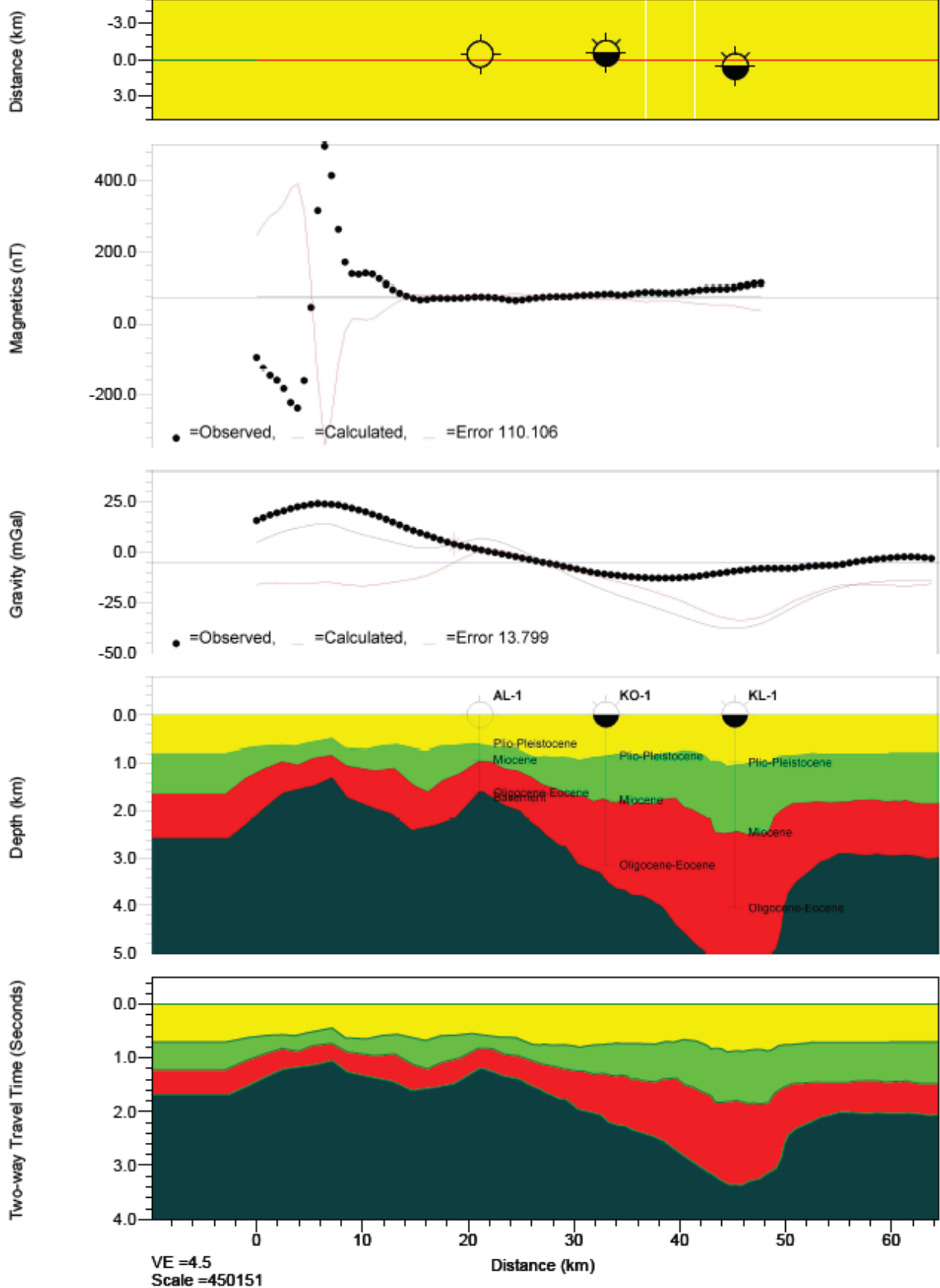
L88P Profile
Generated with GM-SYS

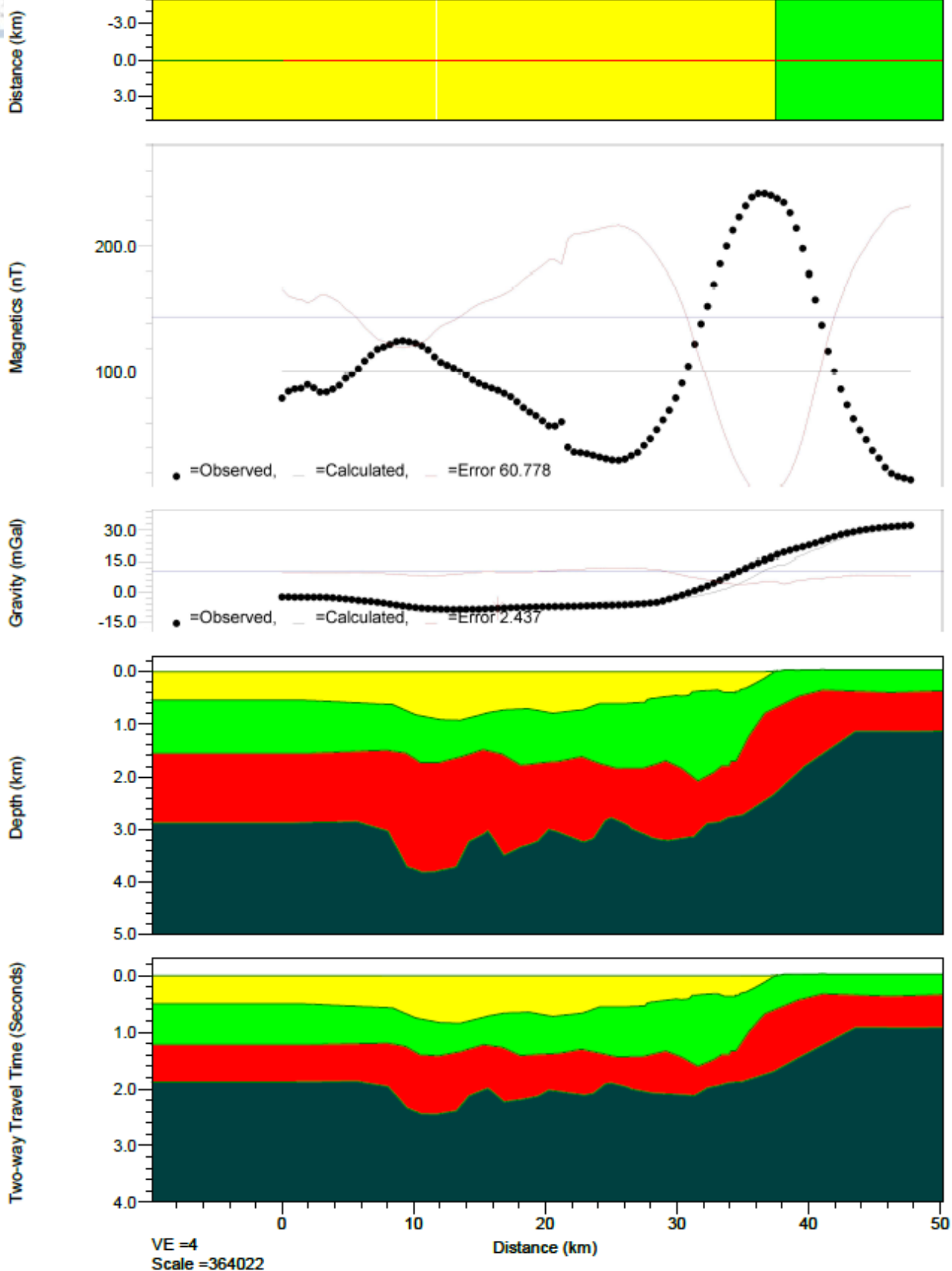Figure 4.15.4: The L88P section analysis.
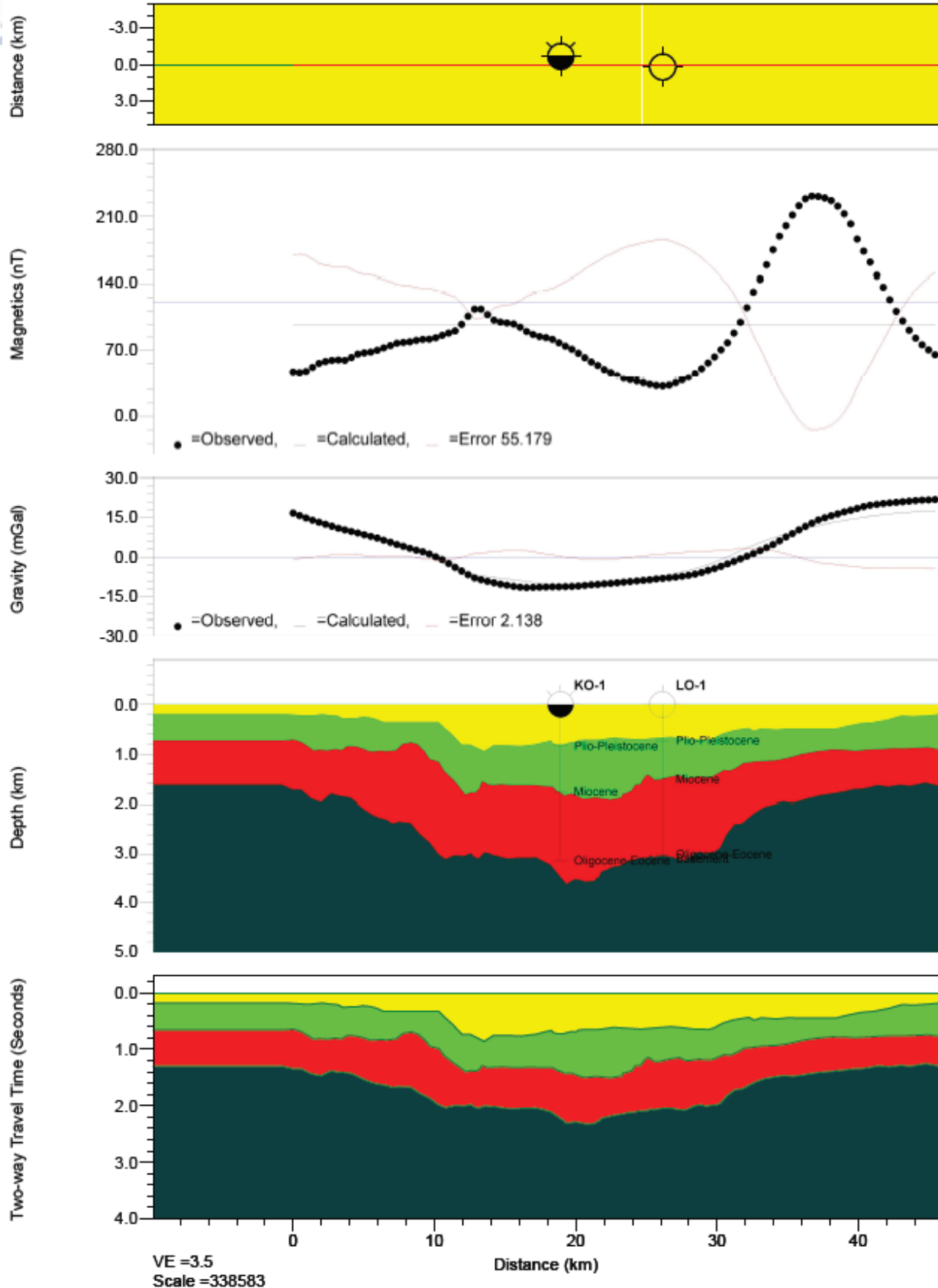
L9P Profile

Generated with GM-SYS

Figure 4.15.5: The L9P section analysis.
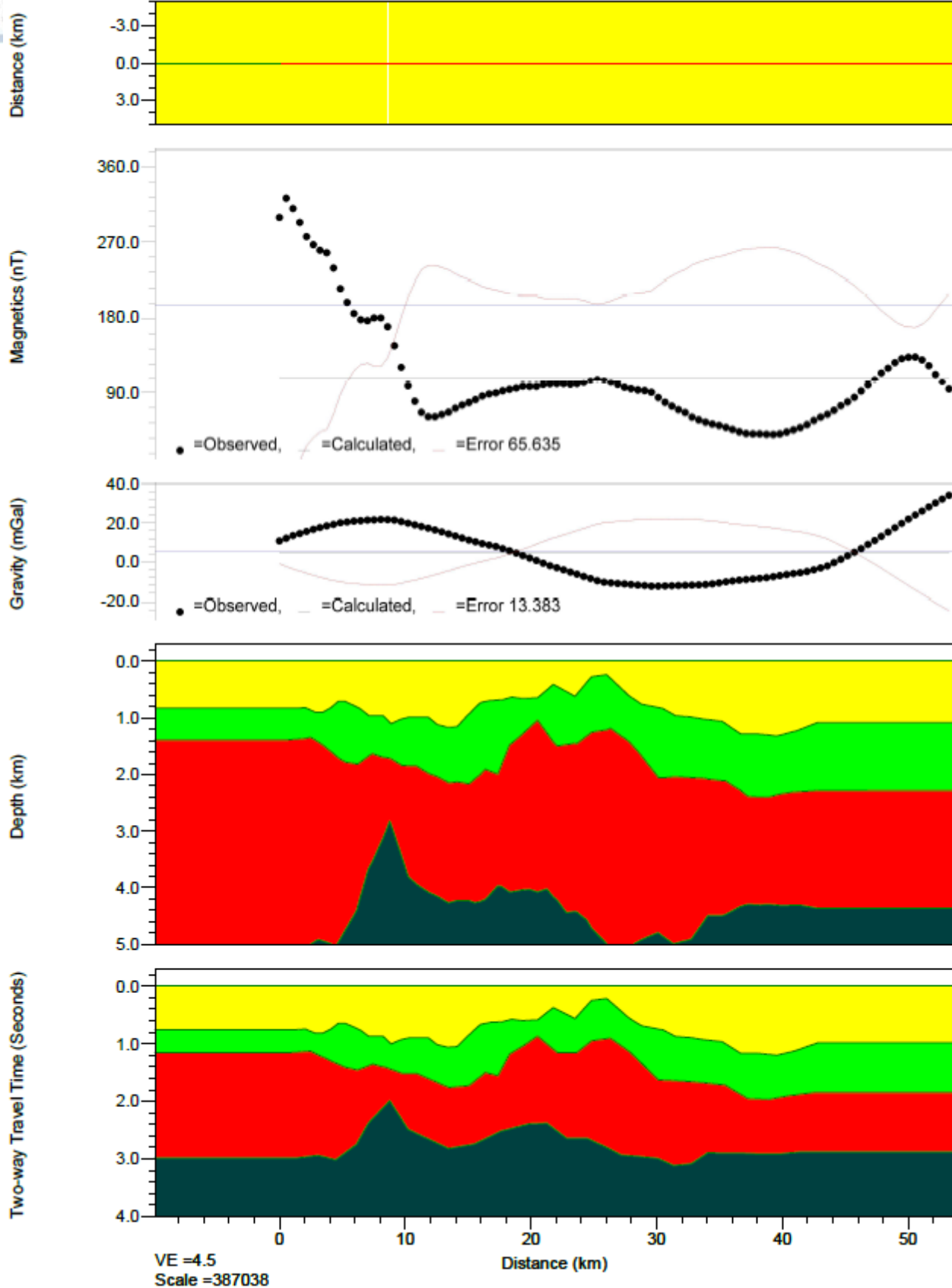
Figure 4.15.6: The SPEV203 section analysis.

Figure 4.15.7: The L105P section analysis.

102

CHAPTER 5

NATURAL GAS STORAGE AT ONSHORE THERMAIKOS BASIN

According to a number of studies that have been conducted at the onshore Thermaikos basin, it is resulted that it consists a favorable area for the development of underground hydrocarbon storages and that there are four possible locations that comply with some specifications concerning underground gas storage, despite of the lack of complete evidence (Sivenas et al., 1997). Figure 5.1 shows these locations of interest with yellow circles.

More specifically, by studying every available seismic and well data for the basin, Sivenas et al. (1997) located four targets, in Loudias (10 km south of Chalkidona, at Loudias 1 well), Alexandria (8 km north of Alexandria, at Alexandria 1 well), Klidi (5 km NW of Klidi 1 well, between Aliakmon and Loudias rivers) and Platy (3 km north of Korifi 1 well, between Alexandria and Loudias targets) areas. The first three targets are consisted of sand layers in alternations with Miocene clays in anticlinal type tectonic structures, at depths up to 1200 meters, dating at Miocene and Pleistocene. These structures were detected by the seismic explorations of years 1978-1979, 1980 and 1988.

The Platy target consists of coral (reef) limestone of Lower Miocene (not after 26 Ma). However, there is no borehole that has drilled that limestone yet; its presence is assumed by seismic sections only, at depths between 1300 – 1500 m. The Platy limestone indicates that in the beginning of Miocene, there were conditions of shallow, rich in oxygen water, which favored the development of coral formations. During Upper Oligocene, the coral limestones had their widest expansion in the area of Mediterranean Sea.
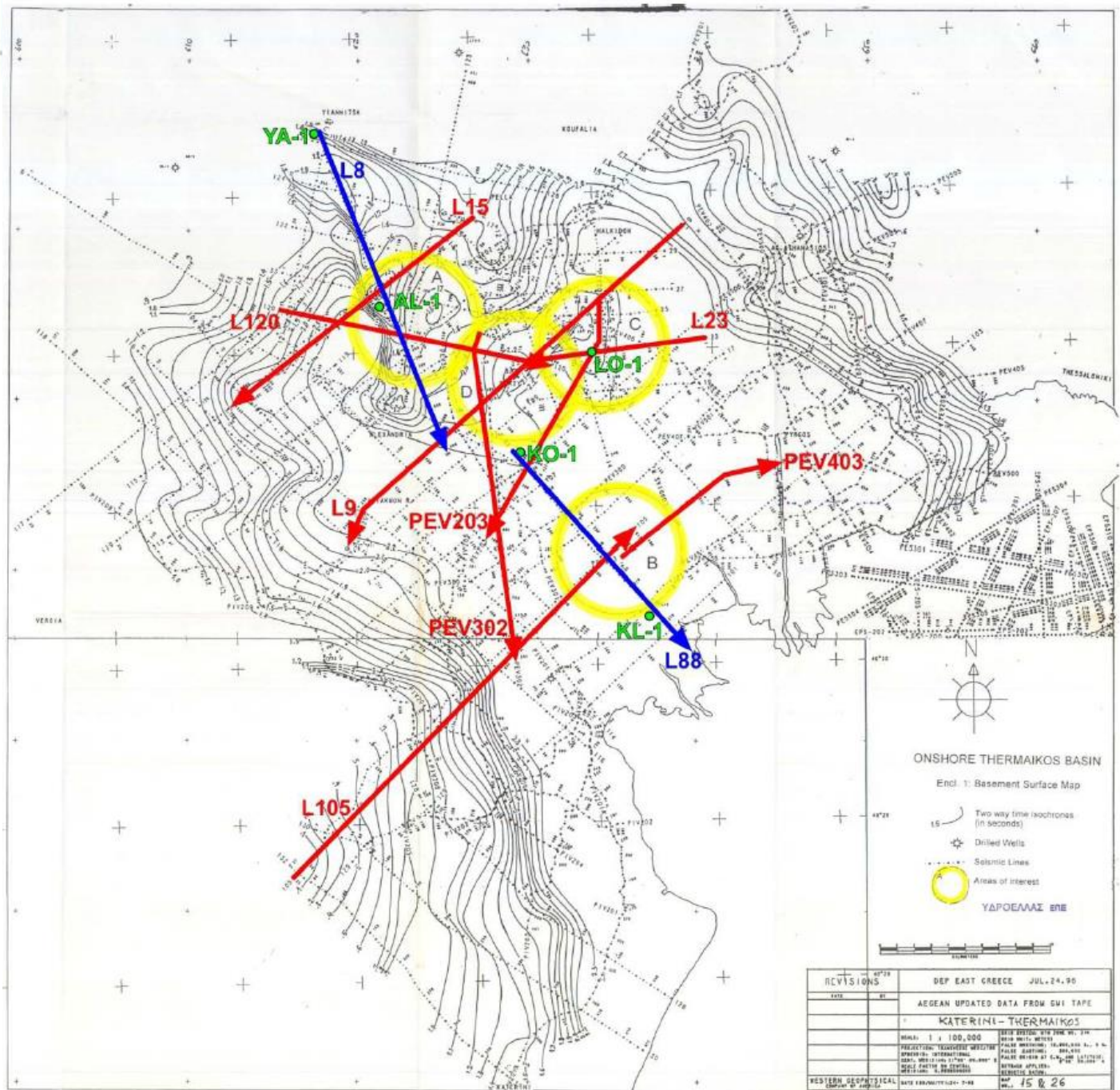
Figure 5.1: Basement isobath map of onshore Thermaikos basin. Seismic lines are depicted with red arrows, well locations with green points, while yellow circles show areas that could possibly store natural gas (after Sivenas et al. 1997, modified by Tsokas et al. 2013).

If the above structures are found tectonically closed, with appropriate geometry and petrophysical characteristics, they should be considered suitable for gas storage.

Tsokas et al. (2013) resulted that Compensated Neutron Log (CNL) at Loudias 1 well showed that between 793 and 835 m there is clay that could possibly acts as cap rock. This possible cap rock is, also, present at Alexandria 1 well, between 797 and 813 m, and probably at the whole basin.

Under this formation and until a depth of 1100 – 1200 m (depending on each well) there are sands (or marly sands) with clay intercalations. Sands are of thin thickness (3 – 6 m), but of adequate porosity, so they could be considered as reservoirs. Moreover, sonic logging proved that sands do not present high pressure, a fact that could lead to the assumption that they carry water.

Gas storage in underground aquifers lies in the replacement of rock pore water with gas. Specific studies should be made, along with supplementary cross-sections and boreholes, so that the appropriateness of rock layers to store natural gas is verified and defined, by studying the layers' geometry, their thickness, the salt dome's characteristics (if found any) etc.

With the presence of underground storage spaces, satisfying quantities of natural gas can be provided at peak seasons and the safe and constant gas supply in possible import breaks can be guaranteed. It is, also, important for the country that a natural gas stock is present, in cases where local interruptions of supply take place (e.g. strikes, accidents, pipe destructions, terrorist attacks) (Sivenas et al., 1997). Underground storages must be accompanied by a number of other infrastructures, such as central conducting high-pressure pipes, measurement stations, valve stations etc., in order to provide safety on gas transportation.

106

CHAPTER 6

CONCLUSIONS

The aim of the present Master Thesis was to summarize the main geophysical exploration methods used for the detection of underground geologic structures, which could act as trap for hydrocarbon (oil and/or natural gas) reserves, as applied on the area of onshore Thermaikos basin in northern Greece.

For this purpose, data of the gravity and magnetic field were studied, along with seismic sections and borehole data (including geologic and logging). It can be, therefore, concluded that the area of onshore Thermaikos basin is a typical area of a sedimentary basin, with large sediment's thickness at the central part. Thickness decreases as we move to the basin's boundaries, since the basement's rocks (mostly ophiolites) are found closer to the surface. At the basin's flanks, basement's rocks reach the surface, especially at the northern part.

The basement's rocks are responsible for high anomaly values of the magnetic field. The large distance between gravity stations (approximately 4 km) where the measurements were made, in addition to the poor quality of the available gravity measurements because of their limited frequency content, does not permit the detailed study and interpretation of the processing results.

The available seismic section profiles were detailed, but due to the above-mentioned limitations regarding gravity data, full matching between gravity and seismic data during depth modeling was not possible in some cases. As a result, detail that could be visible on the 2-D depth models are missing.

107

108

REFERENCES

Books – Articles

Baranov, V. (1957). A new method for interpretation of aeromagnetic maps: pseudo-gravimetric anomalies. *Geophysics*, vol. 22, pp. 359-383.

Behrend, D., Denker, H. & Schmidt, K. (1996). Digital gravity data sets for the Mediterranean Sea derived from available maps. *BGI Bulletin d' information*, vol. 78, pp. 31-39.

Beltrão, J. F., Silva, J. B. C. & Costa, J. C. (1991). Robust polynomial fitting method for regional gravity estimation. *Geophysics*, vol. 56, pp. 80-89.

Bhattacharyya, B. K. (1978). Computer modeling in gravity and magnetic interpretation. *Geophysics*, vol. 43, pp. 912-929.

Brown, S. A. M. & Robertson, A. H. F. (2004). Evidence for Neotethys rooted within the Vardar suture zone from the Voras Massif, northernmost Greece. *Tectonophysics*, 381, pp. 143-173.

Casten, U. & Makris, J. (2001). *Erkundung der Krustenstruktur von Kreta durch detaillierete Schwere- und Magnetfeldmessung-gen*. Project Report DFG: Ca 83/8-1 bis 3 Ma 719/54-1 bis 3.

Chailas, S., Tzanis, A., Kranis, H. & Karmis, P. (2010). Compilation of a unified and homogeneous aeromagnetic map of the Greek Mainland. *Bulletin of the Geological Society of Greece, Proceedings of the 12th International Congress, Patras*, 11 pp.

Claerbout, J. F. (1985). *Imaging the earth's interior*. Blackwell Scientific Publications.

Cordell, L. & Grauch, V. J. S. (1985). Mapping basement magnetization zones from aeromagnetic data in the San Juan basin, New Mexico. In "The utility of regional gravity and magnetic anomaly maps", Society of Exploration Geophysicists, pp. 181-197.

Cordell, L. & McCafferty, A. E. (1989). A terracing operator for physical property mapping with potential field data. *Geophysics*, vol. 54, pp. 621-634.

Dobrin, B. M. & Savit, C. H. (1988*). Introduction to Geophysical Prospecting. 4th Edition*. New York: McGraw-Hill College, 867 pp.

Gardner, G. H. F., Gardner, L. W. & Gregory, A. R. (1974). Formation velocity and density – The diagnostic basics for stratigraphic traps. *Geophysics*, vol. 39, pp. 770-780.

Gazdag, J. (1978). Wave equation migration by phase shift. *Geophysics*, vol. 43, pp. 1342-1351.

Geosoft Inc. (2014). Oasis Montaj How-To Guide, Complete Workflow for Oasis Montaj, [online] 260 pp. Available at: http://updates.geosoft.com/downloads/files/how-to-guides/Oasis_montaj_Complete_Workflow.pdf [Accessed 24 August 2019].

Grigoriadis, V. N. (2009). *Geodetic and geophysical approach of the earth's gravity field and applications in the Hellenic area. PhD Dissertation*. Thessaloniki: School of Rural and Surveying Engineering, Aristotle University of Thessaloniki, 181 pp. (in Greek).

Grigoriou, I., Loukoyannakis, M., Mitsakis, D. & Tiraskis, P. (1988). Radial and wave theory for the interpretation of tectonic events. In: *4th Congress of the Geological Society of Greece*. Athens: Geological Society of Greece (in Greek).

Henderson, R. G. & Zietz, I. (1949). The upward continuation of anomalies in total magnetic intensity fields. *Geophysics*, vol. 14, pp. 517-534.

Institute of Geology and Mineral Exploration (IGME). *Geological Map of Greece, 1:50000 scale*. Alexandria, Arnissa, Edhessa, Epanomi, Katerini, Kilkis, Kolindros, Koufalia, Kozani, Plati, Piryoi, Thessaloniki, Velvendos, Veroia, Yiannitsa sheets.

Kellogg, H. E. (1988). *Paleogene stratigraphy and petroleum potential of the greater Thermaikos basin area, eastern Greece*. DEP-EKY Report, 25 pp.

Kiriakidis, L. G. (1985). Geophysical studies of the eastern margin of the Vardar zone in Central Macedonia, Greece. PhD Dissertation. *Scientific Annals of Faculty of Sciences of Aristotle University of Thessaloniki*, vol. 23, annex 38.
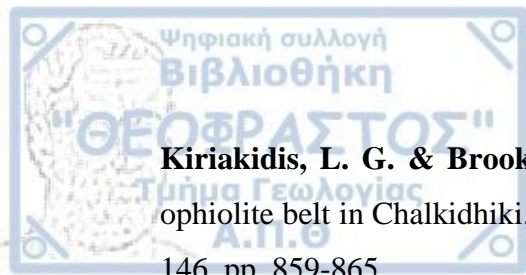
Kiriakidis, L. G. & Brooks, M. (1989). A geophysical study of the Vardar Zone ophiolite belt in Chalkidhiki, Northern Greece. *Journal of the Geological Society*, vol. 146, pp. 859-865.

Lagios, E., Chailas, S. & Hipkin, R. G. (1996). Newly compiled gravity and topographic data banks of Greece. *Geophysical Journal International*, vol. 126, pp. 287-290.

Lagios, E., Chailas, S., Hipkin, R. G. & Drakopoulos, J. (1994). *Gravity and topographic data banks of Greece*. Athens: Department of Geophysics and Geothermal Energy of National and Kapodistrian University of Athens.

Lagios, E., Hipkin, R. G., Angelopoulos, A. & Nikolaou, S. (1988). *Recompilation of the Gravity Anomaly Map of Greece*. Athens: Institute of Geology and Mineral Exploration.

Lalechos, N. (1983). *Correlations and observations in molassic sediments in onshore and offshore areas of northern Greece*. DEP-EKY Report, 19 pp.

Loukoyannakis, M. Z., Tsokas, G. N. & Mountrakis, D. M. (1990). A geological model of the south-west sector of Axios basin as deduced by the interpretation of seismic reflection lines, *Bulletin of the Geological Society of Greece*, vol. 25, pp. 329-345 (in Greek).

Makris, J. & Stavrou, A. (1984). *Compilation of Gravity Maps of Greece*. Hamburg: Institute of Geophysics, Hamburg University, 12 pp.

Mercier, J. (1966). Étude géologique des zones internes des Héllénides en Macedoine centrale. Contribution à l' étude du metamorphisme et de l' evolution magmatique des zones internes des Héllénides. *Annales géologiques des pays Helléniques*, 20, pp. 1-753.

Morelli, C., Gantar, G. & Pisani, M. (1975a). Bathymetry, gravity and magnetism in the strait of Sicily and the Ionian Sea. *Bollettino Geofisica e Teoretica Applicata*, vol. 17, pp. 39-58.

Morelli, C., Pisani, M. & Gantar, G. (1975b). Geophysical studies in the Aegean Sea and in the Eastern Mediterranean. *Bollettino Geofisica e Teoretica Applicata*, vol. 18, pp. 127-167.
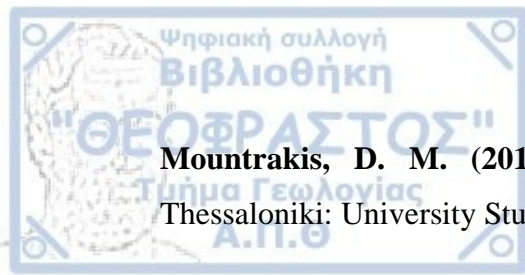
Mountrakis, D. M. (2010). *Geology and Geotectonic Evolution of Greece*. Thessaloniki: University Studio Press, 373 pp. (in Greek).

Nettleton, L. L. (1939). Determination of density for reduction of gravimeter observations. *Geophysics*, 4, pp. 8176-8183.

Onajite, E. (2014). *Seismic Data Analysis Techniques in Hydrocarbon Exploration*. Boston: Elsevier, 237 pp.

Parasnis, D. S. (1952). A study of rock densities in the English Midlands. *Geophysical Journal International*, 6, pp. 252-271.

Peters, L. J. (1949). The direct approach to magnetic interpretation and its practical application. *Geophysics*, vol. 14, pp. 290-320.

Schneider, W. (1978). Integral formulation for migration in two and three dimensions. *Geophysics*, vol. 43, pp. 49-76.

Sheriff, R. E. & Geldart, L. P. (1995). *Exploration Seismology, 2nd Edition*. Cambridge University Press.

Sivenas, P., Ciobotariu, S. & Voudouris, P. (1997). *Onshore Thermaikos Basin*. Athens: HYDROHELLAS Report, 47 pp. (in Greek).

Smith, R. A. (1959). Some depth formulae for local magnetic and gravity anomalies. *Geophysical Prospecting*, vol. VII, pp. 55-63.

Taner, M. T., Koehler, F. & Sheriff, R. E. (1979). Complex seismic trace analysis. *Geophysics*, vol. 44, pp. 1041-1063.

Tsokas, G. N. (1996). Interpretation of the Bouguer anomaly of Milos Island (Greece). *Journal of Volcanology and Geothermal Research*, vol. 72, pp. 163-181.

Tsokas, G. N. (1999). *Geophysical survey using Potential Field methods*. Thessaloniki: Department of Publications, Aristotle University of Thessaloniki, 139 pp. (in Greek).

Tsokas, G. N., Hansen, R. O., Fytikas, M., Vassilelis, G. D. & Thanassoulas, C. (1995). Geological and Geophysical study of the island of Kimolos (Greece) and Geothermal implications. *Geothermics*, vol. 24, pp. 679-693.

Tsokas, G. N., Vafidis, A., Georgakopoulos, A., Papadopoulos, C., Andronikidis, N., Kritikakis, G., Stampolidis, A., Tsourlos, P. & Stamataki, S. (2013). *Design of*
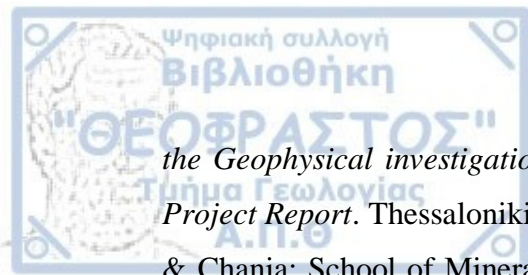
the Geophysical investigations and borehole drilling on shore of Thermaikos basin. Project Report. Thessaloniki: School of Geology, Aristotle University of Thessaloniki & Chania: School of Mineral Resources Engineering, Technical University of Crete, 163 pp. (in Greek).

Xanthopoulos, N., Tsokas, G. N., Nikolaou, S. & Kiriakidis, L. G. (1990). Geophysical investigations at the northern side of the Axios River Basin (N. Greece). *Bulgarian Geophysical Journal*, vol. 16, pp. 53-62.

Yilmaz, Ö. (2001). *Seismic Data Analysis. Processing, Inversion, and Interpretation of Seismic Data. Volume I.* Series: Investigations in Geophysics, Society of Exploration Geophysicists, 1000 pp.

Web Sites

ArcGIS Desktop, ArcMap, ESRI, viewed 10 July 2019, <http://desktop.arcgis.com/en/arcmap/ >.

Geosoft Inc., Oasis Montaj, viewed 25 April 2019, <https://geosoft.com/products/oasis-montaj>.